Lpt-protein dynamics reveal that Lipopolysaccharide promotes trans-envelope bridge formation

HARVARD UNIVERSITY
Graduate School of Arts and Sciences

DISSERTATION ACCEPTANCE CERTIFICATE

The undersigned, appointed by the

Department of Chemical Biology

have examined a dissertation entitled

Lpt-protein dynamics reveal that Lipopolysaccharide promotes trans-envelope bridge formation

presented by Lisa Toerk

candidate for the degree of Doctor of Philosophy and hereby certify that it is worthy of acceptance.

Signature _____

Typed name: Prof. Daniel Kahne

Signature _____

Typed name: Prof. Ethan Garner

Signature _____

Typed name: Prof. Thomas G. Bernhardt

Signature _____

Typed name: Prof. Timothy J. Mitchison

Signature _____

Typed name: Prof.

Date: 08/15/2022

Lpt-protein dynamics reveal that Lipopolysaccharide promotes trans-envelope bridge formation

A dissertation presented

By

Lisa Toerk

to

The Committee of Higher Degrees in Chemical Biology

in partial fulfillment of the requirements for the

Degree of Doctor of Philosophy

in the subject of

Chemical Biology

Harvard University

Cambridge, Massachusetts

August, 2022

Dissertation Advisor: Daniel Kahne Lisa Toerk

Lpt-protein dynamics reveal that Lipopolysaccharide promotes trans-envelope bridge formation

Abstract

Gram-negative bacteria have two lipid bilayers, the inner membrane and the outer membrane as part of their cell envelope structure.[1] A special feature of the outer layer is its asymmetric membrane structure, comprised of phospholipids in the inner leaflet and lipopolysaccharide (LPS) in the outer leaflet. The presence of LPS in the outer leaflet of the outer membrane provides a robust physical barrier, protecting Gram-negative bacteria from external toxins, making them especially difficult to kill with *e. g.* antibiotics.[2-3] LPS is a large amphipathic molecule comprised of fatty acyl chains attached to polysaccharides, whose biosynthesis is completed in the inner membrane, and which then needs to be transported from its synthesis site to the cell surface.[4] LPS must be extracted from the inner membrane, moved across the aqueous periplasm that separates the two membranes, then translocate through the outer membrane and assembled on the cell surface.[5] LPS transport and assembly requires seven conserved lipopolysaccharide transport components (LptA-G), which are proposed to form a continuous protein bridge spanning the periplasm that provides a path for LPS to reach the cell surface.[6-7] However, this model has not been validated in living cells. It is also unknown how stable the proposed bridges are, what influences their formation and breakage and what is their order of assembly and disassembly. This thesis presents live cell single molecule tracking results to address

these questions. In chapter 2 we show that Lpt protein dynamics are consistent with the bridge model and that half of the inner membrane Lpt proteins exist in a bridge state. In chapter 3 we describe the life time measurement of the bridge in cells. We found that bridges persist for 5-10 seconds, showing that their organization is highly dynamic. In chapter 4 we present evidence that Lpt-bridge formation is facilitated by LPS, providing a mechanism by which the production of LPS can be directly coupled to its transport. Finally, bridge decay kinetics suggest that two different kinds of bridges may exist, whose stability differs according to the presence (long lived) or absence (short lived) of LPS. Taken together, the data of this thesis support a model in which LPS is both a substrate and structural component of highly dynamic Lpt bridges that promote outer membrane assembly.

Table of Contents

List of Figures

List of Tables

Acknowledgments

I would like to thank my advisor Dan Kahne for his guidance and advices during my whole PhD. The project described in this thesis would not have been possible without his help. His immense scientific knowledge and admirable ability of logical thinking were absolutely essential for this project. I have learned a lot from him about how to interpret data and how to transform data into a confined story. I'm very grateful that I was able to be part of his lab. Further, I would like to thank Ethan Garner. His idea on how to use microscopy to look at Lpt-bridges in live cells was absolutely fundamental for my PhD project. I'm really grateful for his willingness to share his knowledge and skills about single molecule tracking with me and his generosity to let me use the microscope at any time. Next, I would like to thank Tom Bernhardt. His insights for how to construct Lpt-halo fusion strains were absolutely essential for the work presented in this thesis and I have learned a lot from him about the different approaches to modify bacterial genetics. Further, I would like to thank Tim Mitchison for his honest feedback about my data and interpretation, which helped me to stay critical and initiated a number of important control experiments. I want to thank all members of my DAC committee for their helpful feedback and advice throughout my PhD and for editing and commenting on my paper draft.

Also, I would like to thank Matthew Holmes, who taught me how to perform single molecule experiments with the TIRF microscope. Thank you also to all other members of the Garner lab,

who always were helpful when I ran into problems with the microscope. Especially thank you to, Georgia Squyres, Yingjie Sun and Daniel Henthorn.

I further would like to thank all past and present members of the Kahne lab, who make the lab not only a scientific stimulating research experience, but also a fun and friendly environment. Especially thank you to the LPS subgroup, and to Stephen Early, who generously let me work with the LptCA-fusion protein, which he designed. Further, thank you to Cait Moffat for continuing the Lpt-single molecule tracking technique in the Kahne lab.

Outside of the lab, I would like to thank my Boston friends from hiking, dancing and stadium workout group. Finally, thank you to my family, who is always there for me and supportive in everything I do!

1. Chapter 1: Introduction to Lipopolysaccharide transport and functionality in *Escherichia coli*

1.1. The gram negative bacterial cell envelope and the role of LPS

In 1884 the Danish scientist Hans Christian Gram first was able to distinguish two large groups of bacteria from each other using a staining procedure, which he originally developed to visualize bacteria in stained lung tissues.[8] He was able to distinguish between cells, which are retaining the stain, gram positive bacteria, and cells which are not retaining the stain, gram negative bacteria. Responsible for the differential staining behavior is the fundamental difference in the cell envelope structure of gram negative and gram positive bacteria. While the cell envelope of gram positive bacteria only consists of one lipid membrane and a thick peptidoglycan cell wall, gram negative bacteria have two lipid bilayers the inner membrane (IM) and the outer membrane (OM) and only a thin peptidoglycan cell wall. (Figure 1) The purple Gram stain is retained in the thick peptidoglycan layer of gram positive bacteria, but not in the thin cell wall of gram negative bacteria.

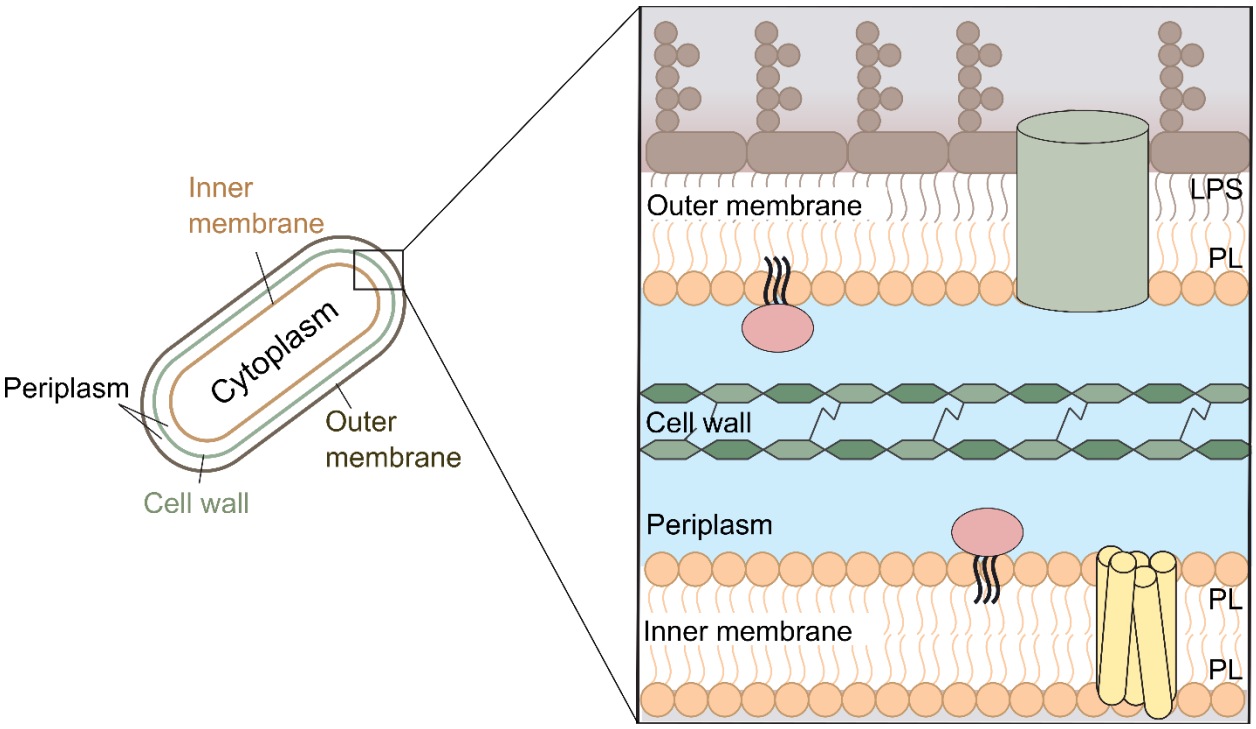

Figure 1: Gram negative bacteria cell envelope contains two lipid membranes. Scheme depicting the cell envelope of gram negative bacteria. The cell envelope of gram negative bacteria consists of four components: the inner membrane, the periplasm, the cell wall and the outer membrane. Lipopolysaccharides are found in the outer leaflet of the outer membrane and give it its unique features. (LPS = Lipopolysaccharide, PL = Phospholipids)

The inner membrane separates the cytoplasm from the periplasm in gram negative bacteria and is built of a phospholipid bilayer. The inner membrane contains alpha-helical transmembrane proteins and lipid proteins serving various different functions in the cell, such as lipid biosynthesis, energy production, cell wall synthesis and transport.[9-10] The periplasm is the aqueous cell compartment between the inner membrane and the outer membrane. It is densely packed with proteins[11], important, for example, for nutrient transport or cell envelope biosynthesis. Interestingly, no ATP is present in the periplasm, which means that processes in this compartment either need to be coupled to an energy source at the inner membrane or must proceed without

chemical energy. The space between the inner membrane and the outer membrane also contains the peptidoglycan cell wall, which holds the major part of the turgor pressure and is responsible for the shape of the cell.[12]

The outer membrane surrounds the periplasm and serves as first protective layer between the cell and the external environment. Unlike most other biological membranes the outer membrane is an asymmetric lipid bilayer with phospholipids in the inner leaflet and Lipopolysaccharides (LPS) in the outer leaflet.[1-3] The outer membrane contains lipid proteins which are anchored to the inner leaflet of the outer membrane with a lipid tail[13] and beta barrel proteins, which are able to span both membrane leaflets and often serve as porins.[14-15] One of the main roles of the outer membrane is it's unusual permeability barrier function.[9] Unlike a phospholipid bilayer the outer membrane does not only prevent large, hydrophilic molecules to enter the cell, but also blocks the diffusion of small hydrophobic molecules to pass the outer membrane. This characteristic makes gram negative bacteria uniquely resistant to antibiotics and host defense mechanisms.[16-18] Further, it has been shown that the outer membrane contributes, due to its stiffness and strength, to the mechanics of the cell envelope and also holds parts of the turgor pressure.[19]

Responsible for these unique characteristics of the outer membrane is lipopolysaccharide, LPS. LPS is a large glycolipid, which is a major structural component of the outer membrane and occupies roughly three third of the outer membrane outer leaflet. [1-3, 20] It is an essential component of the outer membrane in most gram negative bacteria.[16] The structural and chemical properties of LPS allow LPS to form strong lateral interactions between itself, which transform the outer membrane into a stiff barrier.[21-23] Further, LPS has been shown to be important for virulence and it gets recognized by the host immune system.[4, 24]

1.2. LPS structure and functionality

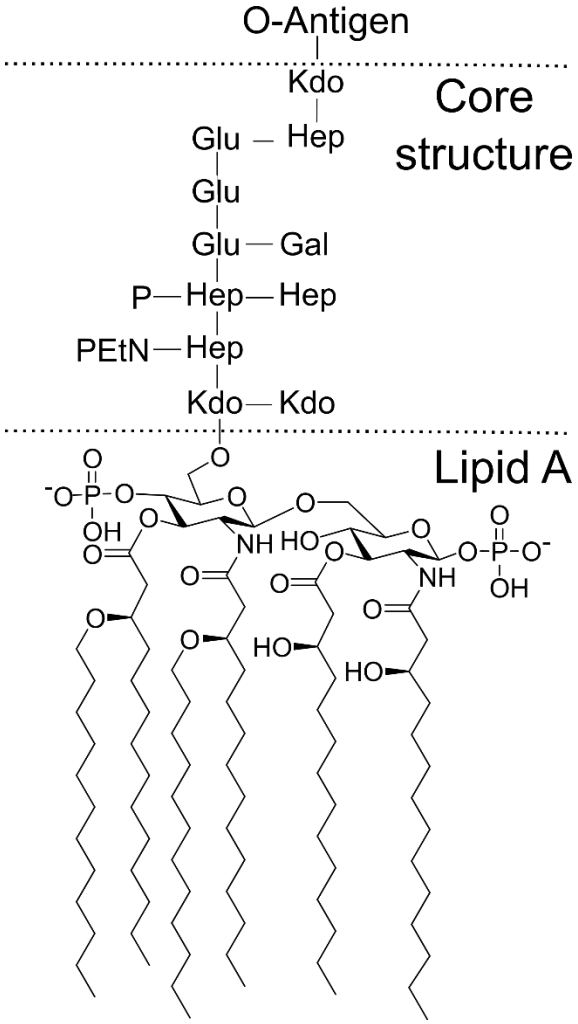

Figure 2: Strong lateral interactions between LPS molecules are responsible for the unique characteristics of the outer membrane. An example structure of a lipopolysaccharide from E. coli is shown. Lipid A is the conserved lipid anchor, which is comprised of the hexa-acylated di-glucosamine diphosphate. The core oligosaccharides are connected to lipid A via the conserved Kdo (3-deoxy-D-*manno*-oct-2-ulosonic acid) sugars. Lipid A plus the core oligosaccharides form the so called Ra-LPS, which lacks the O-antigen unit. The common E coli K12 laboratory strain lacks the oligosaccharide. Kdo: 3-deoxy-D-*manno*-oct-2-ulosonic acid, Hep: L-glycerol-D-manno-heptose, Glu: D-Glucose, Gal: D-Galactose, PEtN: Phosphoethanolamine, P: Phosphate.

Lipopolysaccharide, LPS, is a complex glycolipid, whose structure can be divided into three regions: lipid A, the core sugars and the O-Antigen.[4, 25-26] (Figure 2) Lipid A is the conserved lipid anchor of LPS based on a biphosphorylated di-glucosamin disaccharide which is typically found with four to seven acyl chains. Lipid A is also known as endotoxin. As conserved portion of the LPS molecule, Lipid A is able to activate the mammalian innate immune system, including that of humans.[27-29] Even though Lipid A is highly conserved, it has been shown that it can undergo modifications dependent on the environmental conditions.[24, 29-32]

The second structural unit of LPS are the core sugars. The core sugars are polysaccharides, which are connected to the base Lipid A structure through the unique Kdo (3-deoxy-D-*manno*-oct-2-ulosonic acid) sugar unit. The direct linkage between Lipid A and the sugar moiety Kdo is highly conserved in all gram negative bacteria. The other core sugars are usually conserved within species but can vary among different gram negative species.[33-34]

The LipidA-core sugar structure can be further glycosylated with the addition of the third structural unit of LPS, the O-antigen. The O-antigen is a large polysaccharide, which is highly variable in its chemical structure, but usually consists of linear and branched chains of repeating polysaccharide subunits.[35-38] The O-antigen is often responsible for the interaction with the environment, such as the host defense mechanism. The O-antigen is not essential, for example, the most common E. coli lab strain K12 lacks the O-antigen portion of LPS. LPS missing the O-antigen is also called, Ra-LPS.

Even though the overall structure of LPS is conserved, structural variations in each region can occur depending on the species or the environmental condition.

As discussed above the outer membrane of gram negative bacteria has unique barrier and stability functionality. Responsible for the special characteristics of the outer membrane are the chemical properties of the LPS structure. Analogous to phospholipids, the acyl chains of Lipid A provide the hydrophobic portion of LPS, which prevents the passage of hydrophilic molecules through the outer membrane. Further, the high number of fatty acyl chains of LPS allow the molecules to pack very tightly at the outer leaflet of the outer membrane. This dense packing is further elaborated by metal cations, which connect the negative phosphate groups of Lipid As with each other. Together with the strong hydrogen bonds between the core sugars of neighboring LPS molecules, all these lateral interactions result in a stiff outer membrane with especially low permeability.[21-23]

1.3. LPS synthesis

The biosynthesis of LPS takes place in the cytoplasm and at the cytoplasmic leaflet of the inner membrane. It begins with the biosynthesis of Kdo_2-Lipid A, which involves a series of nine conserved enzymatic steps catalyzed by the so called LpX proteins. These first conserved enzymatic steps to produce the Kdo_2-Lipid A are also known as the Raetz pathway.[4, 24] The Raetz pathway starts with the precursor UDP-*N*-acetylglucosamine (UDP-GlcNAc), which is also a precursor for the peptidoglycan biosynthesis. The first three enzymes, the acyltransferase LpxA, the deacetylase LpxC and the acyltransferase LpxD, convert UDP-GlcNAc into UDP-2,3-diacylglucosamine by the addition of two acyl chains.[39-43] The first step, the acylation of UDP-GlcNAc by LpxA is unfavorable. Therefore, the first committed step in the Lipid A synthesis is the deacetylation of UDP-monoacyl-N-acetylglucosamine by LpxC leading to UDP-monoacyl-glucosamine.[41, 43] This characteristic makes LpxC an attractive antibiotic target and extensive

efforts have produced LpxC inhibitors, which indeed prevent LPS synthesis and lead in most gram negative strains to cell death.[44-49]

Following the action of LpxC, UDP-monoacyl-glucosamine is acylated a second time, this time by the enzyme LpxD, to produce UDP-2,3-diacylglucosamine.[42, 50] The next two steps are catalyzed by the membrane associated enzymes LpxH and LpxB. LpxH removes the sugar nucleotide carrier from UDP-2,3-diacylglucosamine resulting in 2,3-diacylglucosamin-1-phosphate, also known as Lipid X. LpxB then catalyzes the condensation between Lipid X and UDP-2,3-diacylglucosamine, the product of the LpxD step. The resulting tetraacylated glucosamine disaccharide is inserted into the inner leaflet of the inner membrane and is also known as Lipid A disaccharide.[51-52]

The following four enzymes are responsible for finishing Kdo_2-Lipid A synthesis; LpxK, WaaA, LpxL, and LpxM. They are all integral membrane proteins. The kinase LpxK phosphorylates Lipid A disaccharide at the 4' position producing the biphosphorylated lipid IV_a.[53-54] In the next step WaaA adds sequentially two Kdo sugar groups to lipid IVa. Finally, two acylchains are added to Kdo_2-Lipid IVa by the acyltransferases LpxL and LpxM producing Kdo_2-LipidA. LpxL transfers a lauryol group and LpxM adds a myristol group.[55-57]

Following the Kdo_2-lipid A biosynthesis, the core oligosaccharides are extended from the Kdo moiety by the successive addition of sugars by glycosyltransferases generating Ra-LPS at the cytoplasmic leaflet of the inner membrane.[4, 34, 58]

Parallel to the Ra-LPS biosynthesis the O-antigen is prepared. The O-antigen is a large polysaccharide consisting of linear and branched chains of repeating polysaccharide subunit. Its precursors are synthesized separately from Ra-LPS by the sequential action of glucosyltranferases,

at the inner leaflet of the outer membrane and are attached to the lipid carrier undecaprenyl pyrophosphate.[38]

Both the Ra-LPS and the O-antigen precursors are synthesized at the cytoplasmic leaflet of the inner membrane and then need to be switched to the periplasmic leaflet of the inner membrane. Responsible for this process are the two flippases, MsbA, Wzx.[38, 59-62] MsbA is an ABC transporter, which flips LPS in an ATP dependent fashion. Wzx, is responsible for flipping the O-antigen precursor. The O-antigen precursors are polymerized by the two proteins Wzy and Wzz and the completed O-antigen is ligated to the Ra-LPS by the O-antigen ligase WaaL at the periplasmic site of the inner membrane.[50, 63-66] In the E coli K12 lab strain no O-antigen is added to Ra-LPS and Ra-LPS is the final synthesized LPS product, which needs to be transported from the periplasmic leaflet of the inner membrane to the outer leaflet of the outer membrane.

1.4. LPS transport

1.4.1. LPS transport challenges

As discussed above LPS is completely synthesized at the inner membrane and then needs to be transported from its synthesis side to the outer leaflet of the outer membrane. There are a number of challenges, which the transport system needs to overcome. First, the unique structure of LPS poses difficulties for the transport. LPS is a really large molecule, with a large hydrophobic portion, the fatty acyl chains, and a large hydrophilic portion, the core sugars and the O-antigen. In the aqueous periplasm the hydrophobic lipids need to be shielded from the water, and to pass the outer membrane the hydrophilic portion needs to be shielded. Second, LPS has to be transported against a concentration gradient. However, there is no ATP in the periplasm. Therefore, the energy source for LPS transport can only be in the cytoplasm and somehow needs

to be connected to the whole transport process. Third, a lot of LPS molecules have to be transported in order to fill the whole outer membrane in a short amount of time. Insufficient LPS transport to the outer membrane leads to membrane leakiness and cell death. In addition, also LPS spilling into the periplasm creates toxicity by activating the σ^E response. Therefore, LPS transport needs to be carefully regulated with LPS biosynthesis and cell growth.[67]

1.4.2. Identification of the seven essential LPS transport proteins

Seven essential proteins have been identified over the years to be responsible for transporting LPS from the inner membrane to the outer membrane. The first LPS transport protein, which was identified was LptD. LptD mutants showed up 1998 in a genetic selection designed to select for mutants, which allow maltodextrin to pass the outer membrane without its specific channel, LamB, being present.[68] The LptD mutants increased the permeability of the outer membrane suggesting that LptD is important for outer membrane integrity. Further interest in LptD was sparked in 2002, when it was found that LptD is located upstream of the gene encoding SurA. SurA has been identified as periplasmic chaperon protein, which transports outer membrane proteins.[69] It was found that LptD and SurA are co-transcribed from the same operon and controlled by the σ^E stress response. σ^E monitors the cell envelope and increases cell envelope biogenesis upon stress.[70],[71] Motivated by this observation, Braun et al. proofed that LptD is essential for outer membrane biogenesis.[72] Shortly after, it was shown that LptD is essential for LPS transport. In an *N.meningitis* mutant strain, lacking LptD, LPS was not able to reach the surface. LPS neither got cleaved by the extracellular neuraminidase nor did it get modified by the outer membrane enzyme PagL.[73]

The second Lpt-protein, LptE, was discovered by Wu, T. et al. using a biochemical approach.[74] Affinity tag purification of LptD pulled down LptE, and analogously, affinity tag purification of LptE co-purified LptD, suggesting that these two proteins form a complex in the outer membrane. It further was shown that LptE is essential in E. coli and that depletion of LptE lead to the same phenotypes in cells as depletion of LptD; leaky membranes and a buildup of phospholipids in the outer membrane. Finally, it was shown that depletion of either LptD or LptE prevented the modification of newly synthesized LPS at the outer membrane by the palmitoyltransferase, PagP, which proofed that LptD and LptE are required for LPS transport to the outer membrane.

The genes encoding the proteins LptA and LptB were first found in a genetic screen for essential genes in E. coli.[75] Based on the fact that the genes encoding LptA and LptB are part of a conserved locus encoding LPS biosynthesis enzymes it was hypothesized that they are involved in LPS transport.[76] Sucrose gradient centrifugation showed that cells with either depleted LptA or LptB lead to the accumulation of LPS in the inner membrane, demonstrating their importance for LPS transport.[77] The same experiment also proofed that LptC is required for LPS transport. LptC was found to be in the same operon as LptA and LptB and is also essential in E. coli.[5] Based on protein sequencing it was predicted that LptB is a cytoplasmic protein with a nucleotide binding domain, which can associate to an ATP binding cassette in the inner membrane. LptA was predicted to be a soluble periplasmic protein and LptC was predicted to be an integral transmembrane protein.[78]

ABC transporter usually require an inner membrane protein with 12 transmembrane domains or two inner membrane proteins with 6 transmembrane domains each. Since the identified inner membrane protein LptC only contains one trans membrane domain, it was likely that one or

two more inner membrane proteins are involved in LPS transport.[79] To find the missing inner membrane proteins a reductionist bioinformatics approach was used by searching the small genome of *Blochmannia floridanus* for an envelope protein which is conserved and essential in *E. coli*.. This way the two transmembrane proteins LptF and LptG were identified.[80] Their involvement in LPS transport was proven by the accumulation of LPS in the inner membrane upon depletion of these two proteins. Depletion strains also showed the same phenotype that was observed for depletion strains of the other Lpt-proteins; a leaky and unstable outer membrane.

With the discovery of LptF and LptG all seven essential Lpt-proteins required for LPS transport have been identified. The cytoplasmic protein LptB forms an ABC transporter at the inner membrane with the transmembrane proteins LptF, LptG and LptC. LptA was shown to be located in the periplasm and LptD and LptE were observed to form a complex in the outer membrane. In the following section the structure and functionality of the inner membrane complex and the outer membrane complex will first be discussed separately. Afterwards, it will be discussed how the inner membrane complex works together with the periplasmic protein LptA and the outer membrane complex to transport LPS from the inner membrane to the outer membrane.

1.4.3. The inner membrane complex $LptB_2FGC$ extracts LPS from the inner membrane

At the inner membrane $LptB_2FGC$ build a 2:1:1:1 complex. $LptB_2FG$ is a heteromeric ATP binding cassette (ABC) transporter, which associates with the transmembrane protein LptC.[81] The exact role of LptC in the inner membrane complex is still unclear. Even though LptC is essential, a single mutation in LptF can suppress a LptC deletion.[82] Further, a soluble LptC lacking the transmembrane domain is able to support LPS transport and cell viability.[83] In the current model LptC is thought to play a crucial role in interacting with the periplasmic Lpt-protein LptA to hand

LPS over to LptA.[6, 84-87] A mutation in LptC, LptC(G153R), which prevents the interactions between LptC and LptA, fails to transport LPS and cannot support cell viability.[83] In addition it recently has been show that the transmembrane domain of LptC plays a role in regulating the ATPase activity of the inner membrane complex and might be important for the coupling of the ATPase activity with the extraction of LPS from the inner membrane.[88-89]

LptC co-purifies with $LptB_2FG$, and the purified complexes $LptB_2FG$ and $LptB_2FGC$ exhibit ATPase activity.[81, 90] The dimer of LptB forms the nucleotide binding domain of the ABC transporter, which is able to bind and hydrolyze ATP. Based on its location in the inner membrane, it has been predicted that the inner membrane complex, $LptB_2FGC$, is responsible for pulling out LPS from the inner membrane and passing it to the periplasmic protein LptA in an ATP dependent fashion. A combination of in vivo and in vitro photo crosslinking experiments and the resolution of crystal structures of the inner membrane complex support the predicted model. *p*-benzoylphenylalanine (*p*BPA) photo crosslinks to nearby residues upon UV-irradiation.[91] With the help of an orthogonal aminoacyl tRNA synthetase developed by Schultz et al. p-BPA was incorporated into different sites in the periplasmic domains of LptC and LptA.[92] This way a number of interaction sites between LPS and the periplasmic domains of LptC and LptA were identified.[93] The identified binding sides were then used to study the release of LPS to the periplasmic domains in LptC and LptA in right side out vesicles.[94-96] Preparation of vesicles containing photo cross linkable LptC and LptA with and without ATP, showed that LPS crosslinks to these binding sides are dependent on ATP hydrolysis and suggest that multiple rounds of ATP hydrolysis are needed to extract LPS from the inner membrane to move it further towards the outer membrane.[93]

Crystal structures of the inner membrane complex $LptB_2FG$ showed that LptB interacts with LptFG through a conserved groove. Hydrolysis of ATP leads to the collapse of the groove

inducing conformational change in LptFG, which extracts LPS from the inside cavity of the inner membrane complex to the periplasmic domain of LptC.[88-89, 97-99] As already mentioned above the transmembrane domain of LptC is thought to coordinate ATPase activity with the extraction of LPS. Further, crystal structures of the $LptB_2FGC$ complex identified a gate in the β-jelly roll domain of LptF, which can prevent the backflow of LPS into the membrane once it was extracted.[88] Crosslinking experiments in vivo with a catalytic dead LptB, LptB(E163Q),[97-98] and crosslinking experiments in vitro with and without ATP showed that, while ATPase hydrolysis is needed to extract LPS from the inner membrane, LPS is able to enter the cavity of the inner membrane complex without ATP hydrolysis.[89] A number of strong interaction sites between the inner cavity of $LptB_2FGC$ and LPS have been identified.[100] For example the Lysine residue in LptG, K34, possesses a strong electrostatic interaction with the phosphate groups of LPS. Mutation of this residue to LptG(K34D), results in transport defects and cell death. LptG(K34D) is suppressed by the activation of the BasSR two component system,[101] which modifies the phosphates of the LPS to restore the interaction in the inner cavity between LptG and LPS.[100]

Summing up all the observations about the inner membrane complex, it is believed that $LptB_2FGC$ extracts LPS out of the inner membrane in an ATP dependent fashion and gives it to the periplasmic protein LptA.

1.4.4. The outer membrane complex LptDE inserts LPS into the outer leaflet

At the outer membrane LptD and LptE build a stable 1:1 complex.[72-74, 102] LptD is a large β-barrel outer membrane protein containing a C-terminal β-barrel and an N-terminal periplasmic domain.[103-104] LptD is transported to the outer membrane by SurA and gets folded by the Bam complex.[105-106] It contains two sulfide bonds, which connect the C–terminal β-barrel with the N-

terminal periplasmic domain.[107] LptE is a lipoprotein, which gets transported to the outer membrane via the Lol pathway.[108-109] Strong interactions between LptD and LptE have first been observed by overexpressing and co-purifying both proteins.[102] In vivo photo crosslinking between LptE and LptD showed a number of crosslinks between LptE and the inside of the C-terminal β-barrel domain of LptD. This suggested that LptE resided inside the barrel of LptD.[110] Crystal structures supported this suggestion, showing that LptE and LptD form a plug-and-barrel conformation, in which LptE resides in a cone like structure within the barrel of LptD.[103-104, 111] On the other side of the LptD barrel the N-terminal periplasmic domain of LptD extends from the β-barrel and forms a β-jelly-roll structure.

The solved crystal structures of the outer membrane complex allowed to hypothesize a potential model on how the outer membrane complex integrates LPS into the outer membrane. Weak hydrogen bonds and distorting prolines on the first and last β-strands, β-1 and β-26, suggest a lateral gate through which the lipid A portion of LPS could pass through the outer membrane to the outer leaflet. The O-antigen and core-sugars could pass through the inside of the barrel of LptD. This hypothesis was supported by in vivo photo-crosslinks between LPS and LptD at the periplasmic domain, at the connection between the periplasmic domain and the β-barrel and at the proposed lateral gate.[112]

It is unknown what the exact role of LptE is. In some organisms LptE is not directly involved in LPS transport but acts more as a chaperon for LptD assembly.[113-114] LptE's involvement in proper LptD assembly is supported by the observation that LptD cannot be overexpressed without LptE,[102] and that the presence of LptE is necessary for the folding of LptD by the Bam complex.[107, 115] Further, it has been shown that LptE is required for the proper rearrangement of the disulfide bonds in LptD, whose proper alignment have been shown to be

necessary for LPS transport. It also was proposed that the rearrangement of the disulfide bonds might play a regulatory role for building the LPS transport machine, which ensures that the outer membrane complex is completely assembled before LPS transport begins.[116]

1.4.5. Hypothesized LPS transport models

As mentioned above one of the most intriguing questions about LPS is, how the large amphipathic LPS molecule is able to pass through the aqueous periplasm from its synthesis site to the outer leaflet of the outer membrane. The large hydrophobic lipid portion of Lipid A needs to be shielded from the aqueous periplasm. Since the discovery of the seven LPS transport proteins, people have been working on figuring out how these seven Lpt-proteins work together to transport LPS from the inner membrane to the outer membrane. Two main models have been postulated on how LPS transport could occur: The chaperon model, in which LptA serves as soluble periplasmic chaperon that shuttles LPS to the outer membrane. And the bridge model, in which all seven Lpt-proteins come together to form a continued bridge spanning from the inner membrane to the outer membrane along which LPS can move.[69, 86, 117] (Figure 3)

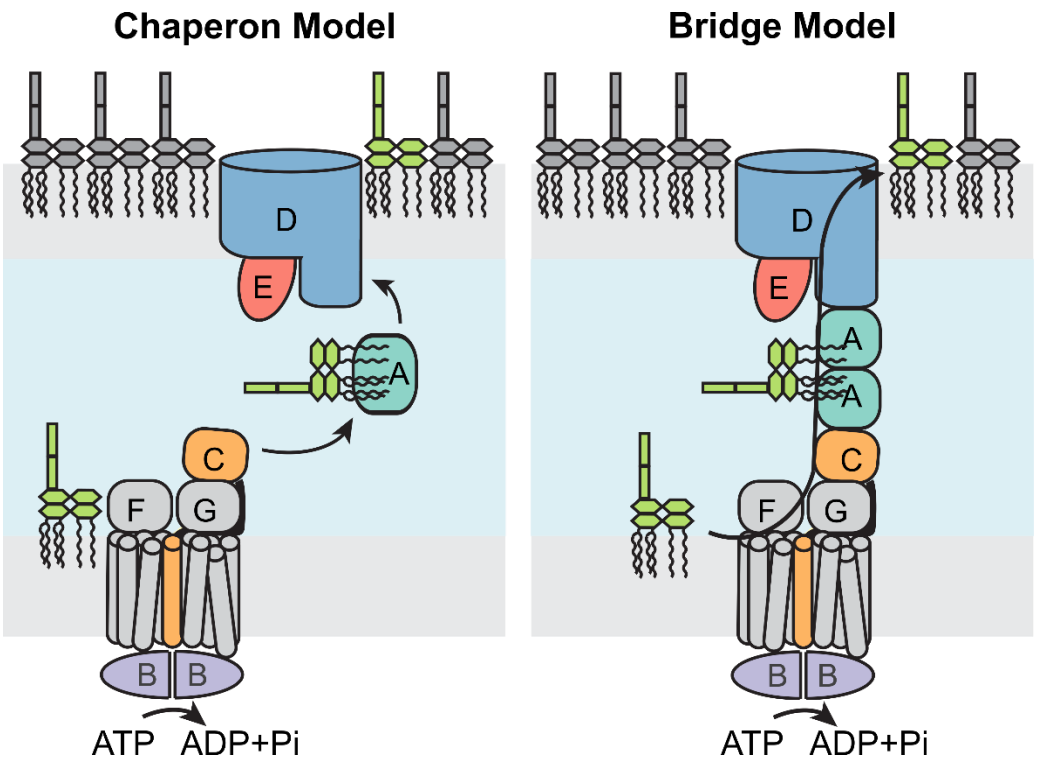

Figure 3: A chaperon and a bridge model are proposed for LPS transport. Scheme depicting proposed LPS transport models. The left hand side shows the chaperon model: LptA serves as soluble chaperon, which transports LPS from the inner membrane to the outer membrane by diffusing through the periplasm. The right hand side shows the bridge model: All Lpt-proteins come together to form a trans-envelope bridge connecting the inner membrane with the outer membrane along which LPS can move from its synthesis site to the cell surface.

The chaperon model is thought to function analogous to the transport of lipoproteins to the outer membrane by the Lol pathway, similar to the Lpt-proteins, also the Lol pathway consists of an inner membrane ABC transporter a soluble periplasmic component and an outer membrane complex.[108-109, 118-119] In the chaperon model LptA is thought to function analogous to LolA as soluble periplasmic chaperon, which transports LPS from the inner membrane to the outer membrane.[120] LptA would come to the inner membrane to collect LPS from the inner membrane

complex. It would shield the fatty acyl chains of LPS from the periplasm and diffuse to the outer membrane complex LptDE, where LPS would be released to the outer membrane.

In contrast to the chaperon model, the bridge model proposes that LptA forms stable interactions with the outer membrane complex and the inner membrane complex at the same time. The resulting trans-envelope bridge would connect the inner membrane and the outer membrane so that LPS would be able to cross the periplasm by moving along the bridge.[87] The bridge model has the advantage that the energy source, the ATPase activity of the ABC transporter is directly connected to all Lpt proteins and to every step of the LPS transport process. This might be able to explain how LPS can be transported against a concentration gradient even though no ATP is present in the periplasm.

1.4.6. Previous approaches and results to elucidate the LPS transport model

Since the postulation of the two LPS transport models a number of studies have tried to shed light onto the mechanism of LPS transport. A first hint for LPS transport at the site of inner and outer membrane adhesion points provided a pulse chase labeling electron microscopy experiment, which showed that newly transported LPS showed up at the sites of membrane adhesions.[121] Membrane adhesion sites were first observed by electron microscopy in 1968 and were called Bayer bridges.[122] However the existence of these so called Bayer bridges and their involvement in LPS transport has been questioned, when improved electron microscopy methods identified that adhesion sites can be an artifact of the method in which the cells were plasmolyzed and fixated.[123-124]

A more convincing observation, which questioned the chaperon model was that LPS is not released from the inner membrane of spheroplasts upon the addition of a concentrated periplasmic portion.[125] While LPS remains in the inner membrane, lipoproteins are released from the inner membrane, identifying LolA as soluble chaperon.[108, 119] In contrast to that, a pulse chase experiment showed that LPS can be transported even after removal of the soluble periplasmic portion.[125]

The first biochemical observation suggesting a strong interaction between all Lpt-proteins was, that outer membrane proteins LptDE and the periplasmic proteins LptA co-purify with the inner membrane complex $LptB_2FGC$.[6] Further, fractionation of cells on a sucrose gradient identified a fraction, slightly lighter than the outer membrane fraction, called OM_L, which contained all Lpt proteins from the inner membrane, the periplasm and the outer membrane.[6] Pulse chase experiments previously demonstrated that newly transported LPS transiently accumulates in the OM_L fraction, suggesting that Lpt-proteins in this fraction might be involved in active LPS transport.[126]

Structural work and sequence analysis revealed that LptA, the periplasmic C-terminal domain of LptC, LptF and LptG, and the periplasmic N-terminal domain of LptD are structural homologous to each other.[69, 85, 103, 127-128] The homologous periplasmic domains are composed of about 15 antiparallel β-sheets, which build a slightly-twisted β –jellyroll. This observation suggests a model in which the β–jellyrolls could interact with each other and form a continuous hydrophobic groove, which binds lipid A and shields the lipid tail from the periplasm. This model was supported by in vivo photo crosslinking experiments, which showed that the N-terminal edge of LptA's β –jellyroll crosslinks with the C-terminal edge of LptC, and that the C-terminal edge of LptA crosslinks to the edge of LptD's β –jellyroll.[85]

The first attempt to visualize a Lpt-bridge, was the in vitro reconstitution of LPS transport machinery in proteoliposomes.[7, 129] Purified inner membrane Lpt-complexes and outer membrane Lpt-complexes were integrated into separate liposomes labeled with two distinct fluorescent dyes. Fluorescent-activated Cell Sorting (FACS) and confocal microscopy showed that the presence of the soluble periplasmic LptA induces a stable long lived association between the inner membrane and outer membrane proteoliposomes. Crosslinking of LPS to LptD showed that LPS is transported from one liposome to the other liposome.[7] A more quantitative observation of LPS transport along the reconstituted Lpt-bridges in proteoliposomes was achieved by monitoring the amount of LPS transported from the inner membrane proteoliposome to the outer membrane proteoliposme using a Dansyl-PMB probe, which changes florescent intensity upon binding to transported LPS.[129]

1.4.7. Perspective: Unanswered questions about LPS transport that will be addressed in this thesis

All of the portrayed studies above support the bridge model for LPS transport. However, none of the above studies is able to give a definite proof for the existence of an Lpt-bridge in cells or gives information about how the hypothesized bridges are forming and breaking.

The spheroplast experiment was able to point out that LPS transport does not follow the classic chaperon model as observed for the Lol pathway. However, it does not provide evidence that LPS transport instead occurs over Lpt-bridges. The fractionation and pulldown experiments suggest a strong interaction between the Lpt-proteins, which is supported by the structural homology of the periplasmic domains and the observed crosslinks between the β–jellyroll interfaces. However, even though the crosslinks support the proposed architecture of a potential

bridge, the same interface crosslinks might also be observed, if LptA does not simultaneously interact with the inner membrane and outer membrane complex at the same time, but rather acts as a shuttle. The in vitro reconstitution of LPS transport in proteoliposomes was the first direct proof that Lpt-proteins are able to form bridges outside of the cell and transport LPS. However, even though the reconstitution is a great tool to study mechanistic details of the LPS transport machinery, it unfortunately still does not give us direct information about the behavior and existence of Lpt-protein bridges in cells. Up to this point the bridge model has not been validated in living cells. We do not know if these proposed bridges really exist in cells and how they would form and break.

Therefore, I set out during my PhD to answer the following questions:

- Is there evidences for Lpt-bridges in living cells?
- How stable are these bridges?
- What influences bridge formation and bridge breakage?
- How do bridges form and break?

Chapter 2 will describe the development of a single molecule tracking experiment with TRIF-M, which allowed to determine the dynamic profiles of LptA, B, C, D and E in cells. The identified dynamic profiles of the Lpt proteins support a bridge model and are therefore the first direct evidence for a LPS transport bridge in live cells. It will be described that all imaged Lpt-proteins have an immobile state, which was able to be identified as the bridge state.

In chapter 3, the development of an experimental set up will be explained to measure the lifetime of Lpt-bridges in cells using single molecule tracking. It was found that Lpt-bridges are

transient in cells with an average lifetime <10s and that bridge decay kinetics show a biexponential behavior.

In chapter 4 evidence will be presented that LPS facilitates Lpt-bridge formation, a mechanism by which LPS levels are coordinated with LPS transport. It further will be shown that bridge decay kinetics suggest that two different kind of bridge states may exist. In one state structural LPS is present stabilizing the bridge and therefore leading to longer lifetimes. In the other state likely no structural LPS is present resulting in faster breakage.

In the discussion of chapter 4 a model for LPS transport in cells will be postulated based on the data of this thesis.

2. Chapter 2: Single molecule tracking of Lpt-proteins provides evidence for LPS transport bridges in live cells.

2.1. Introduction

As discussed in chapter one LPS comprises the outer leaflet of the outer membrane in gram negative bacteria. (1.1.) The tight packing of the fatty acyl chains of LPS and the strong hydrogen bonds and lateral electrostatic interactions between the oligosaccharides of LPS are responsible for the distinct permeability barrier of the outer membrane and its unique stiffness and strength. (1.2.) The large amphipathic LPS molecule is completely synthesized at the inner membrane and then needs to be transported from the inner membrane through the periplasm to the outer leaflet of the outer membrane. Chapter one explained the discovery of the seven essential Lpt-proteins, found in the cytoplasm, inner membrane, periplasm and the outer membrane, which are

responsible for the transport of LPS from its synthesis site to its location of function. (1.4.2.) These lipopolysaccharide transport proteins, LptA-E are proposed to form a continuous trans-envelope protein bridge, along which LPS could move (1.4.6.) (Figure 4).

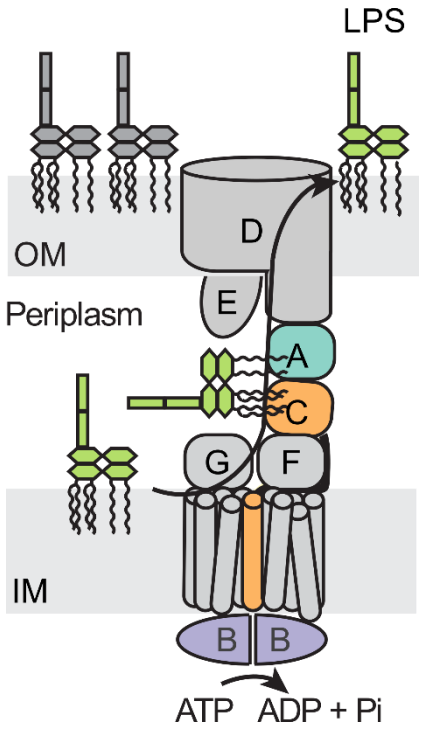

Figure 4: If Lpt-proteins form a trans envelope bridge, then all Lpt-proteins will have an immobile state. Scheme depicting proposed Lpt-bridge along which LPS is transported. Since outer membrane proteins are usually immobile, we predict that also the movement of LptA, B and C will be restricted, if Lpt-bridges are formed in cells.

While a number of studies support the proposed bridge model for LPS transport, up to now it has not been possible to observe Lpt-bridges in cells. In this chapter, we will look at the dynamic profiles of the Lpt-proteins using single molecule tracking. We will show that the Lpt-protein dynamics support the model of LPS transport bridges in cells. Our initial hypothesis was that, if the Lpt-proteins form indeed a bridge, then all Lpt-proteins should have a dynamic state in which they all move in tandem. It is known that the mobility of proteins in the inner membrane and outer

membrane is usually quite different. Outer membrane proteins show greatly restricted diffusion within the membrane bilayer due to the strong intermolecular interactions of LPS and the formation of outer membrane protein islands.[19, 121, 130-131] (This is discussed in more details below.) In contrast, inner membrane proteins are usually able to diffuse freely within the inner membrane throughout the cell.[132-133] Our hypothesis was, if the outer membrane Lpt-proteins, LptD, E form indeed bridges with LptB, F, G, C, and A, it could affect their mobility by restricting their diffusive behavior.

2.1.1. Outer membrane mobility

Already shortly after the discovery that gram negative bacteria have an additional outer membrane, studies suggested that the outer membrane is largely immobile. Mühlradt *et al.* showed, using pulse chase labeling of freshly synthesized LPS with ferritin, that newly incorporated LPS in the outer membrane does not move more than 300 nm. LPS molecules first appear in clusters, which over time distribute further than the 300 nm limit. However, since the outer membrane area doubles in that time scale, Mühlradt *et al.* concluded that the motion of these clusters is dominated by patterns of outer membrane incorporation rather than diffusion.[121, 130]

Analogous to the immobility of LPS, also the outer membrane proteins were found to be immobile.[131, 134-137] In 1978 electron microscopy of ferritin labeled porins in *Salmonella typhimurium* identified that newly inserted porins appear in patches, which increase in number over time but not in size. Therefore, it was concluded that outer membrane proteins are immobile within their patches.[135] This early observation was supported by more recent studies, in which the insertion of outer membrane proteins LamB or BtuB was observed with pulse chase single

molecule tracking. These studies identified that outer membrane proteins are inserted into the outer membrane in discrete insertion events.[131, 136] Outer membrane proteins form cluster islands of ~500 μm in size, which contain the Bam complex responsible for folding the outer membrane proteins.[137] The insertion of the outer membrane proteins is highest at the mid cell region and does not appear to happen at cell poles. The mobility of the outer membrane proteins is then restricted by the tight interaction with the other outer membrane proteins and by the restricted area of the island.[138] The only movement of outer membrane proteins observed occurs over longer time scales, when newly inserted outer membrane proteins at the mid-cell push older outer membrane protein islands towards the poles.

2.1.2. Inter membrane crosstalk

While as discussed above outer membrane proteins are largely immobile, inner membrane proteins are usually able to diffuse around relatively freely throughout the cell.[132-133] However, analogous to our hypothesis that the interaction of LptA, B, and C with immobile LptD and LptE could restrict their mobility, previous studies have indeed shown that trans-envelope protein interactions can dictate the motion and location of inner membrane proteins. For example single particle tracking suggested that the diffusion of inner membrane protein, TonB, is more confined during stronger interactions with the outer membrane protein ferric enterobactin transporter, FepA, an outer membrane β-barrel protein, important for nutrient uptake.[139] Bergman *et al.* observed that the inner membrane ABC transporter, AcrB, accumulates at old poles of cells dependent on the location of the outer membrane efflux channel TolC.[140] More recently, Rassam *et al.* showed that the inner membrane proteins of the Tol-Pal system, important for virulence in most gram negative bacteria,[141] mimic the dynamics of the outer membrane proteins, which are bound to ColE9, when

it establishes a translocon complex. They observed using single molecule tracking, FRAP and colocalization microscopy that the usually free diffusing inner membrane protein TolA becomes nearly immobile in the presence of ColE9. In this immobile state TolA localizes into islands mirroring the outer membrane proteins. Rassam *et al.* conclude that the change in mobility is due to the trans-envelope bridge induced by the bacteriocin, formed between the inner membrane Tol-Pal complex and the outer membrane proteins.[142] This study gave very clear evidence that inter membrane crosstalk via trans-envelope bridges can define inner membrane protein organization in *E. coli* and directly influence inner membrane protein dynamics.

2.1.3. Approach for single molecule tracking of Lpt-proteins

2.1.3.1. TIRF-M

In order to resolve the dynamics of single Lpt-proteins, Total internal reflection microscopy (TIRF-M) was used.[143-147] In TIRF-M the illumination laser beam hits the sample in an angle greater than the angle required for total internal reflection of the beam at the interface between the solid coverslip and the liquid media of the sample. The laser beam is completely reflected back into the microscope slide, producing an evanescent wave, which excites fluorophores closest to the interface. The evanescent wave starts at the solid-liquid interface and decays exponentially over approximately 100-200 nm. This way TIRF-M is able to specifically excite fluorophores closest to the glass surface, which reduces background fluorescence[148] and with this constitutes the perfect microcopy technique to image bacterial cell envelope proteins.[149-154]

2.1.3.2. Labeling strategy

With roughly a minimum of ~500 molecules/cell for each Lpt-protein, the copy number of Lpt-proteins is pretty high in *E. coli* cells.[155] Therefore, expressing fluorescent protein Lpt-protein fusions from the chromosomal side would not allow the detection of single molecules. Instead, it was decided to use self-labeling enzymes to tag Lpt-proteins. This allowed to label only a small subset of Lpt-proteins per cell using a low concentration of the labeling dye to resolve single Lpt-molecules.[149, 152] Halo-Tag was chosen as self-labeling enzyme, since it has been shown that Halo-Tag-fusion proteins can be expressed in the cytoplasm and periplasm of *E. coli* cells and that Halo-Tag-substrates are able to pass the *E. coli* cell envelope.[156] Halo-Tag-JF-549 dye[157] was used to label the Lpt-Halo-tag fusion proteins, since it is extremely stable and bright and has been successfully used in previous single molecule tracking experiments in bacteria.[149, 152]

2.1.3.3. Strategy for the construction of Halo-Tag-Lpt fusion strains

The main challenge for designing Lpt-Halo-Tag fusion proteins is that the Halo-Tag should not impact the functionality of the Lpt-protein. To ensure that their functionality is not affected, fusion proteins were constructed with a 15-amino acids or 30-amino acids linker between the protein and the Halo-Tag. In addition, the labeling site (N-terminus or C-terminus) was chosen based on previous experimental experiences with the respective Lpt-protein from in vitro studies. For LptB it has been known that labeling the N-terminus is less distracting than labeling the C-terminus. For LptC we decided to also label the N-terminus, since the tag then might reach into the cytoplasm and would not interfere with the connection site between LptC and LptA. For LptA both terminal sides are interaction sites. For in vitro studies LptA is usually labeled at the C–terminus. Therefore, also in this study it was decided to label LptA at the C-terminus and a long

linker of 30-amino acids was chosen to ensure that Halo-Tag does not prevent the interaction between LptA and LptD. For LptD the tag was added at the C-terminus, because LptD interacts at the N-terminus with LptA. Further, LptD is usually His-tagged at the C-terminus for in vitro or crosslinking studies with a long linker between the His-tag and LptD. Therefore, it was decided to tag the C-terminus of LptD using the long linker used in previous studies in addition to the 30-amino acid linker attached to the Halo-Tag. LptE was labeled at the N-terminus, since previous experience showed that labeling the C-terminus might give complications. The designed constructs are shown in figure 5.

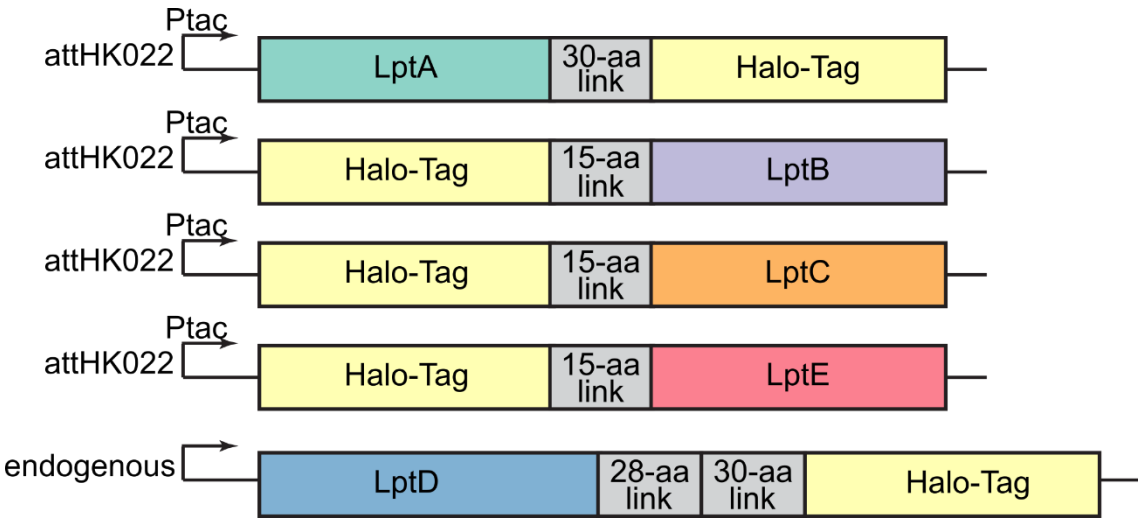

Figure 5: Halo-Tag fusions were expressed of Lpt proteins to label and detect single molecules. Scheme depicting the construct created for labeling Lpt-proteins with Halo-tag. LptA, B ,C and E Halo-Tag fusion proteins were expressed from a phage attachment site, while the endogenous copy of the respective Lpt-protein was knocked out. LptD Halo-Tag fusion protein was expressed from the native chromosomal site.

Besides ensuring that the structure and functionality of the Lpt-proteins is not compromised by fusing it with the Halo-Tag, another challenge is to ensure that the expression levels of the Lpt-

proteins remain the same with the tagged fusion. Therefore, Lpt-Halo-Tag fusion proteins were expressed from a phage attachment site under the control of an inducible Ptac promoter, while the wild type chromosomal copy of the respective Lpt-protein was knocked out. The expression from a phage attachment side rather than a plasmid allows to have homogenous expression levels of the Lpt-proteins in all cells. Further, no antibiotic is needed to retain a plasmid. The Ptac promoter allows to express the Lpt-Halo-Tag protein at wild type levels by adjusting the inducer concentration. Knocking out the endogenous copy of the respective Lpt-protein ensures that the protein dynamics are not disrupted by overexpression of the Lpt-protein. LptD was labeled by introducing the Halo-Tag at the native chromosomal side of LptD.

2.2. Results

2.2.1. Production of Lpt-Halo-Tag fusion proteins in *E. coli*

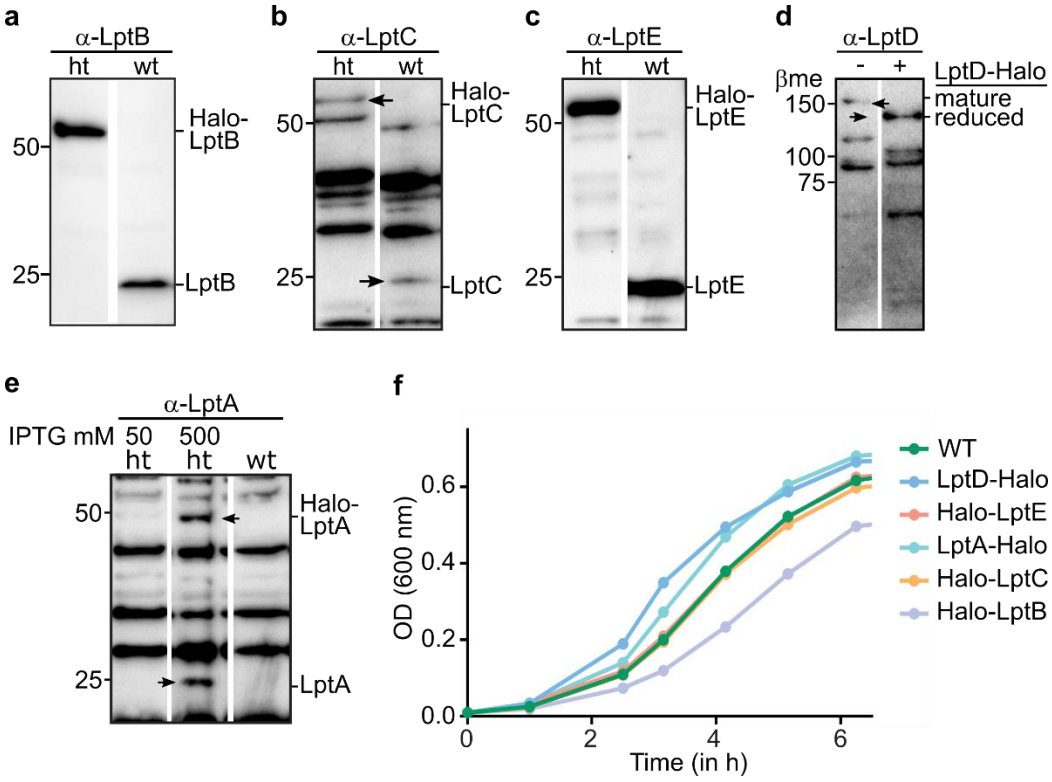

Figure 6: Lpt-Halo-tag fusions are expressed and support cell growth. a, α-LptB immuno blot of LT17 (left lane, ht), and TB28 (right lane, wt). The two lanes are from the same blot, but are not next to each other. **b**, α-LptC immuno blot of LT16 (left lane, ht) and TB28 (right lane, wt). The two lanes are in the same blot but were not next to each other. **c**, α-LptE immuno blot of LT19 (left lane, ht), and TB28 (right lane, wt). The two lanes are in the same blot but were not next to each other. **d**, α-LptD immuno blot of LT18 without (left lane, ht), and with βme treatment. **e**, α-LptA immuno blot of LT23 (left lane, ht), and TB28 (right lane, wt).The α-LptA antibody is not strong enough to detect wild type levels of LptA. The two lanes are in the same blot but were not next to each other. **f**, Growth curves of LT16 (Halo-LptC), LT17 (Halo-LptB), LT18 (LptD-Halo), LT23 (LptA-Halo), LT63 (Halo-LptE) and TB28 (WT).

The production of Halo-Lpt fusion proteins was confirmed by immuno blots. (Figure 6. a-e) The fusion of 35 kDa Halo-Tag introduced a shift of the corresponding Lpt-protein band to

higher molecular weight. Wild type LptB, 26.8 kDa, LptC, 21.7 kDa, and LptE, 21.4 kDa, usually run around 25 kDa. For the corresponding Lpt-Halo-Tag fusion protein it was possible to observe a band slightly above 50 kDa, confirming that the full length Halo-LptB, Halo-LptC or Halo-LptE fusion protein is expressed. (Figure 6. a-c) No bands at lower molecular weights were visible, which shows that the endogenous Lpt-protein was successfully knocked out and that the Halo-tag fusion did not get cleaved. The antibody of LptA is unfortunately too weak to show wild type levels of LptA on an immune blot. (Figure 6 e) Only at higher concentrations of IPTG to induce the Halo-LptA fusion protein a band corresponding to Halo-LptA was visible at around 50 kDa. Upon overexpression of the Halo-LptA fusion also a band at around 25 kDa showed up, which likely corresponds to LptA with cleaved off Halo-Tag. Also for LptD it was possible to observe a band for the LptD-Halo fusion protein at higher molecular weights than untagged LptD. (Figure 6 d) While wild type LptD usually runs ~120 kDa without reduction by βme and below 100 kDa with reduction, the bands corresponding to LptD-Halo run at ~150 kDa and ~140 kDa.

To ensure that the Halo-Lpt fusion proteins are still able to transport LPS and to support cell viability growth curves of the strains expressing Halo-Lpt fusion proteins were measured in comparison to the wild type strain. Figure 6 f shows that cells expressing the Lpt-Halo-tag fusion proteins as the sole source of the respective Lpt-protein were viable and displayed similar growth rates as wild type cells. Since no substantial cleavage of the Halo-Tag Lpt proteins were observed in immune blots, it can be concluded that Lpt-Halo-Tag fusion proteins are able to transport LPS to sustain cell viability and that their behavior in cells closely resembles wild type Lpt-protein behavior.

2.2.2. Single molecule tracking of Lpt-Halo-Tag fusion proteins

To observe the motion of single Lpt-proteins, we labeled the Lpt-Halo-Tag fusion proteins with low concentrations of Halo-Tag-ligand-JF549. Total internal reflection fluorescence microscopy (TIRF-M) was used to resolve single molecule tracks which describe the positions of the protein in Cartesian coordinates. As discussed in the introduction, TIRF-M allows to specifically resolve the dynamics of single molecules at the inner membrane and outer membrane. Soluble proteins in the periplasm or cytoplasm cannot be detected.

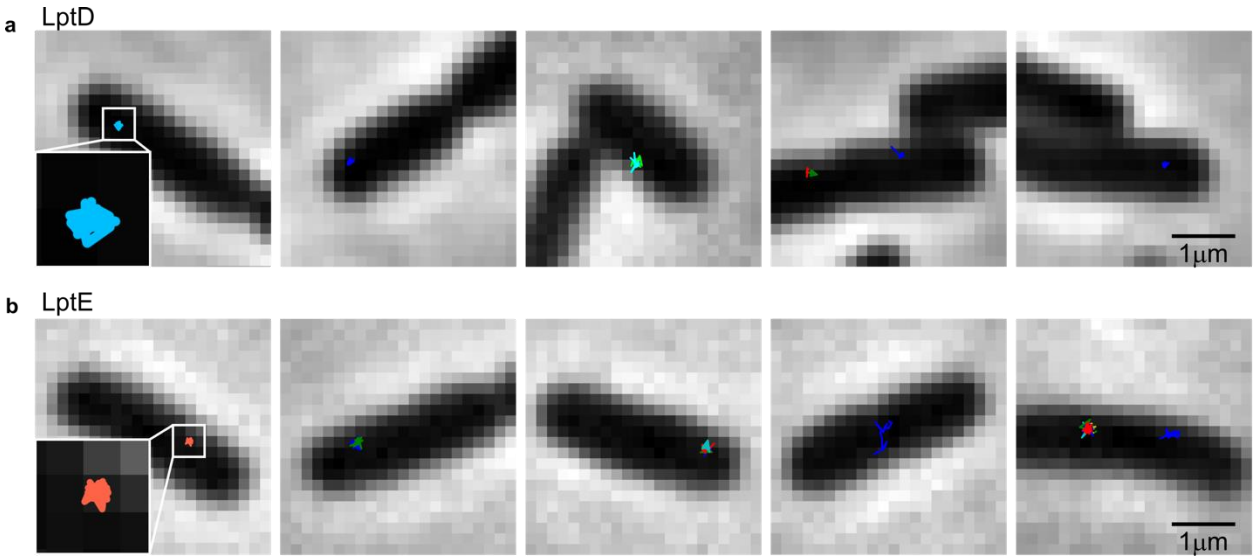

Figure 7: LptD and LptE trajectories show confined dynamics. Representative trajectories of LptD and E are shown. Trajectories were overlaid over the corresponding phase image. Each trajectory is represented in a different color. The color was chosen randomly.

In figure 7 representative trajectories of LptD and LptE are shown, which were collected using 100 ms exposure time. The trajectories are overlaid over the corresponding phase image, which display the outline of the cell. Most of the LptD and LptE trajectories presented a confined

behavior of the proteins, suggesting that LptD and LptE are mostly immobile. In contrast to that the observed trajectories for LptA, B and C showed a more complex dynamic profile for the corresponding protein. Figure 8 highlights representative trajectories of LptA, B and C overlaid over the corresponding phase image. For LptA, B and C trajectories were visible, which behaved like LptD and E and mainly stayed at the same location. However, also trajectories could be observed that span a larger area, suggesting that the corresponding proteins diffuse around more freely.

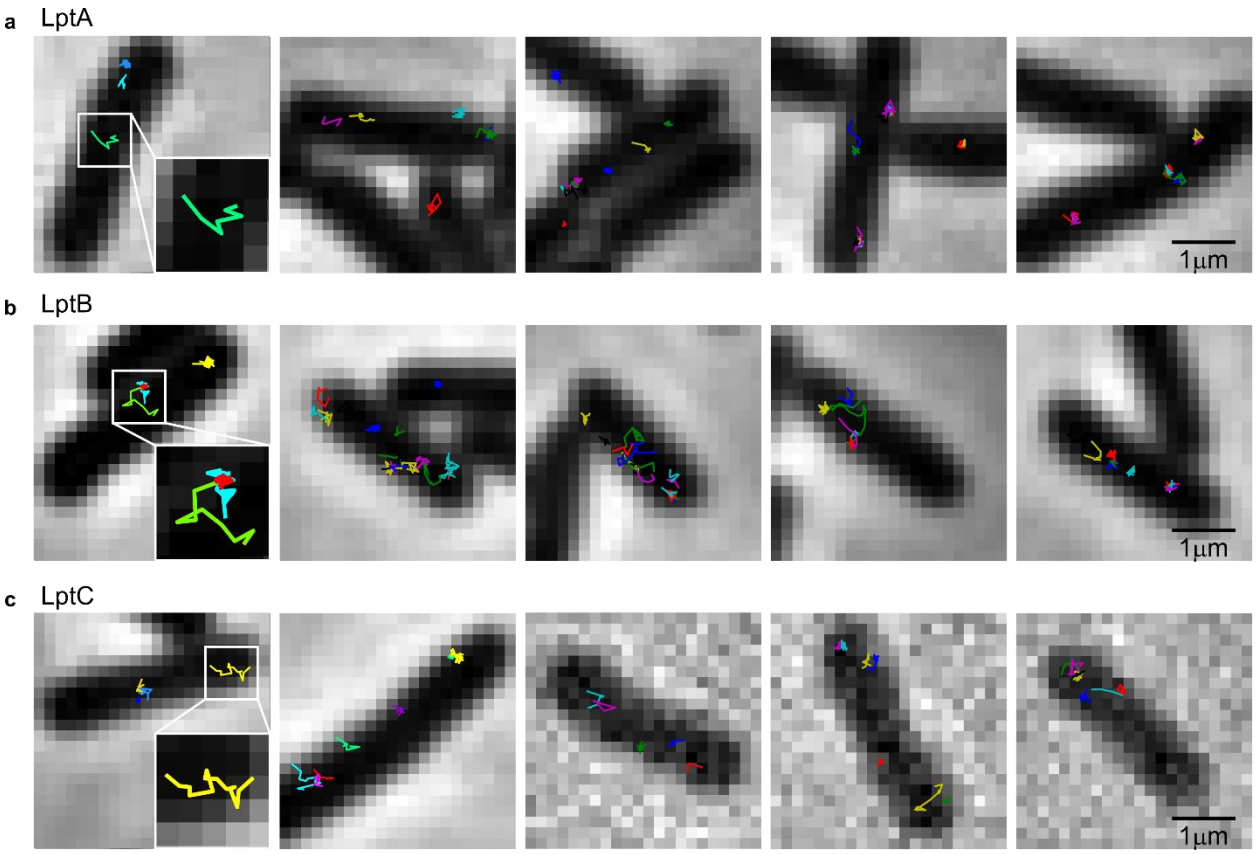

Figure 8: LptA, B and C trajectories show a complex dynamic profile. Representative trajectories of LptA, B and C are shown. Trajectories were overlaid over the corresponding phase image. Each trajectory is represented in a different color. The color was chosen randomly.

2.2.2.1. Mean squared displacement analysis reveals switching behavior of Lpt-proteins

To get a better quantitative picture of the Lpt-protein dynamics the mean squared displacement (MSD) was calculated for the measured trajectories and plotted against the time delay τ. (Figure 9) The MSD versus τ plots were very flat for LptD and LptE, indicating that their movement is extremely restricted. In contrast to that, the MSD plots for LptA, B and C were more diverse, some trajectories displayed very confined dynamics, while other trajectories showed unrestricted diffusive behavior. Interestingly, the MSD plots revealed that some of the LptA, B and C trajectories switched between the diffusive and restricted state. MSD analysis is best suited for trajectories, which display the same dynamic behavior over the monitored time scale. Therefore, it was decided to use confinement radius, and cumulative distribution function analysis to analyze the dynamic profiles of the Lpt-proteins going forward. These methods allow to also include switching trajectories in the analysis.

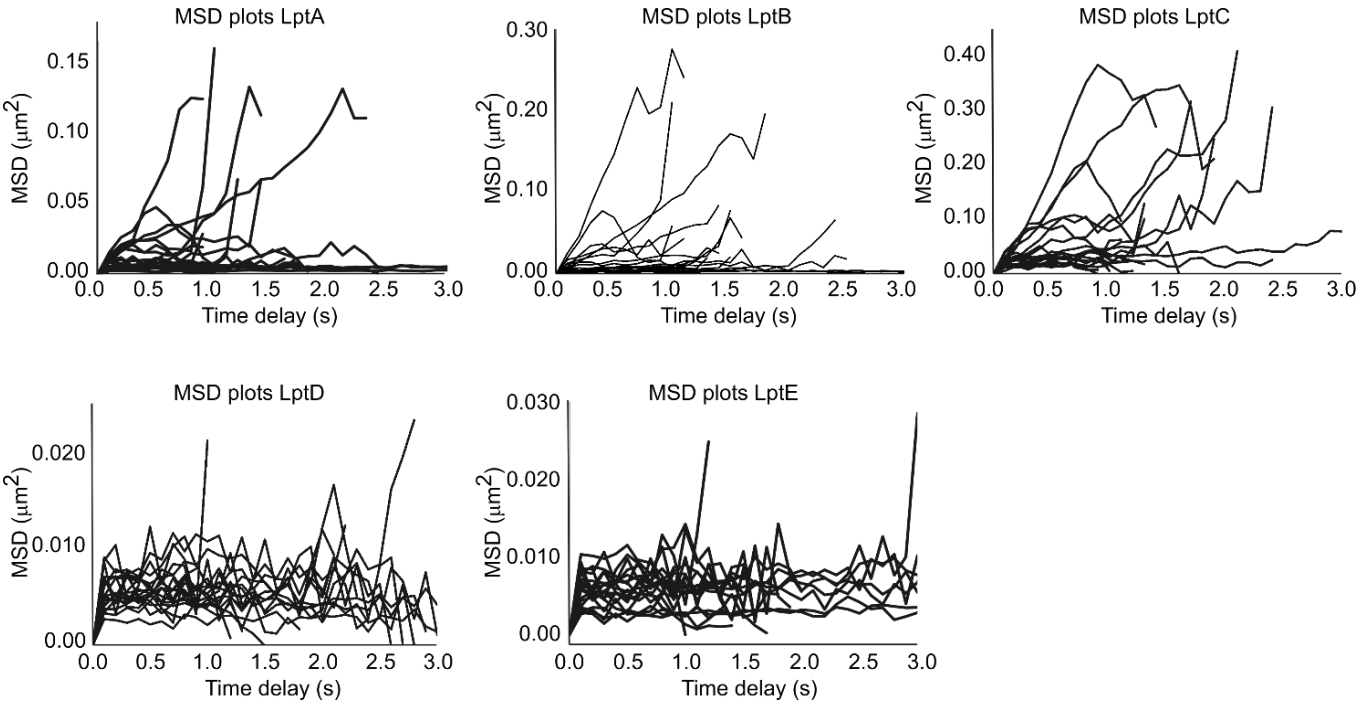

Figure 9: Mean square displacement versus τ curves show inhomogeneous dynamics for LptA, B, and C. 20 random sampled msd versus τ plots are shown for trajectories collected from LptA, B, C, E and D. MSD plots for LptA, B and C trajectories showed immobile, mobile and also switching trajectories. LptD and E showed mostly immobile trajectories.

2.2.2.2. Confinement radius analysis identifies that all Lpt-proteins have an immobile state

To characterize the type of motions each of these labeled proteins displayed, the area was monitored that the proteins sample in a given amount of time, *i.e.*, the confinement radius. For that we calculated the average x, y position (the centroid, blue point), from the x, y position (black dots) of each time point within a track (Figure 10 a). The average of the distances between the blue point and the black points is defined as the confinement radius. For each labeled protein, we binned the confinement radii and plotted the frequency of the binned radii to understand their dynamics. (Figure 10 b)

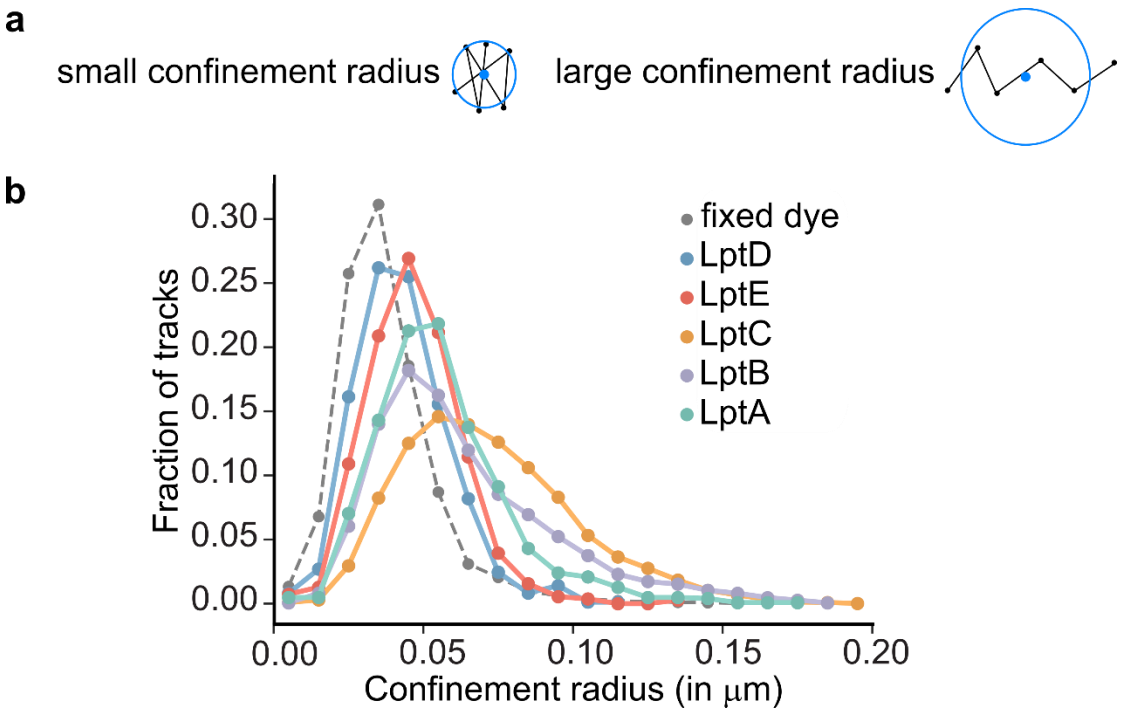

Figure 10: Confinement radius analysis reveals an immobile state for all Lpt-proteins. **a,** Scheme depicting the confinement radius measurement. (blue dot = centroid of the track, black dots = Cartesian coordinates of the track) **b,** Confinement radius histograms for the different imaged Lpt-protein tracks in comparison to the confinement radius measured for the trapped dye tracks (fixed). **c,** The confinement radius was measured for tracks consisting of five frames. Trajectories with less than 5 frames were excluded and trajectories with more frames were cut to the length of 5 frames. Results are representative of at least two independent experiments.

To determine the localization precision of our experimental set up, we collected tracks of a dye trapped within an agar pad. The confinement radius distribution of the trapped dye served as example on how a completely immobile spot would look like under the microscope. For all imaged Lpt-proteins the confinement radius histogram overlapped to a large extent with the fixed dye distribution, indicating that all five Lpt-proteins have an immobile state. Confinement radii plots of Lpt proteins D and E looked very similar to each other and closely resembled the trapped dye

distribution. The small shift to larger confinement radii for LptD and E compared to trapped dye is presumed to reflect experimental errors related to the difference between the random motion of the dye and the bacterium within the agar pad. These outer membrane proteins were clearly less mobile than any of the inner membrane proteins, as judged by the maxima and distribution of the histogram. Our results for LptD and E are consistent with previous studies that have shown that proteins in the outer membrane have highly restricted dynamics as discussed in the introduction (2.1.1.).

The histograms of LptB and LptC displayed a shift in their maxima to larger confinement radii and had longer distribution tails than LptD and LptE, indicating that they have greater mobility. The histogram of the confinement radii of LptA was also shifted to the right compared to LptD and E, but the frequency of trajectories dropped sharply as the confinement radius increases. Therefore, LptA is more mobile than LptD and E but less mobile than LptB and LptC. For all imaged Lpt-proteins the confinement radius histogram overlapped to a large extent with the trapped dye distribution, indicating that all five Lpt-proteins have an immobile state.

2.2.2.3. CDF analysis confirms the immobile state of LptA, B and C and predicts two dynamic states

To better understand the dynamic profiles for LptA, B, and C we carried out a cumulative distribution function (CDF) analysis for the respective protein's tracking data. Fitting the cumulative distribution of squared displacements allows to determine for multi component diffusion systems the number of dynamic states, the diffusion constants for the different dynamic states and the fraction of tracks in the different states.[158-159] We first calculated for each trajectory the displacement r between the positions of the protein separated by the lag time Δt. The

cumulative probability $P(r^2, \Delta t)$ was constructed of the pool of displacements across multiple tracks for each protein by counting the number of squared displacements $\leq r^2$ normalized by the sample size. The resulting cumulative probability describes the probability to find the protein starting at the origin within a circle of radius r after the lag time Δt. Figure 11 shows the CDF plots for LptA, B, C and D.

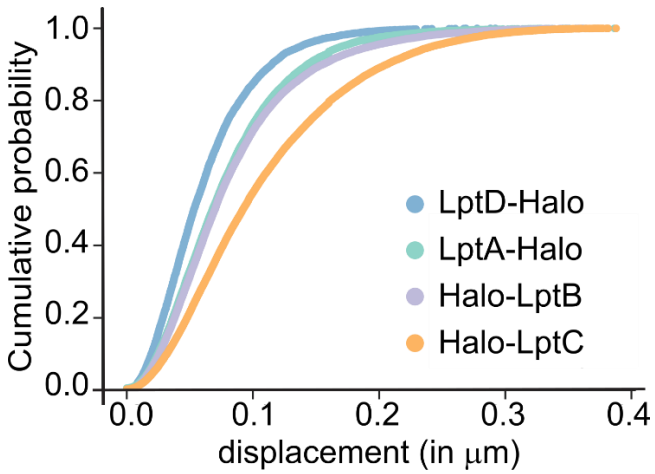

Figure 11: Cumulative distribution function of displacements shows larger mobility for LptA, B and C than LptD. Cumulative distribution function of displacements with Δt=200 ms for single molecule tracks of LptA, B, C and D is plotted. The CDF curve of LptA, B and C were clearly shifted towards lager displacement compared to LptD, indicating that they are more mobile.

As expected from the confinement radius plots, the CDF curve for the immobile LptD protein was shifted furthest to the left, small displacements, indicating no imaged LptD molecule moved further than 100 nm within Δt. In contrast to that, the CDF curves of LptA, B, and C were clearly shifted to larger displacements, again confirming their mobile behavior. While the CDF curves for LptA and LptB looked very similar to each other, the CDF curve for LptC was shifted to larger displacements, indicating that LptC is the most mobile.

To determine the number of different dynamic states for LptA, B, and C we fitted the respective CDF curves with a one component dynamic model (ES1, red line), and a two component dynamic model (ES2, black line). (Figure 12)

(ES1) $$P(r^2, \Delta t) = 1 - e^{-\frac{r^2}{4D\Delta t + 4\sigma^2}}$$

(ES2) $$P(r^2, \Delta t) = 1 - \left(\alpha * e^{-\frac{r^2}{4D_{slow}\Delta t + 4\sigma^2}} + (1 - \alpha) * e^{-\frac{r^2}{4D_{fast}\Delta t + 4\sigma^2}} \right)$$

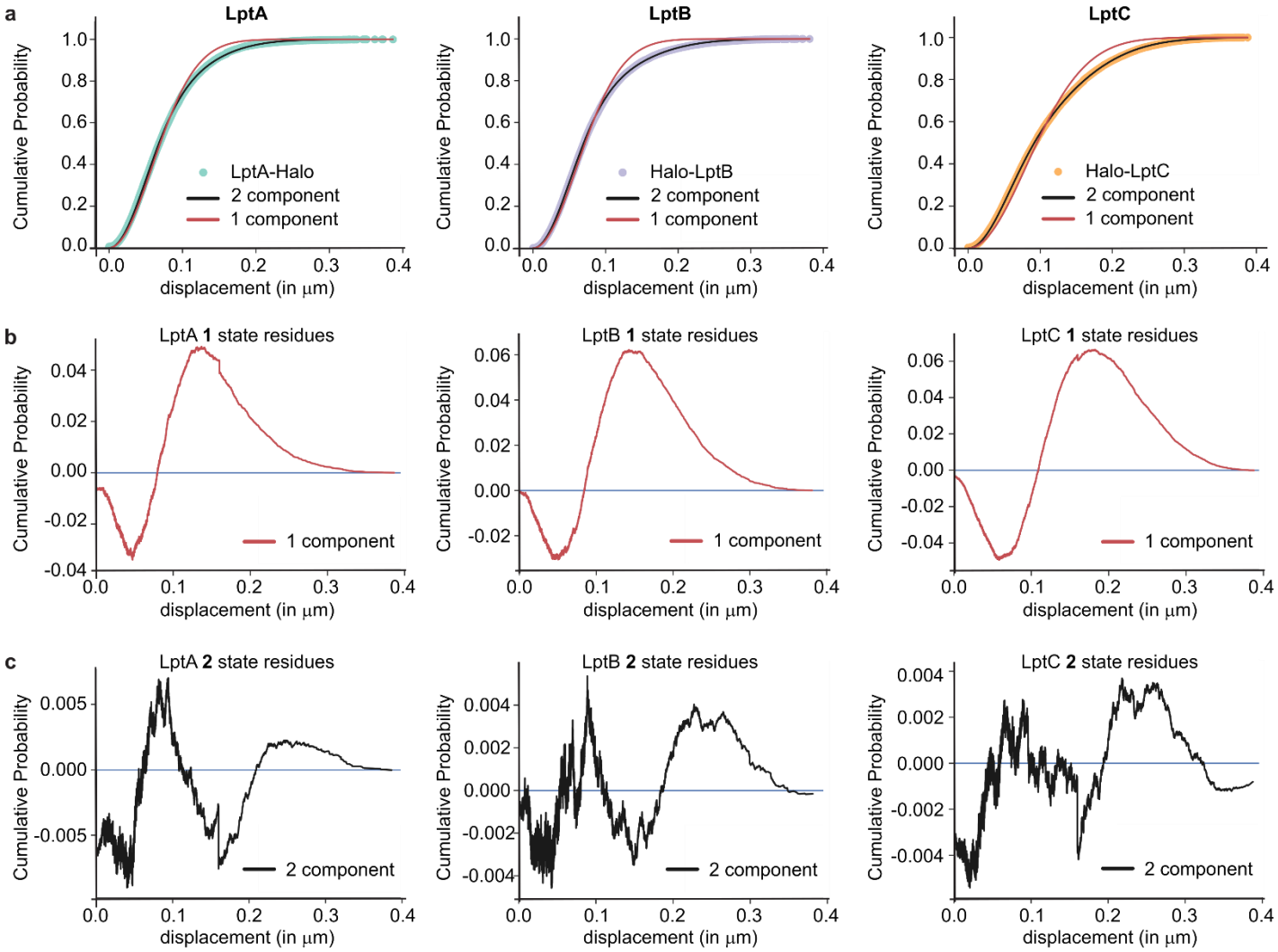

Figure 12: Cumulative distribution function analysis reveals a two component dynamic profile for LptA, B and C a, Cumulative distribution function of displacements with Δt=200 ms for single molecule tracks of LptA, B, C and D is plotted. One state (red line) and two state (black line) dynamic models were fitted to the CDF plots of LptA, B, and C. The corresponding residue plots are shown below. (**b,** residue plots for the one component dynamic model fit. **c,** residue for the two component dynamic model fit.) Equations ES1 and ES2 were used for the fit. For all three proteins the two component model resulted in the best fit without over fitting the curve.

For all three proteins the two component model fitted the data significantly better than the one component model as judged by the residual plots shown in figure 12 b and c. Therefore, it is

possible to conclude that LptA, B, and C exist in two different dynamic states, a slow diffusive and a fast diffusive state. The fit gives us diffusion constants for the two different dynamic states D_{slow} and D_{fast} as well as the fraction of proteins in the slow state, α. For LptA, B, and C, D_{slow} described movement smaller than the average confinement radius of the trapped dye, the precision limitation of our experimental set up, which means that the "slow diffusing state" is actually an immobile state. This is consistent with the observation we made with the mean squared displacement analysis and the confinement radius plots and confirms again that all Lpt-proteins have an immobile state.

a

	Diffusion constant D_{fast} in $\mu m^2/s$	Immobile fraction α
LptA	0.01 ± 0.004	0.59 ± 0.06
LptB	0.02 ± 0.004	0.64 ± 0.03
LptC	0.03 ± 0.004	0.44 ± 0.07

b

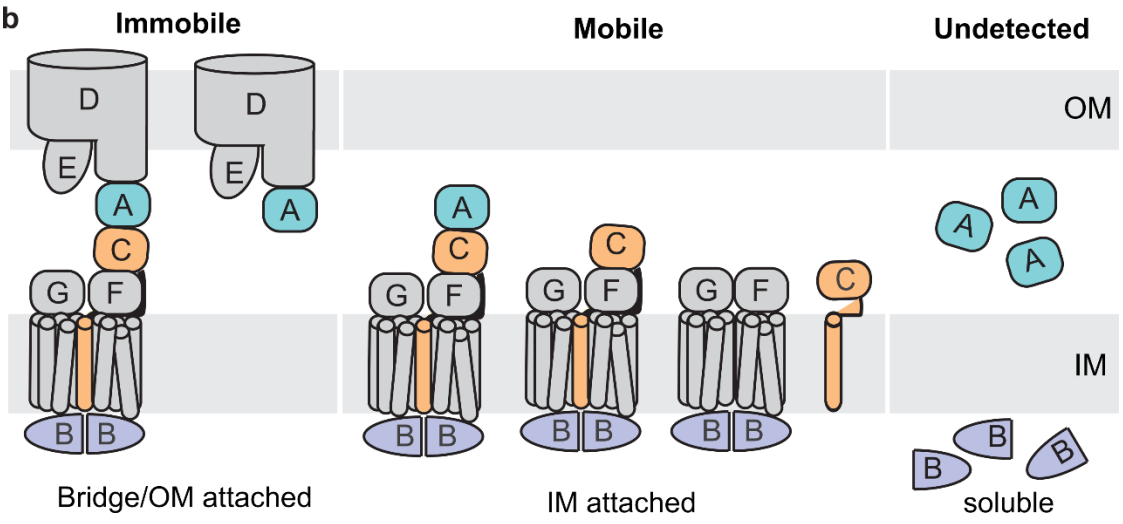

Figure 13: Immobile state of the Lpt-proteins is hypothesized to correspond to Lpt-proteins involved in bridge formation. a, The average Diffusion constant, D_{fast} and alpha values (immobile fraction) with standard deviations for LptA, B and C are reported. These values resulted from the two state dynamic model fit to the CDF plots. CDF plots, fits and residual plots are shown in figure 12. **b,** Scheme depicting the hypothesized model: Lpt-proteins involved in a trans envelope bridge or attached to the outer membrane are predicted to be immobile, while proteins at the inner membrane are mobile. LptA and LptB have a third undetectable soluble state.

We hypothesize that the immobile state of LptA, B, and C corresponds to proteins involved in bridge formation or to proteins, which are in other ways connected to the outer membrane. (Figure 13 b, left) The latter one is especially expected for LptA. LptA would be able to bind to LptDE by

itself independent from the other Lpt-proteins. Therefore we might expect that LptA has an additional immobile state, independent from the full bridge.

D_{fast} describes the mobile state of LptA, B, and C. (Figure 13 a) They are in the same order of magnitude and similar to previously reported diffusion constants of inner membrane proteins in *E. coli*.[160] We hypothesize that Lpt-proteins connected to the inner membrane without any connection to the stiff outer membrane are in the mobile state. (Figure 13, b, middle) Interestingly, the diffusion constant for LptA was the smallest of the three, while the one for LptC was the highest. Since we are expecting smaller diffusion constants for particles with a higher molecular weight, this could indicate that LptA mainly is connected to the inner membrane Lpt-proteins when the whole complex $LptB_2FGC$ is present.

As mentioned above, besides the two diffusion constants, the CDF analysis also allows to determine the fraction of tracks in the immobile state, the value, α. (Figure 13 a) The immobile fraction, α, was very similar for LptA and B. For both proteins about 60 percent of the monitored tracks were in the immobile state, while 40 percent were mobile. For the inner membrane protein LptC the fraction of tracks in the immobile state was lowest with only around 45 percent of LptC tracks being immobile. This observation could be explained by the fact that LptC is a transmembrane protein and we are able to observe all its immobile and mobile states with our experimental set up. In contrast to that, the periplasmic protein LptA, and the cytoplasmic protein LptB have another mobile, soluble state, which we cannot detect. (Figure 13 b) The higher immobile fraction for LptA and LptB suggest that both proteins are mainly involved in bridge formation once they are associated with membrane proteins.

2.2.3. Testing the requirements for immobile Lpt-proteins with the overexpression of LptC(G153R) mutant

We identified that LptA, B and C have two dynamic states, one mobile state, in which the proteins diffuse relatively freely, and one immobile state, in which their movement is restricted. As described above we hypothesized that the immobile state corresponds to proteins involved in a trans-envelope bridge or connected to the outer membrane. (Figure 13 b) We wanted to test, if the immobile states observed for LptA, B and C indeed reflect a bridge involving all seven proteins. To address this question, we decided to disrupted bridge formation to observe the effect on the mobility of the Lpt-proteins. For this we used the LptC mutant, LptC(G153R) (LptC*, Figure 14).

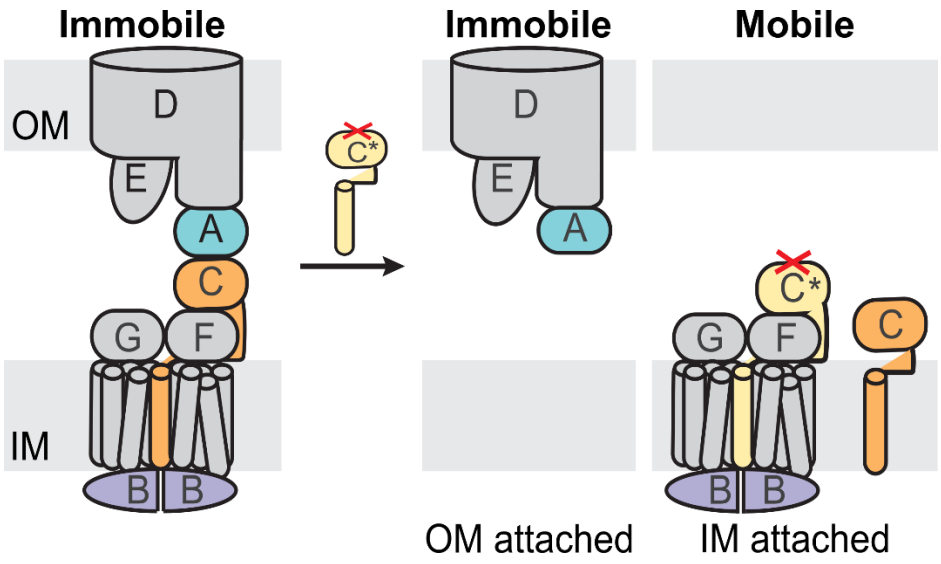

Figure 14: Overexpression of LptC(G153R) leads to the formation of broken bridges in cells. Scheme depicting the effect of LptC(G153R) (LptC*). LptC* is able to connect to the inner membrane complex $LptB_2FG$, but is not able to interact with LptA. This leads to the formation of broken bridges in the cell.

Sperandeo *et al.* showed that the mutant LptC(G153R) is able to form an inner membrane complex with $LptB_2FG$ but is unable to interact with LptA.[83] (Figure 14) Therefore, overexpression of the mutant LptC* leads to the formation of inner membrane complexes that cannot connect to the outer membrane complex LptDE through LptA. The concentration of broken Lpt-bridges in the cell will be high. If the immobile fraction of LptA, B and C indeed corresponds to proteins being involved in a bridge, then we would expect under this condition the immobile fractions that correspond to bridges to decrease.

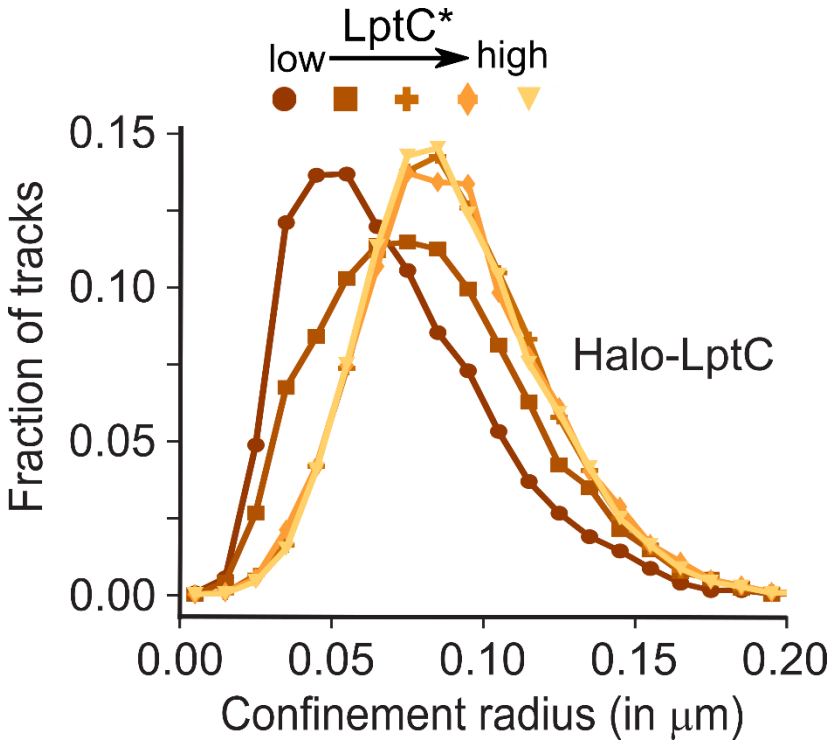

Figure 15: Overexpression of LptC(G153R) (LptC*) leads to the complete mobilization of Halo-LptC. Confinement radius plots of Halo-LptC tracks measured in the presence of different levels of LptC(G153R). The confinement radius distribution with circles as marker corresponds to no induction of LptC*, while the triangle corresponds to the highest level of induction of LptC* (0.04 μM). Each confinement radius distribution corresponds to tracks measure of wild type Halo-LptC.

We monitored the dynamics of Halo-LptC while we increased the production of LptC* to different levels by changing the inducer concentration. Confinement radius plots of Halo-LptC in cells with different levels of LptC* overexpression showed that small levels of LptC* lead to the complete mobilization of LptC. (Figure 15) All wild type LptC was replaced in the Lpt-complexes by LptC* and became mobile. This evidences that the confinement radius plot maxima for wild type LptC (circle marker, no inducer was added) consisted of two states and that the immobile state of LptC indeed depends on the connection of LptC to the outer membrane Lpt-proteins through LptA.

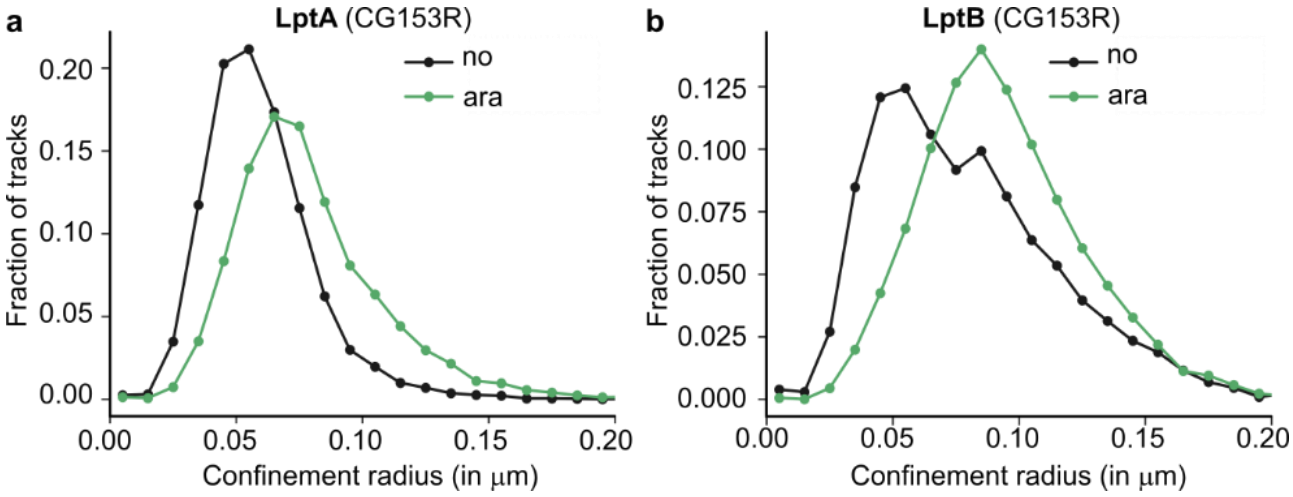

Figure 16: Overexpression of LptC(G153R) (LptC*) also increases mobility of LptA and LptB. Confinement radius plots of Halo-LptA (**a**) and Halo-LptB (**b**) tracks measured with (green) and without (black) induction of LptC* (LptC(G153R)) expression. The confinement radius distribution of LptA and LptB were shifted to larger radii upon overexpression of *lptC**.

Similar to Halo-LptC, also the confinement radius plots of LptA and LptB showed a shift to larger confinement radii upon overproduction of LptC*. (Figure 16) This indicates that also LptA and LptB became more mobile. To get a better quantitative understanding of the dynamic change, we analyzed the monitored tracks using the cumulative distribution function analysis and

compared the resulting α values, the fraction of tracks in the immobile state with an without induction of LptC* expression. Figure 17 displays the fitted fraction of tracks in the immobile state for LptA, B and C measured when LptC* production is not induced (low) and when LptC* is overexpressed (high).

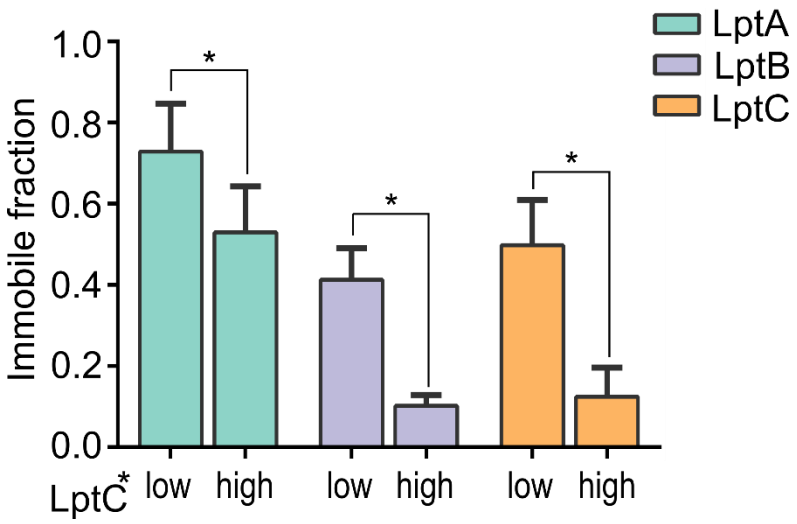

Figure 17: LptA has an additional immobile state, it associates with LptDE in broken bridges. Average alpha values with standard deviations (error bars), which indicated the immobile state, gained from the CDF analysis of single molecule LptA, B, and C tracks, imaged with (high) or without (low) inducing LptC(G153R) production are shown. *P*-values were obtained from a t-test, **P* <0.05, ***P*<0.005.

For both Halo-LptC and Halo-LptB the immobile fraction dropped below 10 percent when LptC* was overproduced. Therefore, we can conclude that the immobile state for LptC and LptB is dependent on their connection to the outer membrane proteins LptDE through LptA. In contrast to Halo-LptB and Halo-LptC, the immobile fraction of Halo-LptA behaved differently. The immobile fraction remained higher under low LptC*and dropped less at high LptC* (Figure 17, green) A simple interpretation for the higher amount of immobile Halo-LptA is that it can still associate with the outer membrane proteins LptDE even when bridges are broken (see Figure 13).

This interpretation is consistent with previous studies, which showed that LptA largely co-fractionates with the outer membrane fraction containing LptD and LptE when cells are fractionated on a sucrose gradient.[6] To ensure that the fused Halo-Tag does not influence the preferred binding side of LptA, we fractionated cells expressing the LptA Halo-Tag fusion protein and confirmed via immuno blot that Halo-LptA still fractionates analogous to wild type LptA to 90 percent with the outer membrane proteins LptD and E. (Figure 18)

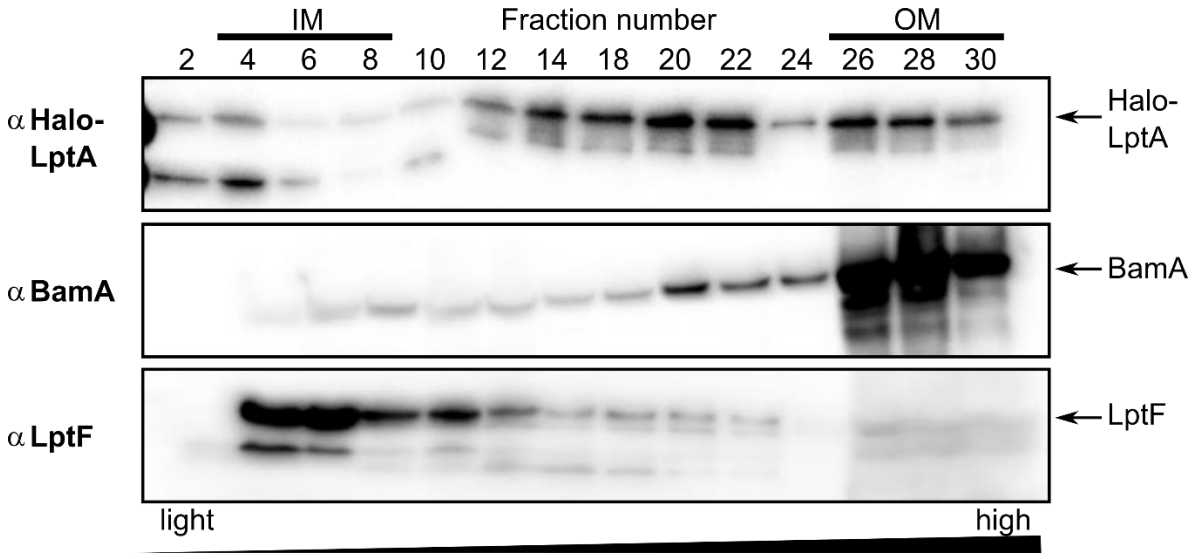

Figure 18: Halo-LptA fractionates analogous to wild type LptA with the outer membrane proteins LptD and E. Immuno blot analysis of sucrose gradient fractions of cells expressing Halo-LptA are shown. (upper blot) α-LptA blot, the arrow indicates the band corresponding to Halo-LptA. (middle blot) α-BamA blot was run as reference for an Lpt independent outer membrane protein. (lower blot) α -LptF, was run as control for an inner membrane protein.

The α-LptF blot serves as control for an inner membrane protein and α-BamA serves as control for an Lpt independent outer membrane protein. The top blot is the α-LptA blot and shows the fractionation results for Halo-LptA. Halo-LptA runs as discussed in (2.2.1) at around 50 kDa.

Nearly no Halo-LptA is detected in the inner membrane fraction. A large amount of Halo-LptA fractionated in the OM_L fractions (fractions 18-22), which as discussed in (1.4.6) was identified as fraction containing proteins most likely involved in a trans-envelope bridge. Almost all detectable Halo-LptA, which was not in the OM_L fraction, co-fractionated with the outer membrane proteins LptDE. This shows that Halo-LptA behaves analogous to wild type LptA and also preferentially binds to the outer membrane proteins LptD and E. This is consistent with our observation that Halo-LptA stays partially immobile even when bridges are broken by the overexpression of LptC*. (Figure 17) Nevertheless, our experiments also showed that the fraction of immobile LptA did decrease when bridges were broken due to production of LptC*, implying that some LptA must be bound at the inner membrane, too.

To ensure that the changes in the dynamic behavior of LptA, B and C are not artifacts of changed expression levels of the proteins upon overexpression of LptC*, LptC(G153R), we confirmed via immuno blot that the levels of LptB and LptA remained unchanged when LptC* is overexpressed. (Figure 19)

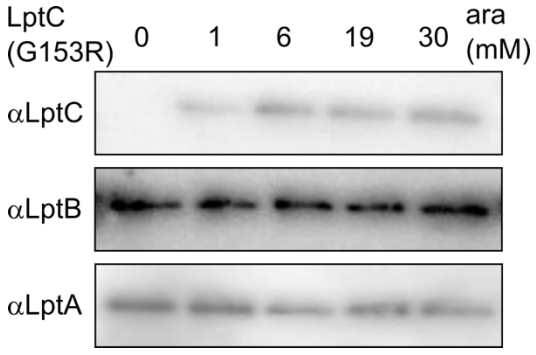

Figure 19: LptA and LptB expression levels remain constant upon overexpression of LptC(G153R). α-LptA and α-LptB immuno blot analysis for the LT16 strain containing pBAD33LptC(G153R) treated with different arabinose concentrations to induce LptC(G153R) expression.

2.2.4. Testing the requirements and source of mobile Lpt-proteins with the overexpression of wild type LptC

We observed that the immobile fraction of LptB and LptC depends on their connection to the outer membrane proteins LptD and E through the periplasmic protein LptA. While LptB and LptC became highly mobile when bridges are broken upon overexpression of LptC(G153R), LptA remained partially immobile bound to LptDE. However, nevertheless also for LptA we observed a drop in the immobile fraction, suggesting that some LptA is mobile. Based on our hypothesis shown in figure 14, we proposed that Lpt-proteins which are mobile are proteins which are connected to the inner membrane, but do not have any connection to the outer membrane. The observation of mobile LptA is inconsistent with the model that LptA is bound to LptD when it is not in a bridge. Therefore, we wanted to characterize the nature of this mobile LptA, which probably is bound to inner membrane proteins. We wondered how the dynamic behavior might be influenced, if we increase potential binding partners at the inner membrane. Therefore we decided to overexpress wild type LptC, while we monitored the dynamics of Halo-LptA, B and C. (Figure 20)

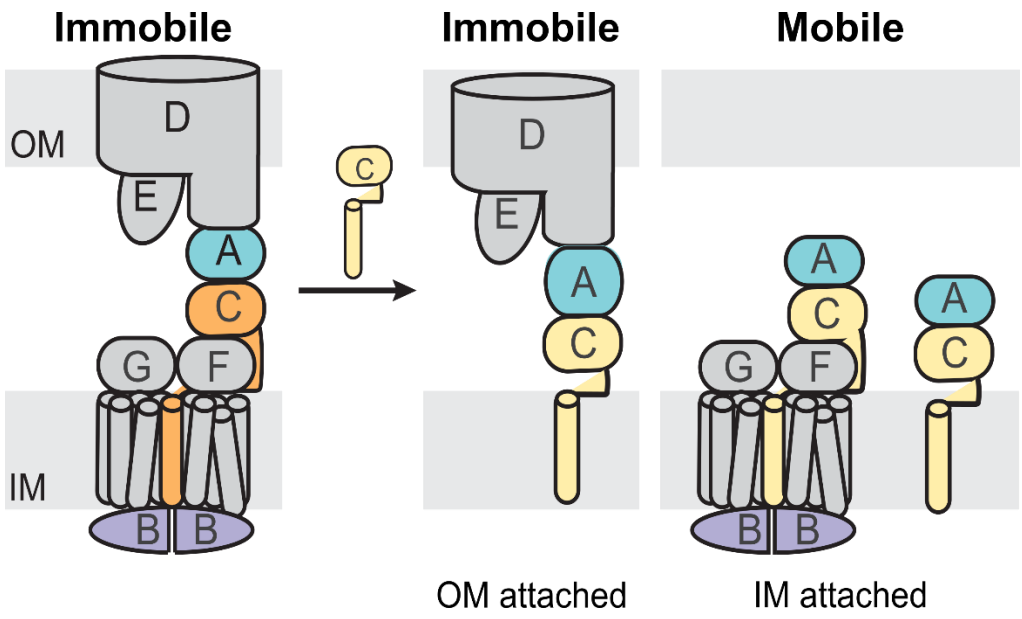

Figure 20: Overproduction of wild type LptC leads to the formation of more inner membrane complexes. Scheme depicting the overexpression of wild type LptC. Untagged wild type LptC is depicted in yellow. Halo-LptC is depicted in orange.

Figure 21 shows confinement radius distributions for Halo-LptA, B and C without induction of wild type LptC (black) and with overproduction of wild type LptC (green). For all three proteins the confinement radius distribution broadened and shifted to the right, to larger confinement radii, suggesting that LptA, B and C became more mobile upon overproduction of wild type LptC.

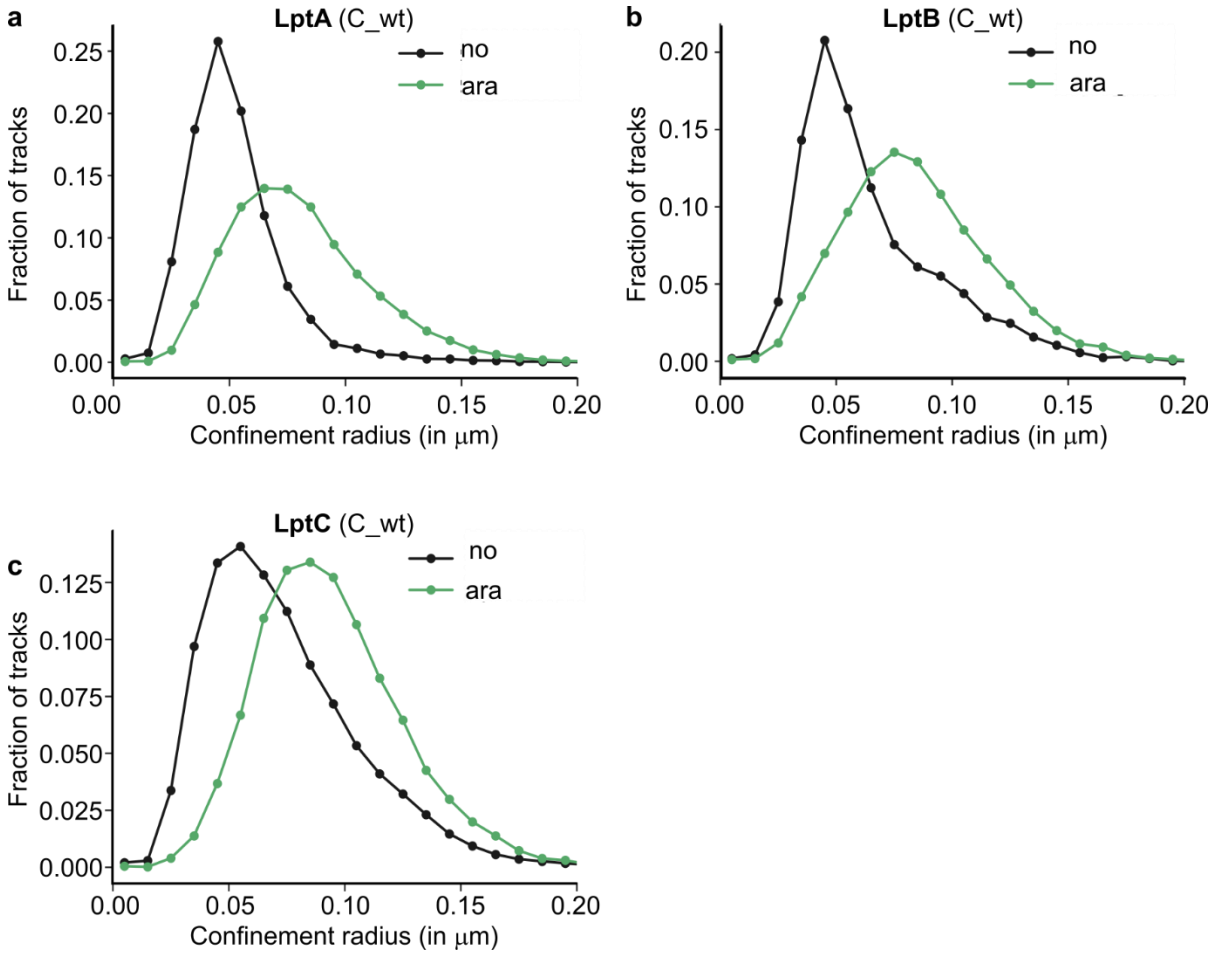

Figure 21: Overeproduction of wild type LptC results in more mobile LptA, B and C. Confinement radius plots for LptA, B, and C under wild type conditions (black line) and under overexpression of LptC(G153R) (green line).

To quantify the change in the dynamic states we did a cumulative distribution function analysis of the monitored tracks and determined the fraction of proteins in the immobile state, with (high) and without (low) the induction of wild type LptC. (Figure 22)

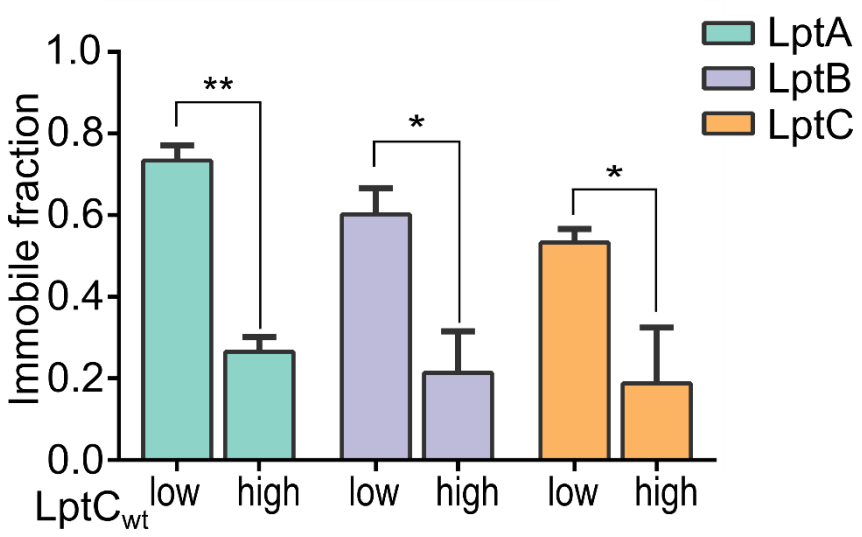

Figure 22: More mobile inner membrane complexes are formed upon overproduction of wild type LptC. Average alpha values with standard deviations (error bars), which indicated the immobile state, gained from the CDF analysis of single molecule LptA, B, and C tracks, imaged with (high) or without (low) inducing wild type LptC expression are shown. *P*-values were obtained from a t-test, **P* <0.05, ***P*<0.005.

We observed a drop of the immobile fraction for all three Lpt-proteins to about 20 percent, implying that a lot of more mobile complexes were present in the inner membrane under this condition. One possible explanation for this observation is that wild type LptC is able to attract LptA and LptB out of solution to the inner membrane to build more mobile inner membrane complexes, which led to an increase in the mobile fraction and therefore to a decrease in the immobile fraction of tracks. As discussed in Figure 14, LptA and LptB have a third soluble state in which they are soluble in the periplasm or cytoplasm. Soluble proteins are undetectable with our experimental set up due to their fast movement. However, LptA and LptB from the cytoplasm and periplasm can become detectable once they connect to the inner membrane, which slows down their movement. If overexpression indeed led to the attraction of soluble LptA and LptB to the inner membrane, then we would expect to see an increase in detectable tracks per cell. Therefore,

we measured the total number of protein tracks per cell surface for Halo-LptA, Halo-LptB, and LptC when wild type LptC was overproduced, and normalized them to the number of tracks found under endogenous levels of LptC. (Figure 23)

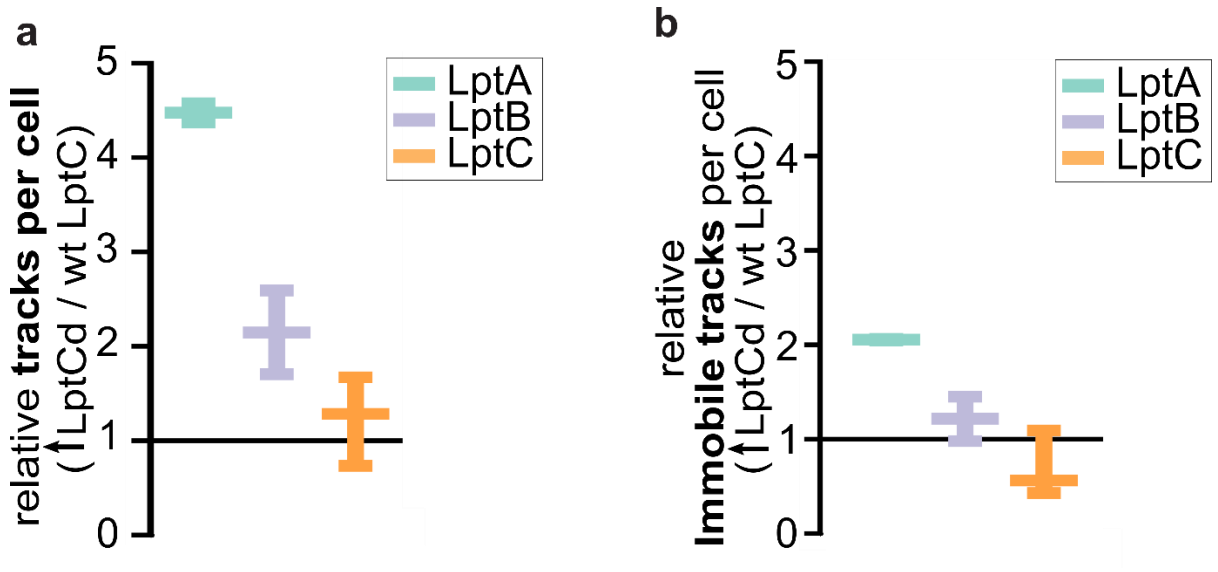

Figure 23: LptA has an immobile state outside of the bridge, LptB does not. a, The quotient of LptA, B and C tracks per cell surface under wild type condition and LptA, B and C tracks per cell surface under LptC overexpression is plotted. **b**, The quotient of immobile LptA, B and C tracks per cell surface under wild type condition and immobile LptA, B and C tracks per cell surface under LptC overexpression is plotted on the left side. **a, b**, The median of at least two independent experiments is plotted with minimum and maximum as whiskers. A median quotient higher than 1 indicates an increase in (immobile-) tracks per cell and smaller than 1 indicates a decrease upon overexpression of LptC.

As expected, the number of tracks per cell for Halo-LptC did not change because as inner membrane protein all of its states are observable. However, for LptA and LptB, the normalized number of tracks per cell increased, implying that LptA and LptB are indeed recruited to the inner membrane when LptC is overexpressed. Interestingly, this increase was more pronounced for LptA

than LptB, which would occur, if LptA can bind to both the inner membrane complex and excess LptC in the membrane while LptB can only bind to the inner membrane complex. (Figure 20)

To test if the number of bridges in the cell changed, we also determined the normalized number of immobile tracks for LptA, B and C. The number of immobile tracks for LptC slightly decreased. This is expected due to the exchange of Halo-LptC in bridges with unlabeled overexpressed wild type LptC. For Halo-LptB we found that the number of immobile tracks per cell remained unchanged while for Halo-LptA the immobile tracks per cell increased upon overexpression of wild type LptC. The fact that for both proteins, Halo-LptA and Halo-LptB, no decrease in the immobile tracks per cell is observed, shows that the decrease in the immobile fraction observed in figure 23 was indeed due to the increase in new mobile complexes at the inner membrane rather than a decrease in the number of bridges in the cell. The increase in the immobile tracks for Halo-LptA suggests that LptA has an additional immobile state, which is dependent on the overexpression of LptC. We hypothesize that LptA might be able to connect with LptC to LptDE without the inner membrane complex $LptB_2FG$ when high LptC levels are present.

This is not observed for LptB. We hypothesized that binding of LptB to LptC at the inner membrane might be limited by the levels of LptFG. To test this we overexpressed LptFG while we monitored the dynamics of Halo-LptB. (Figure 24)

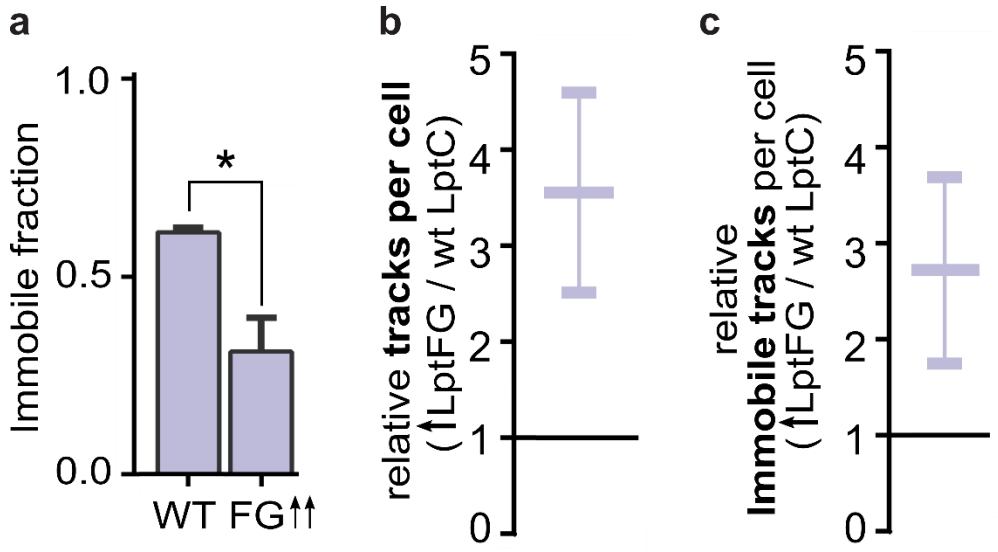

Figure 24: LptFG is required to attract LptB to the inner membrane. a, Average alpha values with standard deviations (error bars), which indicated the immobile state, gained from the CDF analysis of single molecule Halo-LptB tracks, imaged with (FG↑↑) or without (WT) inducing wild type LptFG expression are shown. *P*-values were obtained from a t-test, **P* <0.05, ***P*<0.005. **b,** The quotient of Halo-LptB tracks per cell surface under wild type condition and Halo-LptB tracks per cell surface under LptFG overexpression is plotted. **c**, The quotient of immobile Halo-LptB tracks per cell surface under wild type condition and immobile Halo-LptB tracks per cell surface under LptFG overexpression is plotted. **b,c**, The median of at least two independent experiments is plotted with minimum and maximum as whiskers. A median quotient higher than 1 indicates an increase in (immobile-) tracks per cell and smaller than 1 indicates a decrease upon overexpression of LptC. More immobile LptB is present when LptFG is overexpressed. More Lpt-bridges are formed.

The immobile fraction of Halo-LptB decreased upon overexpression of wild type LptFG, indicating that the mobile fraction increased. The number of detectable fluorescent tracks per cell increased drastically. In fact, the dye concentration had to be adjusted to lower concentration in order to sill detect single molecules. In addition, also the relative number of immobile tracks per cell of Halo-LptB increased. This shows that LptB is able to build more bridges, if LptFG is present. LptB is not able to bind to LptC without LptFG. Therefore, we can conclude that, in

contrast to LptA, the sole source of immobile LptB is the full bridge state with all seven Lpt-proteins present, with the absolute amount of the bridge remaining unchanged upon LptC overexpression. Thus, the immobile state of LptB reports on Lpt-bridges in cells.

By immuno blot analysis we confirmed that the levels of LptA and LptB remained unchanged when wild type LptC is overexpressed. This ensured that the observed changes in the dynamic behavior of LptA, B and C are not artifacts of changed expression levels of the proteins.

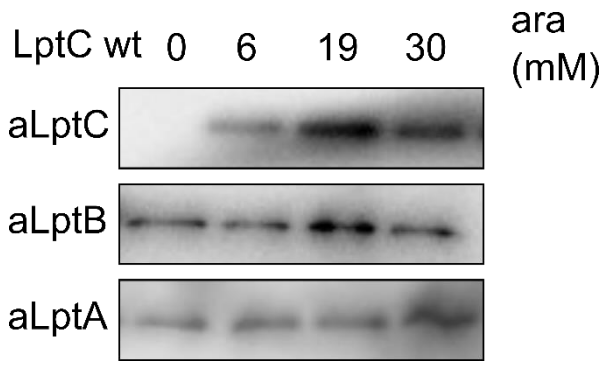

Figure 25: LptA and LptB expression levels remained constant upon overproduction of LptC. α-LptA and α-LptB immuno blot analysis for LT16 strain containing pBAD33LptC treated with different arabinose concentrations to express LptC.

2.3. Discussion

Here we tested the bridge model for LPS transport. Using TIRF-M microscopy we tracked single Lpt-proteins and determined their dynamic profile in live cells. This technique allowed us for the first time to get evidence for an Lpt-bridge in live cells. Our single molecule data support the model in which a protein bridge responsible for LPS transport is formed between the inner

membrane and outer membrane consisting of the cytoplasmic LptB, the inner membrane LptC, and the soluble periplasmic LptA proteins, all connected to the outer membrane LptDE translocon.

Single molecule tracking revealed that the mobility of outer membrane Lpt-proteins LptD and LptE is extremely confined. Any movement that might occur is below the localization precision (< 35 nm) of our experimental setup suggesting that LptD and LptE are immobile. This finding is consistent with previous studies, which showed that outer membrane proteins are largely immobile. The mobility of outer membrane proteins is confined by tight interactions with other outer membrane proteins and by the restricted area of the outer membrane protein islands.[131, 138, 142] One of the main reason for the stiffness and immobility of the outer membrane are the strong lateral interactions between LPS molecules. Newly inserted LPS molecules do not move further than 300 nm.[21, 130] LptD is the largest and slowest outer membrane β-barrel to be folded by the Bam complex.[105] Further it has been shown that LPS transport only occurs, if the LptDE translocon is completely assembled.[116] One hypothesis might be, that protein islands containing the Bam complex form by the insertion of newly synthesized outer membrane proteins. In order to allow protein insertion the outer leaflet might contain phospholipids at that time. Then as last complex, LptDE might be formed. Once it is formed, it could transport LPS into the outer leaflet, filling the surrounding of the outer membrane proteins island. The newly inserted LPS would fix the outer membrane protein island and immobilize it.

While LptDE were immobile, we found a more complex dynamic behavior for LptA, B and C. These Lpt-proteins had two detectable dynamic states: an immobile state and a mobile state. The mobile state is expected for inner membrane proteins or inner membrane associated proteins. Transmembrane proteins in the inner membrane are usually able to diffuse around relatively freely.[132-133] However, the strongly confined state, the immobile state, is unusual for inner

membrane proteins. We showed that the immobile state depends on the connection of LptA, B and C to the outer membrane complex LptDE. This indicates that the dynamics of the proteins in the cytoplasm, inner membrane and periplasm can be dictated by the localization and movement of the outer membrane proteins. As discussed in the introduction this kind of inter membrane crosstalk has also been observed for other trans-envelope protein complexes such as, the Tol-Pal system and the ArcB TolC interaction.[140, 142]

A common feature of these trans-envelope protein bridges is that they are energized by an energy source located at the inner membrane.[142] The Tol-Pal system exploits the proton motor force at the inner membrane,[161] while ArcB acts as ABC transporter. Analogous, in the LPS transport system the ABC transporter $LptB_2FGC$ is located at the inner membrane. By forming a trans envelope bridge the Lpt-proteins are able to power LPS transport from the inner membrane to the outer membrane through the periplasm by using the energy from ATP hydrolysis in the cytoplasm.[7, 98] This way the cell is able to transport LPS against a concentration gradient even though no ATP is present in the periplasm. In contrast, this energy dependency does not seem to be required for outer membrane components, transported from the inner membrane via a chaperon mechanism, such as lipoprotein and beta-barrel proteins.[105, 109, 162]

We found that LptB has only one immobile state. The sole source of immobile LptB is the full bridge state with all seven Lpt-proteins present. Therefore the immobile state of LptB can be used to report on Lpt-bridges in cells. In contrast, we found that LptA and maybe also LptC might be able to be immobile outside of a complete bridge. Upon overexpression of wild type *lptC* our data suggested that LptCA can form a bridge with the outer membrane complex LptDE without the presence of $LptB_2FG$. This observation suggests that unbridged LptDE must be present under wild type conditions and that LptFG might be a limiting component for bridge formation.

However, it is unclear, whether these LptDEAC bridges also exist in wild type cells or, if they are just an artifact of the LptC overproduction condition. In contrast, it is clearer that LptA has an additional immobile state in which LptA is connected to LptDE without the other Lpt proteins being present. We observed that LptA prefers to bind to the outer membrane complex LptDE when bridges are broken, which is consistent with previous studies showing that LptA fractionates with LptDE.[6] This suggests that the LptA-D bond might be thermodynamically more stable than the LptC-A bond and might give a hint on how bridges form or break.

Next to the immobile and the mobile detectable dynamic states, LptA an LptB also have a third soluble state in the cytoplasm and the periplasm. We found that overexpression of LptC was able to attract LptB and LptA out of solution. Interestingly even though LptC increased the recruitment of LptB to the inner membrane. LptBs recruitment was limited by the presence of LptFG, indicating that even though LptB might bind better to LptFGC than LptFG alone, LptB is not able to connect to LptC without LptFG. This observation is consistent with crystal structures of the inner membrane complex.[88] In contrast to LptB, LptA was attracted to the inner membrane by LptC alone. This is not only surprising, because it is counter intuitive to the observation that LptA preferably connects to LptDE in broken bridges, but this observation is also contrary to the common believe that soluble LptA in the periplasm does not exist.[83] This believe was based on the fact that overexpression of LptA is toxic. Our results however suggest that soluble LptA exists in the periplasm and is not toxic under wild type conditions. Instead, probably the level of soluble LptA in the periplasm might be important to determine its toxicity.

Taken together in chapter 2 we answered the question whether there is evidence for Lpt-bridges in cells. We gained insights into the dynamic profiles of the Lpt-proteins and developed with this, a method to test Lpt-bridge formation. We now have a reporter, the immobile state of

LptB, for Lpt-bridges in live cells. The next chapter will use this tool to answer the other questions about Lpt-transport stated in 1.4.7:

- How stable are these bridges?
- What influences bridge formation and bridge breakage?
- How do bridges form and break?

2.4. Materials and Methods

2.4.1. Strain construction

Halo-Lpt strains were constructed by integrating Halo-Lpt fusion proteins at a phage attachment site, while the wild type chromosomal copy of the respective Lpt protein was knocked out.

Strains used in this chapter are listed in Table 1.

LT16 (expressing Halo-LptC)

To create LT16, pHC94C was electroporated into TB28 cells containing the temperature sensitive helper plasmid pTB102. Colonies were selected on media containing tetracycline. To confirm a single copy integration of Ptac::Halo-Tag::15aa-linker::LptC at the phage attachment site attHK022 Sanger sequencing by Eton Bioscience was utilized. To delete the wild type copy of LptC from the chromosome, the ΔLptC::frt::kan::frt allele[6] was transduced into the Halo-LptC strain using P1 transduction. Kanamycin containing media was used to select for transduction and the successful deletion of the chromosomal LptC copy was confirmed with Sanger sequencing by

Eton Bioscience. Following, the kan allele was switched out using the pCP20 plasmid resulting in the strain LT16.

LT17 (expressing Halo-LptB)

LT17 was created analogues to LT16. In this case pHC94B was electroporated into TB28 cells containing the temperature sensitive pTB102. The wild type copy of LptB in the chromosome was deleted by P1 transducing ΔLptB::frt::kan::frt cassette from strain NR2339.[98] The kan cassette was switched out with pCP20 to yield LT17.

LT23 (expressing LptA-Halo)

LT23 was made analogues to LT16. Plasmid pHC94A was used to integrate Ptac::LptA::30aa-linker::Halo-Tag at the phage attachment site. To delete the wild type chromosomal LptA, the ΔLptA::frt::kan::frt cassette was transduced from strain NR1849.[85] The antibiotic kan marker was switched out with pCP20.

LT63 (expressing Halo-LptE)

LT63 was created analogues to LT16. In this case pHC94E was used to integrate Ptac::ss-Halo-Tag::15aa-linker::LptE at the phage attachment side. And the ΔLptE::frt::frt cassette from strain MG1029[113] was P1 transduced to delete the wild type copy of LptE. The kan allele was switched out using pCP20.

LT18 (expressing LptD-Halo)

LT18 was constructed using lambda red recombineering. The frt::kan::frt cassette was PCR amplified from pKD4 with primers LT185, LT183, resulting in a PCR product that has a 50 base pair overlap on its 3'-end to the genome downstream of LptD. The DNA fragment 28aa-linker::30aa-linker::Halo-Tag was PCR amplified from plasmid pBAD18LptD-Halo with primers LT186, LT178. The primers were chosen so that a 75 base pair overlap to LptD was created at the 5'-end. The two PCR products were Gibson assembled® to one fragment, overlap-LptD::28aa-linker::30aa-linker::Halo-Tag::frt::kan::frt::overlap-genome.[163] The Gibson product was PCR amplified with primers LT178, LT184 and electroporated into MG1655 containing temperature sensitive pKD46. Recombineering products were selected with medium containing kanamycin and successful integration of a single 28aa-linker::30aa-linker::Halo-Tag::frt::kan::frt cassette into the correct chromosomal site was confirmed by Sanger sequencing. Following, the kan allele was flipped out using pCP20.

Table 1: List of strains in Chapter 2

strain name	**genotype**	**source**
DH5α(λpir)	F- hsdR17 deoR recA1 endA1 phoA supE44 thi-1 gyrA96 relA1 Δ(lacZYA-argF)U169 Ø80dlacZΔM15 lpir	
E. coli NovaBlue	endA1 hsdR17 (rK – , mK +) supE44 thi-1 recA1 gyrA96 relA1 lac F′[proA+ B+ lacI q ZΔM15::Tn10]	Novagen
MG1655	rph ilvG rfb-50	ATCC
TB28	MG1655 ΔlacIZYA::frt	[164]
LT16	TB28 attHK022 Plac::Halo-15aa-LptC, ΔLptC::frt	this study
LT17	TB28 attHK022 Plac::Halo-15-aa-LptB, ΔLptB::frt	this study
LT18	MG1655 frt::LptD-30aa-Halo::frt	this study
LT63	TB28 attHK022 Plac::Halo-15-aa-LptE, ΔLptE::frt	this study
LT23	TB28 attHK022 Plac::LptA-15aa-Halo, ΔLptA::frt	this study

NR1849	MC4100 ara+ ΔlptA::kan pET23/42lptA-His	85
NR2339	MC4100 ΔLptB::kan	98
ΔC	MC4100 ΔLptC::kan	6
MG1029	MC4100 ΔLptE::kan	113

2.4.2. Plasmid construction

pHC94A

gLptA was PCR amplified from the genome using primers LT41 and LT42. 30aa-linker::Halo-Tag fragment was PCR amplified using primers LT44 and LT9. The two fragments were assembled using Gibson Assembly® Master mix. The resulting LptA::30aa-linker-Halo-Tag fragment was PCR amplified with primers LT214 and LT215 and digested with Xbal/HindIII. Plasmid pHC943 was digested with Xbal/HindIII and the two digested products were ligated to form pHC94A. The ligated product was transformed into DH5α cells.

pHC94B

A Halo-Tag::15aa-linker::LptB fragments was generated by PCR amplifying genomic DNA of LptB with LT78 , LT93, amplifying Halo-Tag::15aa with LT2 ,LT81 and Gibson assembling® both fragments. Halo-Tag::15aa-linker::LptB was PCR amplified with LT208, LT209 digested with Xbal/HindIII and ligated into Xbal/HindIII digested pHC943. The ligated product was transformed into DH5α cells.

pHC94C

Halo-Tag::15aa-linker::LptC was generated by PCR amplifying genomic LptC with LT11, LT26 and Halo-Tag::15aa-linker with LT27, LT67 and assembling these two fragments using Gibson assembly® master mix. The resulting DNA fragment was PCR amplified with LT211, LT210, digested with Xbal/HindIII and ligated into digested pHC943 to form pHC94C. The ligated product was transformed into DH5α cells.

pHC94E

Three DNA segments were PCR amplified: ssLptE (genomic signal sequence from LptE) with LT204, LT202, Halo-Tag::15aa-linker with LT203, LT206, and genomic LptE with LT205, LT207. The three fragments were assembled using Gibson assembly® method to ssLptE:: Halo-Tag::15aa-linker::LptE. The resulting fragment was PCR amplified with LT212 and LT213, digested with Xbal/HindIII and ligated into Xbal/HindIII digested pHC943. The ligated product was transformed into DH5α cells.

pBAD33LptC

gLptC was PCR amplified from the genome with LT247,LT26 and pBAD33 was PCR amplified with LT273, LT274. To generate pBAD33LptC the two fragments were assembled using Gibson assembly®. The assembled product was transformed into NovaBlue cells.

pBAD33LptC(G153R)

pBAD33LptC(G153R) was generated using site-directed mutagenesis. For this pBAD33LptC was PCR amplified with primer LT271, LT272. The product was DPNI digested and transformed into NovaBlue cells.

pBAD33LptFG

To generate pBAD33LptFG gLptFG was PCR amplified from the genome with primers LT299, LT301 and pBAD33 was amplified with primers LT300, LT302. The two PCR fragments were assembled using Gibson assembly® master mix and transformed into NovaBlue cells.

pBAD18LptDHalo

To create pBAD18-LptD-Halo, LptD plus the 28 amino acid linker were PCR amplified from -LptD plasmid with primers LT37, LT188. 30-aa-linker::Halo-Tag was PCR amplified with LT187, LT9 and pBAD18 was amplified with primers LT46, LT40. All three PCR products were Gibson assembled® and the resulting product transformed. pBAD18LptDHalo expresses LptD-Halo-Tag fusion in which the Halo-Tag is fused to LptD with two linkers.

Table 2: Plasmid list for Chapter 2

Name	Description	Source
pBAD33		165
pBAD18		165
pKD4	source of kanamycin-resistance cassette used for recombineering	166
pKD46		

pTB102	helper plasmid [repA(ts) cI857(ts) λPR::intHK022]	167-168
pHC943	attHK022 tetAR lacIq Plac::msfgfp-pbpA	149
pHC94A	Crim plasmid to integrate attHK022 tetAR lacIq Plac::LptA-Halo	this study
pHC94B	Crim plasmid to integrate attHK022 tetAR lacIq Plac::Halo-LptB	this study
pHC94C	Crim plasmid to integrate attHK022 tetAR lacIq Plac::Halo-LptC	this study
pHC94E	Crim plasmid to integrate attHK022 tetAR lacIq Plac::Halo-LptE	this study
pBAD33LptC	cmAR encodes wild type LptC	this study
pBAD33LptC(G153R)	cmAR encodes LptC(G153R)	this study
pBAD33LptFG	cmAR encodes LptFG	this study
pET23/42LptD	encodes wild type LptD	102
pET23/42LptD-Halo	encodes LptD-30aa linker-Halo	this study
pCP20	cat bla cI857 PR::FLP	166

Table 3: Primer list for Chapter 2

Primer	**Sequence (5‘-3‘)**
LT41	ATGAAATTCAAAACAAACAAACTCAGCCTTAATCTTGTG
LT42	GGACCTTGTCCGCTACCCTCAAGATTACCCTTCTTCTGTGCCGGGG
LT44	TTAGCCGCTGATTTCTAAGGTAGAAAGCC
LT9	TTAGCCGCTGATTTCTAAGGTAGAAAGC
LT214	CATGTTTCTAGATTTAAGAAGGAGATATACATATGAAATTCAAAACAAACAAA CTCAGCCTTAATCTTGTG
LT215	CATGTTAAGCTTTTTATTCGGATTATCCGTCATGATTAGCCGCTGATTTCTAAGG TAGAAAGCC
LT93	TCAGAGTCTGAAGTCTTCCCCAAGG
LT2	ATGGCAGAAATCGGTACTGGC

LT81	TATAGGCTTTTGCAAGGTTCTTTGCAGTTAATGTTGCCATGCCGCTTCCTTGGCC
LT78	CAGGGACCGGGCTCAGGCCAAGGAAGCGGCATGGCAACATTAACTGCAAAGAA
LT93	TCAGAGTCTGAAGTCTTCCCCAAGG
LT208	CATGTTTCTAGATTTAAGAAGGAGATATACATATGGCAGAAATCGGTACTGGCT
LT209	CATGTTAAGCTTTTTATTCGGATTATCCGTCATGATCAGAGTCTGAAGTCTTCCC
LT26	TTAAGGCTGAGTTTGTTTGTTTTGAATTTCATAGG
LT27	ATGGCAGAAATCGGTACTGGCTTTC
LT11	GGGCTCAGGCCAAGGAAGCGGCATGAGTAAAGCCAGACGTTGGGTTATCATTG
LT67	CAGTGATAGCACAATGATAACCCAACGTCTGGCTTTACTCATGCCGCTTCCTTG
LT210	CATGTTTCTAGATTTAAGAAGGAGATATACATATGGCAGAAATCGGTACTGGCT
LT211	CATGTTAAGCTTTTTATTCGGATTATCCGTCATGATTAAGGCTGAGTTTGTTTGT TTTGAATTTCATAGG
LT212	CATGTTTCTAGATTTAAGAAGGAGATATACATATGCGATATCTGGCAACATTGT
LT213	CATGTTAAGCTTTTTATTCGGATTATCCGTCATGATCAGTTACCCAGCGTGGTGG
LT202	TACCGATTTCTGCCATCCCGGCGGTGATTAACACCGCCAGAGATAACAACAATG TTGCCAGATATCGCAT
LT203	CGGTGTTAATCACCGCCGGGATGGCAGAAATCGGTACTGGCTTTCCATTC
LT204	ATGCGATATCTGGCAACATTGTTGTTATCT
LT205	TCAGGCCAAGGAAGCGGCTGTGGCTGGCATCTGCGTG
LT206	CACGCAGATGCCAGCCACAGCCGCTTCCTTGGCCTGA
LT207	TCAGTTACCCAGCGTGGTGG
LT271	CTGGAGTTAAATGTTGTTCTGTATAACGTGACGAGGTCT
LT272	AGACCTCGTCACGTTATACAGAACAACATTTAACTCCAG
LT247	ATGAGTAAAGCCAGACGTTGGGTTATCA
LT183	TTTCCATTTCAATTAACCGCACTGCGGATTACGTGGTAAATCAACAAATCAATAT GAATATCCTCCTTAG
LT185	GGCTTTCTACCTTAGAAATCAGCGGCTAATGTGTAGGCTGGAGCTGCTTC
LT178	GCGGCCTGAGCTCCAACTAC
LT186	GAAGCAGCTCCAGCCTACACATTAGCCGCTGATTTCTAAGGTAGAAAGCC
LT184	TTTCCATTTCAATTAACCGCACTGCGG

LT37	ATGAAAAAACGTATCCCCACTCTCCTGG
LT188	GACCTTGTCCGCTACCCTCAAGCTCGAGTGCGGCCGCAAG
LT187	CTTGCGGCCGCACTCGAGCTTGAGGGTAGCGGACAAGGTC
LT40	CCAGGAGAGTGGGGATACGTTTTTTCATGGATCCCCGGGTACCGAGC
LT46	GGCTTTCTACCTTAGAAATCAGCGGCTAATCTAGAGTCGACCTGCAGGCATG
LT273	CCAACGTCTGGCTTTACTCATATGTATATCTCCTTCTTAAAGTTAAACAAAATTA
LT274	CAAAACAAACAAACTCAGCCTTAATTGATTAATACCTAGGCTGCATGC
LT314	TTAATTACCCTTCTTCTGTGCCGG
LT319	CCAACGTCTGGCTTTACTCATATGTATATCTCCTTCTTAAAGTTAAACAAAATTA
LT316	CCGGCACAGAAGAAGGGTAATTAATTGATTAATACCTAGGCTGCATGC
LT299	ATGATAATCATAAGATATCTGGTGCGGG
LT300	CCCGCACCAGATATCTTATGATTATCATATGTATATCTCCTTCTTAAAGTTAAACTC
LT301	TTACGATTTTCTCATTAACAGCCACAGG
LT302	CCTGTGGCTGTTAATGAGAAAATCGTAATTGATTAATACCTAGGCTGCATGC

2.4.3. Immuno blots to observe Lpt-Halo-Tag fusion proteins

For immuno-blots cultures were grown as described above to OD600~0.4 and normalized to OD600~0.3. The cells were pelleted with centrifugation at 8000 rpm for 2 min. The pellets were resuspended in SDS-PAGE sample buffer supplemented with 5% β-mercaptoethanol. Samples were boiled for 10 min and run on home-made Tris-HCl 14% polyacrylamide gels with Tris-glycine running buffer. Proteins were transferred onto Immuno-Blot® PVDF membranes (Bio-Rad). The membrane was blocked with Casein blocking buffer and then incubated with the primary antibody. The sources of rabbit anti-LptC, LptA, LptB, LptE and LptD antisera have been previously reported.[6, 85, 98] Lpt proteins were detected by a donkey anti-rabbit HRP conjugate secondary antibody (GE Amersham). Bands were visualized using ECL™ Prime Western Blotting Detection Reagent (GE Amersham) and Azure c600 imaging system (Azure Biosystems).

2.4.4. Growth curves

Single colonies of the strains were inoculated from streaked plates in M9 media containing 0.2% CAA and 0.4% Maltose. For LT17/LT63/LT23 20 μM IPTG, and for LT16 70 μM was added to the media to induce expression of the Lpt-Halo-Tag proteins. For LT18 and TB28 no inducer was added. The cultures were grown over night at 37°C and then diluted 1:100 into fresh media the next morning. The diluted cultures were grown at 37°C while shaking and OD600 was monitored until they reached the stationary phase.

2.4.5. Culture growth for imaging

Unless otherwise indicated, all cultures in this study were grown as described in the following procedure: Cells were streaked from frozen stocks on LB agar plates and incubated over night at 37°C. Single colonies from the plates were inoculated in M9 media*, supplemented with 0.2% casamino acid (CAA) and 0.4% Maltose as carbon source, serial diluted and grown over night at 37°C. The next day a culture at its mid exponential phase (OD600 = 0.3-0.6) was used as starter culture to produce another round of serial dilutions. These were grown on the shaker at 37°C until they reached OD600 ~0.3. At this point the strains were either stained and imaged, or harvested for western blot.

*To grow LT16, LT17, LT63 and LT23 expression of the respective Lpt-Halo fusion protein was induced by adding 20μM IPTG for LT17/LT63/LT23 and 70μM IPTG for LT16 to the media.

2.4.6. Imaging sample preparation

Cultures of the strains were grown as described above. At OD600~0.3 1mL of the culture was stained with ~5nM Halo-Tag-JF549 and incubated for 10-15 min at 37°C while shaking. The culture was concentrated by spinning it down at 8000rpm for 2min and removing part of the supernatant. 1 μL of the concentrated culture was pipetted onto a 20x60 mm coverslip and covered with a 1.5 mm thick 2% agar pad. The agar pad was made with the media in which the strain was grown in. After ~30 min of imaging a new slide was prepared.

2.4.7. Slide preparation

To reduce background fluorescence the coverslips were cleaned before their use for TIRF microscopy. The coverslips were sonicated for 30 min in 2% Hellmanex™ III, washed with deionized water and sub sequentially sonicated in NaOH for 30 min. The NaOH was washed away with deionized water and the coverslips were washed with EtOH and sonicated in EtOH for another 30 min. Coverslips were washed with EtOH again and stored in EtOH until its usage.

2.4.8. Microscope set up for particle tracking

Total internal reflection fluorescence microscopy (TIRF-M) and phase-contrast microscopy was performed on a Nikon TI microscope equipped with a 100X NA 1.45 TIRF objective and an Andor Ixon EMCCD camera resulting in 160 nm pixels. With an exposure time of 100 ms, 400 – 500 frames (streaming acquisition) were taken at an illumination of 561 nm. A phase-contrast image was taken before and after the fluorescent movie was acquired to segment

the outside of the cells. Movies that displayed drifts were discarded. The imaging was performed in a chamber equilibrated at 37°C.

2.4.9. Fixed dye measurement

Imaging slides were prepared as described above. Instead of applying cell solution to the slide, 12.5 μM Halo-JF549 dye solution was applied. An agarose pad was added above and the sample was imaged as described above.

2.4.10. Imaging of LptC(G153R) mutant samples

pBAD33-LptC(G153R) was transformed into LT16, LT17 and LT23. The strains containing the plasmid were grown as described above with the addition of chloramphenicol to the media to ensure the retention of the plasmid. Imaging samples were prepared analogous to the description above. However, 10 min before staining 0.04 μM arabinose was added to the culture to induce the expression of LptC(G153R). Also the agarose pads were prepared with media containing chloramphenicol and arabinose. For the negative condition no arabinose was added. The movies for particle tracking were taken ~35 min after inducing the expression of LptC(G153R with the same setup as defined above . For the concentration gradient (Figure 15) arabinose concentrations of 0.001 μM, 0.007 μM, 0.02 μM and 0.04 μM were used.

2.4.11. Imaging of wild type LptC overexpression sample

pBAD33-LptC was transformed into LT16, LT17 and LT18. To retain the plasmid chloramphenicol was added to the media and the strains were grown as described above in, Culture

growth. 10 min before staining with JF549-Halo-liganf 0.04 μM arabinose was added to the culture to induce the overexpression of wild type LptC. Imaging samples were prepared as explained above. However, the agarose pad was made with media containing chloramphenicol and arabinose. For the negative control no arabinose was added to the culture or the agarose pad. Single molecule tracking movies were collected ~35 min after the expression of LptC was induced.

2.4.12. Imaging of LptFG overexpression sample

To get high expression levels of LptFG while imaging Halo-LptB we transformed pBAD33LptFG into LT17. The LT17 strain containing the pBAD33LptFG plasmid was grown as described above with the addition of chloramphenicol to the media to retain the plasmid. 10 min before staining, overexpression of LptFG was induced by the addition of 0.04 μM arabinose. Imaging samples were prepared as described above, However, the JF-549-Halo-ligand concentration was reduced to ~2nM, because overexpression of LptFG attracts so much Halo-LptB to the inner membrane that the dye concentration needed to be reduced to detect single molecules. The agar pads were prepared containing chloramphenicol and 0.04 μM arabinose. For the wild type control no arabinose was added and the JF549-Halo-ligand concentration was kept at 5 nM. About 40 min after the induction of LptFG overexpression, Halo-LptB particles were tracked using the imaging set up described above.

2.4.13. Fractionation of Halo-LptA strain

The fractionation of LT23 was done following the protocol used in Chng et al..[6] 1.5L cells were grown of LT23 in LB at 37C to OD600~ 1.2. Cells were pelleted by centrifugation at 4251 x g for 20 min and then resuspended in 15 mL of 10 mM Tris-HCl, pH=8.0 containing 20% (w/w)

sucrose, 1 mM PMSF and 50 μg/mL DNase I. The cells were lysed by a single passage through the cell disrupter. Unbroken cells were removed by centrifugation at 300 x g for 20 min. 1.6 mL of cell lysate was layered on top of the sucrose gradient: bottom 65% (0.5 mL), 55% (1.0 mL), 50% (2.4 mL), 45% (2.4mL), 40% (2.4 mL), 35% (1.4 mL), 30% (0.5 mL). All sucrose (w/w) solutions contained 10 M Tris-HCl, pH=8.0. Samples were centrifuged at 39,000 rpm for 15 h and 0.5 mL fractions were collected manually from the top of each tube. Fractions were diluted with 950 μL of 20 mM Tris-HCl, pH 8.0 and 110 μL 100% (w/w) trichloroacetic acid (TCA, Sigma). Precipitated proteins were collected by centrifugation at 21,000 x g for 30 min, resuspended and analyzed by SDS-page and immuno-blots. α-LptF blot was run as reference for inner membrane proteins and α-BamA blot was run as reference for the outer membrane.

2.4.14. Image analysis

Collected images were not modified for analysis. Images were analyzed with Fiji.[169] For displaying purposes images were cropped for the figures and movies.

2.4.14.1. Particle tracking

Tracks were generated using the software Fiji and the plugin TrackMate.[169-170] Particles were detected with the DoG (difference of Gaussian) detector and tracks were generated with the Simple LAP Tracker with a 200 nm search radius and no frame gaps allowed. Tracks shorter than 4 frames were discarded and the remaining tracks exported for further processing.

2.4.14.2. Data analysis

If not other indicated, further data analysis was done in python using custom-written code. Plots were generated using python Matplotlib or Graphpad PRISM.

2.4.14.2.1. Filtering tracks ins cells

To ensure only tracks inside cells are used for analysis, the phase contrast images to the corresponding movie were converted into binary images using the threshold tool in Fiji. The exported binary images were used as mask to filter out tracks from the exported TrackMate file, which are not in cells. A custom-written python code was used for this.

2.4.14.2.2. Mean squared displacement analysis

Mean squared displacements versus time delay (Msd vs Δt) plots were generated for all tracked proteins. Msd vs Δt plots are shown for 20 representative tracks for each imaged protein in Figure 9. Since tracks indicated switching behavior between different dynamic states we decided to use confinement radius calculation and cumulative distribution function analysis for further analysis.

2.4.14.2.3. Confinement radius analysis

For the confinement radius analysis tracks were filtered to a minimum length of 5 frames. Tracks larger than 5 frames were cut down to 5 consecutive frames. The confinement radius were calculated by determining the average x, y position (centroid) of the trajectory by taking the average of the trajectory coordinates. The average of the distances between the trajectories

coordinates to the centroid gives the confinement radius. Confinement radii histograms were generated using NumPy.histogram function with a given bin size of 0.01.[171] The histogram values were normalized by dividing the incident number per bin by the total number of incidences. The plots were generated using Matplotlib.

2.4.14.2.4. Cumulative distribution analysis

The r^2-displacement was calculated for trajectories by measuring the frame to frame vector displacement along the trajectory by the lag time Δt=200 ms and taking its magnitude. The cumulative probability $P(r^2, \Delta t)$ was constructed from the pool of displacements across multiple tracks for each protein by counting the number of squared displacements $\leq r^2$ normalized by the sample size. The CDF of the r^2-displacements were fitted to analytical functions describing diffusive processes with one or two dynamic states. $P(r^2, \Delta t)$ is the cumulative probability of displacement r in the observation period Δt, D_1, D_2 are diffusion constants for the different states, and α describes the relative fraction between the states.[158-159] 4 sigma square is the error term with σ = 0.034 μM. Sigma was identified as the average of the confinement radii of fixed dye tracks with a frame length = 3, and given as fixed parameter. CDF fit results with smaller error term and without an error term are reported in Supplementary table 1.

(ES1) $$P(r^2, \Delta t) = 1 - e^{-\frac{r^2}{4D\Delta t + 4\sigma^2}}$$

(ES2) $$P(r^2, \Delta t) = 1 - \left(\alpha * e^{-\frac{r^2}{4D_1\Delta t + 4\sigma^2}} + (1 - \alpha) * e^{-\frac{r^2}{4D_2\Delta t + 4\sigma^2}} \right)$$

The CDF for LptA, B, and C under wild type conditions were fitted with both different diffusion models using the lmfit package in python.[172] Residuals of model fits were calculated and used to identify the best model. The two component diffusive model resulted in the best fit for all three proteins. To identify the diffusion constant and the fraction of proteins in the immobile state for the proteins under non wild type conditions, only the two state diffusive model was used. CDF fit results are reported in Supplementary table 1.

2.4.14.2.5. (Immobile-) tracks per cell surface analysis

Cell masks were constructed as binary images as explained above. The cell surface area was calculated by taking the sum of the binary image. Tracks were filtered to have a minimum length of 4 frames and to be inside cells. The number of tracks measured for one 400 frame time-lapse movie was calculated and divided by the corresponding cell surface area. At least three time-lapse movies with their corresponding phase images were used to determine the tracks per cell surface.

To determine the immobile tracks per cell surface, tracks are additionally filtered for a confinement radius < 0.07 μm before the number of tracks is calculated.

3. Chapter 3: Lifetime of Lpt-bridges in cells

3.1. Introduction

The large amphipathic molecule LPS, comprises the outer leaflet of the outer membrane in gram negative bacteria and is responsible for the unique barrier function of this membrane.[10, 16] LPS gets completely synthesized in the cytoplasm and at the inner membrane and then needs to be transported from its synthesis site to the cell surface. In chapter 1, it was discussed that seven essential Lpt-proteins have been identified to be responsible for the LPS transport process.[86] Previous studies suggested a model in which the Lpt-proteins come together to form a trans envelope bridge spanning from the inner membrane through the periplasm to the outer membrane.[7, 173] It is thought that LPS moves along this bridge to the outer membrane while its hydrophobic chains are shielded from the aqueous periplasm. The transport process is energized by the ABC transporter $LptB_2FGC$ located at the inner membrane. This way ATP from the cytoplasm can be utilized to power LPS transport against its concentration gradient. The hypothesized Lpt-protein bridge was able to be reconstituted in vitro.[7]

However, it has not been possible to find evidence for the existence of the bridge in live cells previously. Further a number of important features about this proposed Lpt-bridge are unknown. (1.4.7.) One important open question is for example how stable are Lpt-bridges in cells. For example, a long lived trans-envelope bridge might be an advantage for the cell, because multiple thousand LPS molecules need to be transported during one cell division. However, a long Lpt-bridge lifetime would raise the question, how a stiff bridge connection between the inner membrane and outer membrane might impact the architecture of the bacterial cell envelope and the distribution of LPS molecules in the outer leaflet of the outer membrane. In contrast, short

lived Lpt-bridges would allow the cell to dynamically transport LPS to different locations around the outer membrane and could spontaneously respond to different stimuli. Chapter 3 aims to answer the question, how stable are Lpt-bridges in live cells.

Previous in vitro studies showed that the interaction between the different Lpt-proteins is strong and therefore suggested that Lpt-bridges are stable and might have long lifetimes. The fact that Lpt-proteins co-purify with each other supports the existence of strong interactions between these proteins.[6] In addition, the in vitro reconstituted Lpt-protein bridge between proteoliposomes containing the inner membrane Lpt-complex and proteoliposomes containing the outer membrane Lpt-complex exists long enough to sort the proteoliposomes with Fluorescent Flow Cytometry Spectroscopy (FACS).[7] Furthermore, the connection between the two proteoliposomes is stable enough to be observed under the microscope after FACS sorting. These in vitro experiments propose that Lpt-protein bridges can be stable for multiple minutes to hours.

In chapter 2, a method is described, which we developed in order to observe Lpt-proteins in live cells. We were able to determine the dynamic profiles of the different Lpt-proteins. We found that analogous to most outer membrane proteins, the outer membrane Lpt-proteins LptD and LptE are immobile. The cytoplasmic protein LptB, the inner membrane protein LptC and the periplasmic protein LptA displayed two types of motion. LptA, B and C had a mobile diffusive state, and an immobile state. Experiments with the mutant LptC, LptC(G153R), and overexpression experiments with wild type LptC elucidated that the immobile state of LptA, B and C depends on their connection to the outer membrane proteins LptDE and their involvement in Lpt-bridge formation. Furthermore, we were able to show that the sole source of immobile LptB is the full bridge state with all seven Lpt-proteins present. Thus, the immobile state of LptB directly reports on Lpt-bridges in cells. Therefore, the approach for measuring the lifetime of Lpt-bridges in cells

was, to measure the lifetime of the immobile state of LptB. We also measured the lifetime of the immobile state for LptA and LptC to get information about their involvement in Lpt-bridges.

3.2. Results

3.2.1. Development of bridge lifetime measurement and bleaching control

Since the immobile state was shown to represent a connection to the outer membrane, the mobile state is evidence of broken bridges with a connection to the inner membrane, but no connection to the outer membrane. When Lpt-bridges break the connection between the inner membrane and the outer membrane is disrupted and immobile Lpt-proteins become mobile. Therefore, in order to determine the lifetime of the bridge we wanted to measure the amount of time LptA, B and C stay in the immobile state. Measuring the dwell time of stationary single molecules with TIRF-M harbors multiple challenges. One of the main challenges is to ensure that the lifetime of the immobile state is not artificially shortened due to incorrect tracking of spots. The most straightforward approach to measure lifetimes of immobile Lpt-proteins is to measure the length of the immobile tracks. To determine the dynamics of the Lpt-proteins in chapter 2, the particle tracking data were analyzed with the TrackMate plugin in Fiji to identify spots and construct tracks. (2.4.14.1.) In order to get information about the dynamic profile of the Lpt-proteins the length of the tracks is not critical. However, to determine the lifetime of immobile spots it is important to not artificially shorten the tracks. Fluorescent spots tend to show a blinking behavior under the TIRF-M, which might lead to a low signal to noise ratio in some frames. If the signal to noise ratio of a spot is too low in one or two frames, TrackMate stops the track in the frame of low signal to noise ratio and starts a new track once the signal intensity is higher. This

tracking approach would measure shorter lifetimes than the real lifetimes. To circumvent this problem Squyres *et al.* developed a lifetime measurement approach of single immobile molecules, in which they measured the dwell time of a spot based on the corresponding intensity trace rather than the length of a track.[151] This analysis approach was also used to determine the lifetime of LptA, B and C in the immobile state in this chapter. As illustrated in figure 26, the location of an immobile single molecule spot was identified with TrackMate. Using the code developed in [174] the intensity trace for this spot was measured. The intensity trace was fitted to a Hidden Marcov Model.[175] A single molecule event with a certain lifetime is expected to fit a two state model with an "on" and an "off" state. The lifetime of the immobile spot can then be determined by the dwell time of the spot in the "on" state.

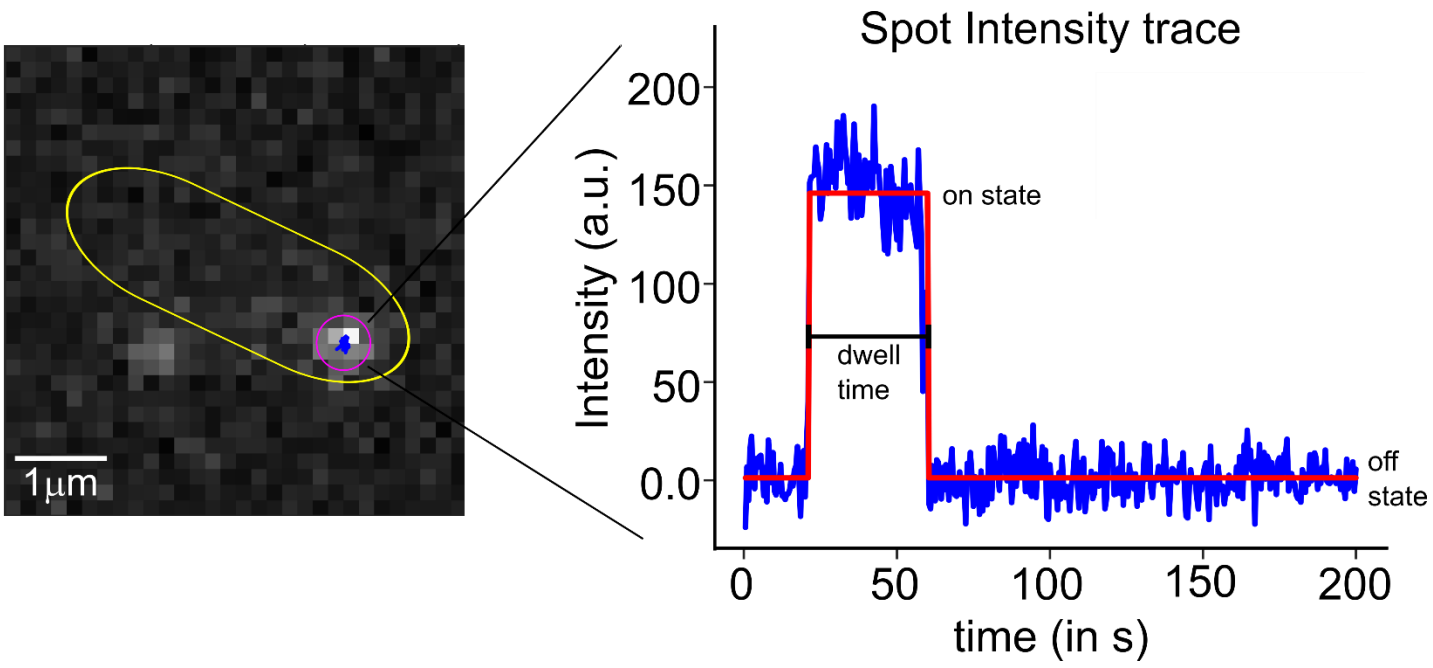

Figure 26: Hidden Markov Model was fitted to spot intensity traces to determine the lifetime of immobile proteins. The location of single molecule spots was identified using the TrackMate plug in in Fiji. Intensity traces of the identified spots were constructed and fit to a Hidden Markov Model. The dwell

time of the spot in the on state (high intensity) was measured as the lifetime of the spot in the immobile state.

Another main challenge of the lifetime measurement is bleaching of the fluorescent dye. Bleaching of the dye before the observed protein leaves the immobile state and starts moving again would result in falsely short lifetimes. Therefore, it is important to determine the right exposure time and laser intensity, which are able to give a good signal to noise ratio of single molecules without bleaching the dye before the protein starts moving again. Troubleshooting indicated that TRIF-M time-lapses of single Halo-Tag-Lpt-proteins with a laser intensity of 50% and an exposure time of 500 ms give a good signal to noise ratio. To test that bleaching of the dye does not dictate the lifetime measurement under these experimental condition, we collected time lapses of Halo-Tag-LptC with 500 ms exposure in 500 ms intervals (Figure 27, green dots) and compared it to lifetimes measured with 500 ms exposure in 1 s intervals (Figure 27, blue dots). This way, fluorescent dyes are exposed to half the amount of light in the measurement with 1 s intervals. Survival probability plots of the measured lifetimes were very similar for the 500 ms interval and the 1 s interval, suggesting that the influence of bleaching to the lifetime of the immobile Halo-Tag-LptC is negligible.

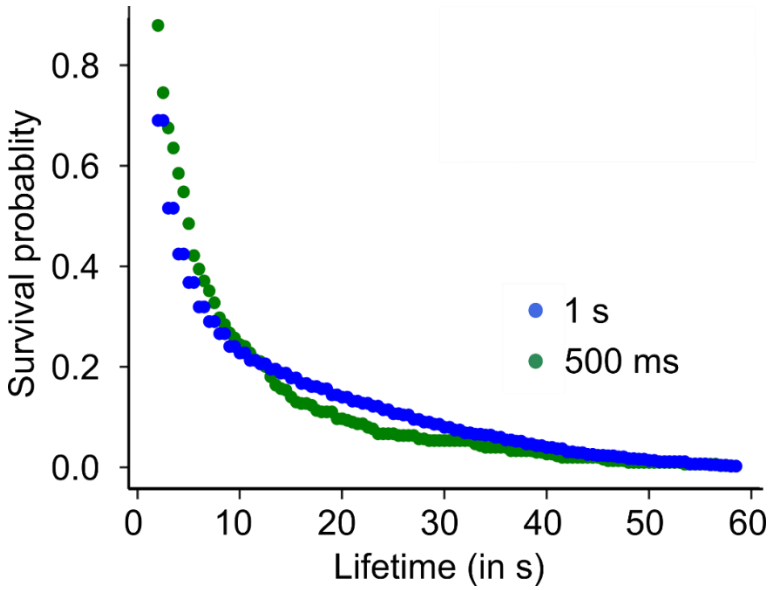

Figure 27: The effect of bleaching to the lifetime measurement is negligible with an exposure time of 500 ms. Bleaching control measurement; Halo-Tag-LptC (LT16) lifetime plots measured with 500 ms exposure in 500 ms intervals (green) compared to 500 ms exposure in 1 s intervals (blue). Results shown are representatives of two independent experiments.

3.2.2. Lifetime of the immobile state of LptA, B and C

To get insights about the stability and breakage of Lpt-bridges in cells, we measured the lifetime of the immobile states for LptA, B and C following the approach described above in 3.2.1. Lifetime distribution plots for immobile LptA, B, and C are shown in Figure 28.

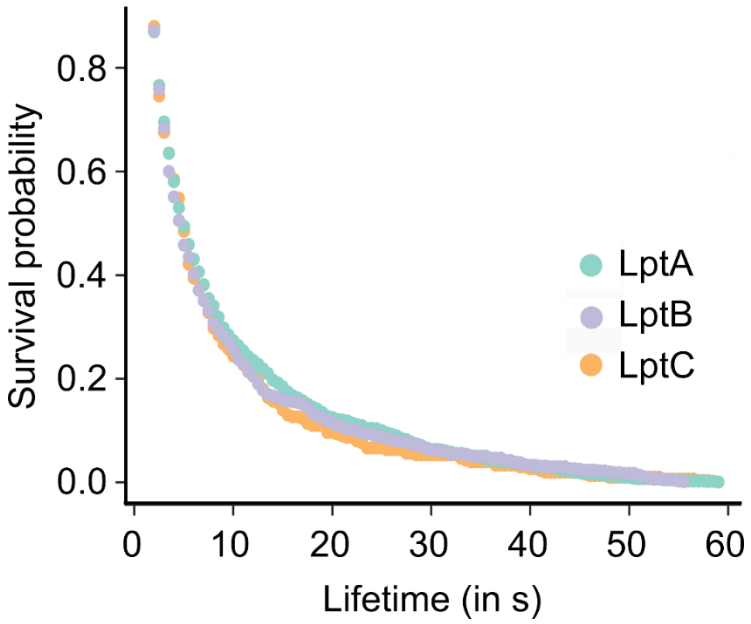

Figure 28: Lpt-bridges are transient. Measured lifetimes for LptA, B, and C in the immobile state are shown in survival probability plots. Lifetimes were measured by fitting intensity traces of immobile spots to a Hidden Markov Model.

The lifetime distribution plots were remarkably similar for LptA, B and C and displayed an average lifetime of ca. 10 s. (Figure 28) This is a relative short lifetime compared to the Lpt-bridge lifetime expected from *in vitro* experiments. This showed that Lpt-bridges are transient in *E. coli* cells. Further, the fact that the lifetime distributions looked nearly identical for LptA, B and C implies that all three Lpt-proteins become mobile at the same time. Thus, all three proteins can report on the lifetime of the bridging state. This is inconsistent with the observation that LptA has an additional immobile state bound to LptDE without being in a complete bridge. We showed above in section (2.2.3.) that LptA is preferably bound to LptDE after the Lpt-bridge breaks (Figure 17 and Figure 18). Therefore, it must be the case that LptDE-bound LptA can exchange rapidly with LptA from the pool of soluble Halo-LptA protein in the periplasm. Because the vast majority of LptA does not contain a fluorophore, the signal from the LptDE-bound state rapidly washes out

under these conditions. The lifetime of LptA bound to LptDE alone is far shorter than the lifetime of the Lpt-bridge.

3.2.3. Fitting of the lifetime distribution reveals two distinct bridge states

To get insights about the mechanism of bridge breaking we tested if the lifetime plots for LptA, B, and C follow a single or a biexponential decay. (Figure 29)

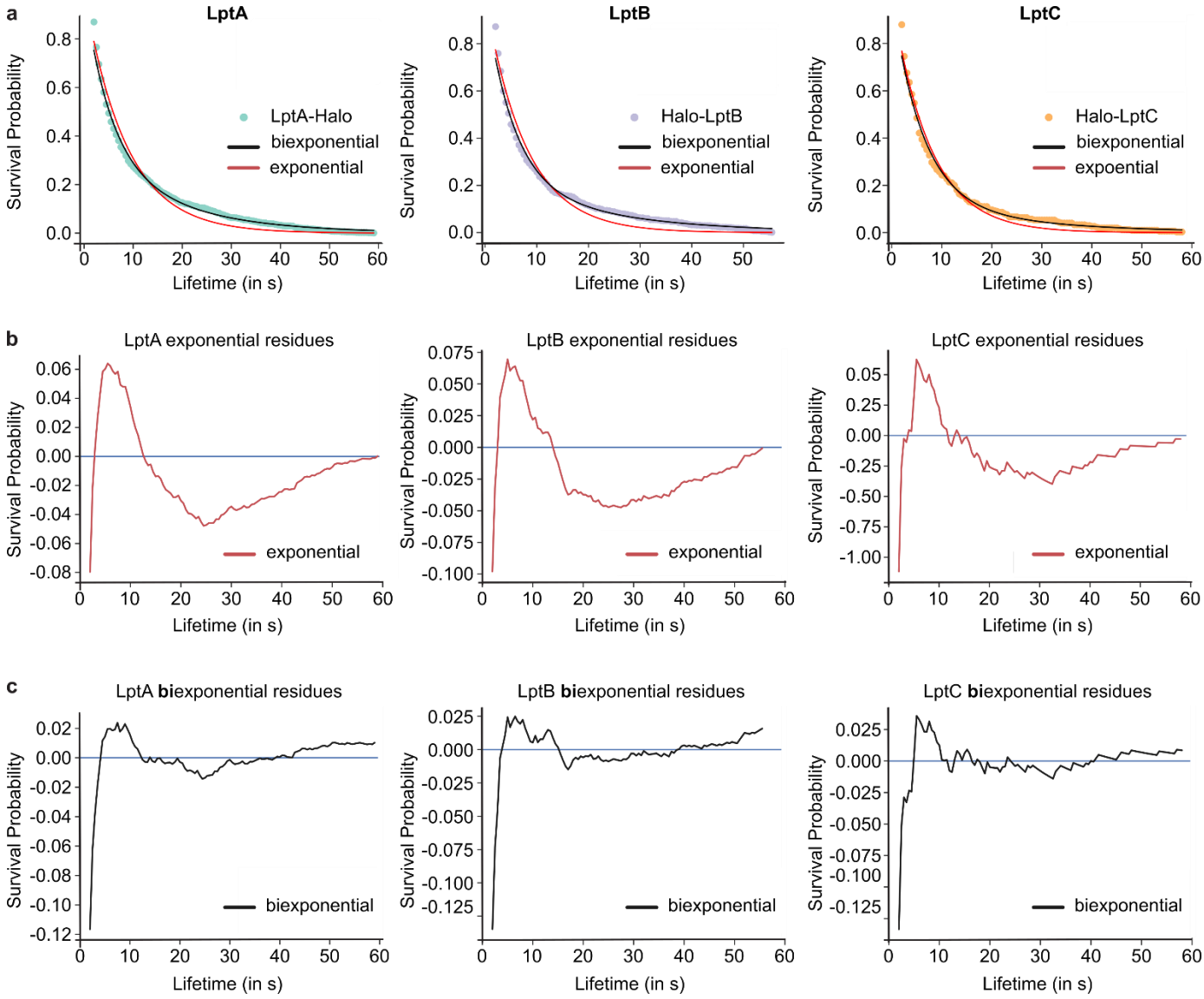

Figure 29: Decay kinetics of the Lpt-bridge is biexponential. a, Single exponential curves (red) and biexponential curves (black) are fitted to the lifetime plots of LptA, B, and C. (line = fit, dots = lifetime data). Fitted values can be found in figure 30 and figure 31. **b**, Residue plots for the single exponential fits are shown (red). **c**, Residue plots for the biexponential fits are shown (black). For all three proteins the biexponential fit resulted in the best fit of the lifetime distribution.

A single exponential fit (red line) did not fit the data for any of the proteins well. In contrast a biexponential function (black line) fitted the lifetime data for LptA, B, and C beautifully, showing

that the bridge breaking mechanism is more complex and involves two processes. The biexponential fit describes the bridge breaking with two rate constants. One quick event with a half-life time of ~4s and a slightly slower event with a half-life time of ~12s. The biexponential behavior implies that two different states of the bridge can break. A plausible scenario is that in one state, the bridge contains LPS; in the other state, no LPS is present.

	exponential g(x)=exp(-kx)	
	k	$t_{1/2}$
LptA	0.12 ± 0.01	6.0 ± 0.2
LptB	0.12 ± 0.02	5.9 ± 0.7
LptC	0.13 ± 0.00	5.2 ± 0.0

Figure 30: The lifetime distributions of LptA, B and C do not fit a single exponential decay. Fitted values of the single exponential fit to the lifetime distribution of LptA, B and C are shown.

	biexponential g(x)=a*exp(-lx)+(1-a)*exp(mx)				
	a	l	$t_{l1/2}$	m	$t_{m1/2}$
LptA	0.64 ± 0.01	0.20 ± 0.01	3.5 ± 0.1	0.06 ± 0.01	12.4 ± 0.9
LptB	0.67 ± 0.01	0.20 ± 0.01	3.5 ± 0.1	0.05 ± 0.01	13.8 ± 1.5
LptC	0.84 ± 0.01	0.22 ± 0.05	3.4 ± 0.8	0.05 ± 0.01	14.8 ± 1.1

Figure 31: The lifetime distributions of LptA, B and C fit a biexponential decay well. Fitted values for the biexponential fit to the lifetime distribution of LptA, B and C are shown. For all three proteins, the lifetime data fit a biexponential decay reflecting two processes with half-lives of ~4s and ~12s.

3.3. Discussion

In this chapter we showed for the first time kinetic information about the Lpt-bridge in cells. Using the live cell microscopy approach introduced in chapter 2, we were able to determine the lifetime of Lpt-bridges in cells by measuring the dwell time of immobile LptB. Chapter 2 established that the only immobile state of LptB is the full bridge state involving all seven Lpt-proteins. We found that individual bridges are transient, existing for less 10 seconds. Further, we found that also the lifetime distributions of immobile LptC and LptA are almost identically to the lifetime distribution of LptB. This suggests that all Lpt proteins become mobile at once and that also LptA and LptC can report of the lifetime of the bridge. In chapter 2 we discussed that LptA preferentially binds to immobile LptDE when bridges are broken, leading to a second immobile state of LptA. Since the lifetime distribution of immobile LptA is very similar to the lifetime

distribution of LptB and LptC it must be the case that LptDE bound LptA exchanges rapidly with soluble Halo-LptA from the periplasm. Since Halo-LptA is only sparsely labeled the signal from the LptDE bound LptA quickly disappears. It is possible to conclude that the lifetime of LptA bound to LptDE alone without the full bridge is way shorter than the lifetime of LptA in the full bridge state.

The stability of the Lpt bridges in cells is way less than predicted by *in vitro* experiments using purified components. As discussed in the introduction of chapter 3 (3.1.), reconstitution of a functional seven protein complex *in vitro* produces bridges between proteoliposomes that last for more than an hour. It is likely that the stability of these bridges is due to multiple bridges existing simultaneously; polyvalent interactions increase the stability of the associated proteoliposomes. Polyvalent interactions likely also occur in cells, but other processes may disrupt the bridges. In a cell, the inner membrane is fluid while the outer membrane is largely fixed by lateral interactions of the LPS in the outer leaflet. Connecting the two membrane bilayers by a continuous bridge in a cellular context may create additional sheer forces adding stress on the protein-protein interfaces that form the bridge. A plausible scenario might even be that moving of LPS along a newly formed bridge makes the outer membrane around the LptDE complex stiffer, leading to breakage of the bridge when the LPS transport is completed. In addition, a layer of peptidoglycan exists in cells in between the inner and outer membranes, and the immobility of this "solid membrane" relative to the two membrane bilayers, may also facilitate breakage.

The measured lifetime distribution of LptA, B and LptC are also able to give us information about the bridge breakage mechanism. We found that the lifetime distributions of all three proteins follow a biexponential decay reflecting two processes with half-lives of ~4s and ~12s. The biexponential behavior implies that there must be two different states of the Lpt-bridge that can

break. One state breaks with a faster rate constant and the other one with a slower. One possible hypothesis is that in the one state, the bridge contains LPS and in the other state, no LPS is present. The influence of LPS to bridge stability might be a potential answer for how the cell is able to coordinate LPS transport with transient bridge formation. This question will be further discussed and tested in chapter 4.

Concluding, chapter 3 answered the question how stable Lpt-bridges are in cells. We found that bridges are highly dynamic and only exist transiently. Further, the biexponential decay behavior of the lifetime distribution suggested that there are two different kind of bridges that are breaking. In the following chapter, chapter 4, we will try to gain insights into the two remaining questions.

- What influences bridge formation and bridge breakage?
- How do bridges form and break?

3.4. Materials and Methods

3.4.1. Strains used in this Chapter

Table 4 contains a list of the strains used in this chapter. The construction of these strains is described in chapter 2 in 2.4.1..

Table 4: List of strains for chapter 3

strain name	genotype	source
LT16	TB28 attHK022 Plac::Halo-15aa-LptC, ΔLptC::frt	this study
LT17	TB28 attHK022 Plac::Halo-15-aa-LptB, ΔLptB::frt	this study
LT23	TB28 attHK022 Plac::LptA-15aa-Halo, ΔLptA::frt	this study

3.4.2. Sample preparation

Cells of LT16, LT17 and LT23 were streaked from frozen stocks onto LB agar plates containing 20 μM IPTG for LT17 and LT23 and 70 μM IPTG for LT16. The agar plates were incubated at 37°C overnight. Single colonies from the plates were inoculated in M9 media, supplemented with 0.2% casamino acid (CAA) and 0.4% Maltose as carbon source. The inoculated culture was serial diluted and grown over night at 37°C. The next day, a culture at its mid exponential phase (OD600 = 0.3-0.6) was used as starter culture to produce another round of serial dilutions in the supplemented M9 media with the addition of 20 μM IPTG for LT17 and LT23 and 70 μM IPTG for LT16. The serial dilutions were grown on the shaker at 37°C until they reached OD600 ~0.3. At this point 1mL of the respective culture was stained with ~5nM Halo-Tag-JF549 and incubated for 10-15 min at 37°C while shaking. The culture was concentrated by spinning it down at 8000 rpm for 2 min and removing part of the supernatant. 1 μL of the concentrated culture was pipetted onto a 20x60 mm coverslip. The coverslip was cleaned in advance, following the procedure explained in 2.4.7.. The concentrated culture on top of the coverslip was covered with a 1.5 mm thick 2% agar pad. The agar pad was made with the media in which the strain was grown in. After ~30/45 min of imaging a new slide was prepared.

3.4.3. Microscope set up for lifetime measurement

Total internal reflection fluorescence microscopy (TIRF-M) and phase-contrast microscopy was performed on a Nikon TI microscope equipped with a 100X NA 1.45 TIRF objective and an Andor Ixon EMCCD camera resulting in 160 nm pixels. With an exposure time of 500 ms, TIRF-M time-lapses were taken with streaming acquisition for 4 min at an illumination

of 561 nm at a 50% laser intensity. A phase-contrast image was taken before and after the fluorescent movie was acquired to segment the outside of the cells. Movies that displayed drifts were discarded. The imaging was performed in a chamber equilibrated at 37°C.

3.4.4. Life time measurement

The phase-contrast images taken before and after each time-lapse were used to generate a cell mask using the threshold tool in Fiji.[169] The analysis approach used for determining single-molecule lifetimes of stationary spots was described and developed by G. Squyres et al.[151] The TIRF-M time-lapses were preliminary analyzed using TrackMate.[170] Spots were detected with the DoG detector and linked with a 2-pixel linking distance and a maximum gap of 10 frames. The Trackmate data were exported to Matlab.

To determine lifetimes from the TrackMate data, the Matlab code published and developed by G. Squyers was used.[174] The tracks from TrackMate were filtered for tracks inside cells using the generated cell masks, and the filtered tracks were converted into spot intensity traces. A 5 x 5-pixel window around the mean spot position was used to calculate the average intensity, and the local background was averaged in a 2-pixel frame around the window. The resulting intensity traces were filtered; only traces with a maximum background-subtracted intensity above 300 counts were included for further analysis. Intensity traces were fitted to a hidden Markov model using the vbFRET package[175] to measure single-molecule lifetimes. Only traces that were best fitted with a two-state model were included. Further, a minimum difference between state 1 (no fluorescence) and state 2 (single-molecule fluorescence) of 40 counts was set. The lifetime is given by the duration of each state 2 event: dwell times less than 2s (four frames) were excluded, as well

as events that overlapped with the start or the end of the trace. Traces with more than 4 events were also discarded.

The resulting lifetimes were exported as NumPy files[171] and further analyzed with custom written python code. Single-molecule lifetimes were plotted as survival probability by dividing the number of lifetimes > i by the total number of measured lifetimes, whereby i is equal to the minimum to maximum measured lifetimes in 500 ms steps. The single and the biexponential fits to the lifetime plots were done using the lmfit package in python.[172]

3.4.5. Bleaching control set up

To measure the contribution of photo bleaching to the lifetime measurement, we repeated the lifetime measurement for Halo-LptC with 1s imaging intervals rather than 500 ms intervals without changing the laser intensity or exposure time. There was no significant difference between the 1s imaging intervals measurements compared to the 500 ms intervals, indicating that photo bleaching contribution was negligible. (Figure 27)

4. Chapter 4: The role of LPS in bridge formation and bridge breakage

4.1. Introduction

In chapter 2, we showed that the dynamics of Lpt-proteins in cells support a bridge model in which the Lpt-proteins come together to span a trans-envelope bridge connecting the inner membrane with the outer membrane. LPS is then able to be transported along this bridge from its synthesis site, the inner membrane, to the outer leaflet of the outer membrane. We showed that the cytoplasmic protein LptB, the inner membrane protein LptC and the periplasmic protein LptA have an immobile state, analogous to the immobile state of the outer membrane proteins LptD and LptE. The immobile state of LptA, B and C was identified to correspond to their involvement in the formation of a trans-envelope bridge. In chapter 3, we tested the stability of the Lpt-bridge in cells by measuring the dwell time of LptA, B and C in the immobile state. We found that Lpt-bridges are transient with an average lifetime of ~10 s. Further, the lifetime distribution of LptA, B and C followed a biexponential decay indicating that there are two different states of the bridge that can break.

The transient nature of the bridge raises the question how LPS transport is coordinated with bridge formation. Calculations show that ~70, 000 LPS molecules are transported to the outer membrane per minute.[67] The short lifetime of the bridge in cells means that LPS must be transported rapidly when the bridge is intact. However, if LPS transport starts before the complete bridge is assembled, it is possible for LPS to spill into the periplasm, creating toxicity by activating the σ^E response.[67] Further, the finding of the biexponential lifetime distribution behavior suggested the existence of two different bridge states, which break. We hypothesized that one state might contain LPS, while the other state might not. If the presence of LPS in the bridge affects the bridge

properties, one prediction is that altering LPS levels could change either the number of bridges or their dynamics. Therefore, we tested in the first part of this chapter the effect of an LpxC inhibitor to the dynamics of the Lpt-proteins. As discussed in 1.3 LpxC catalyzes the first committed step in the LPS synthesis. Thus treatment of cells with the LpxC inhibitor leads to a decrease in cellular LPS concentration. (Figure 32)

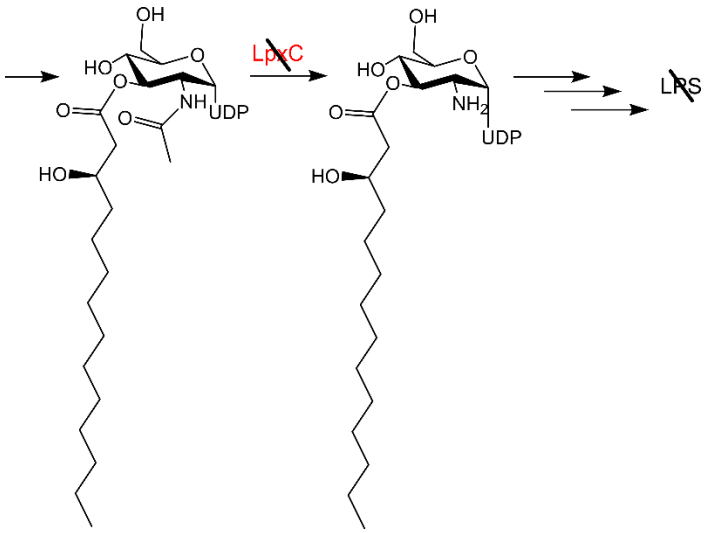

Figure 32: Inhibition of LpxC leads to decreased LPS levels in the cell. The deacetylation of UDP-monoacyl-N-acetylglucosamine by LpxC leading to UDP-monoacyl-glucosamine is the first committed step in the Lipid A synthesis. Inhibition of LpxC leads to a decreased concentration of LPS in the cell.

There are two main interactions, which, when ruptured, would lead to Lpt-bridge breakage: The interaction between LptC and LptA, and the interaction between LptA and LptD. (Figure 33) The biexponential behavior of the bridge lifetime distribution suggests that there are two different states of the bridge that break. We wanted to test if one of these states breaks by the dissociation of the CA-interaction. Therefore we fused the C-A bond and tested its effect on Lpt-bridge dynamics. These experiments are described in the second part of chapter 4.

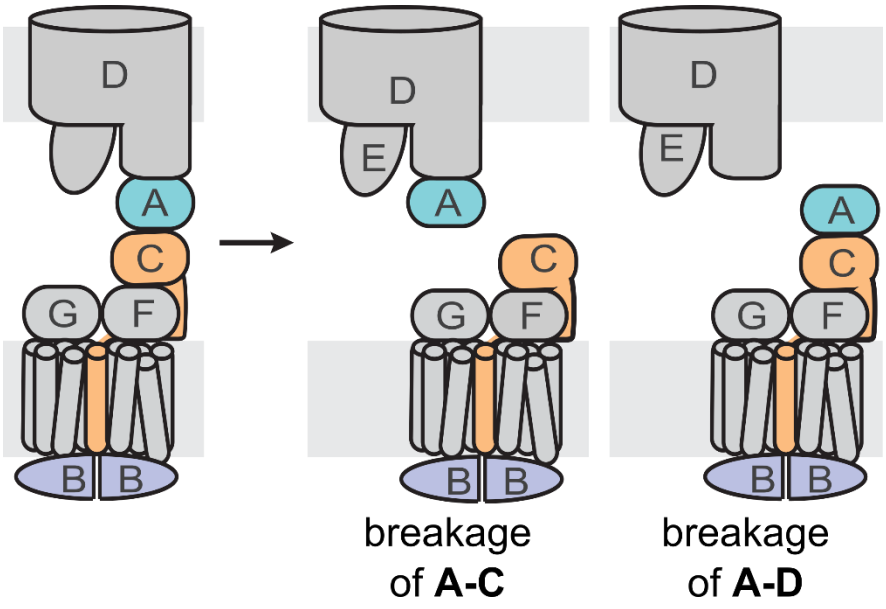

Figure 33: Rupture of the CA-interaction or the DA-interaction would lead to bridge breakage. Model scheme depicting potential bridge breakage mechanisms.

4.2. Results

4.2.1. Bridge lifetimes remain unchanged at lower LPS levels

To test if the presence of LPS affects the dynamics of the bridge, we altered the level of LPS in the cell with the help of an LpxC inhibitor while measuring the lifetime of the bridge. We, therefore, treated cells containing Halo-LptB with an LpxC inhibitor,[49] which decreases intracellular LPS concentration by inhibiting the first committed step of LPS synthesis. The lifetime distribution plot was identical in the presence and absence of LpxC inhibitor, meaning that lowering the cellular concentration of LPS did not affect bridge breakage decay kinetics.

(Figure 34) The lifetime distribution of bridges in cells treated with an LpxC inhibitor still best fitted a biexponential decay.

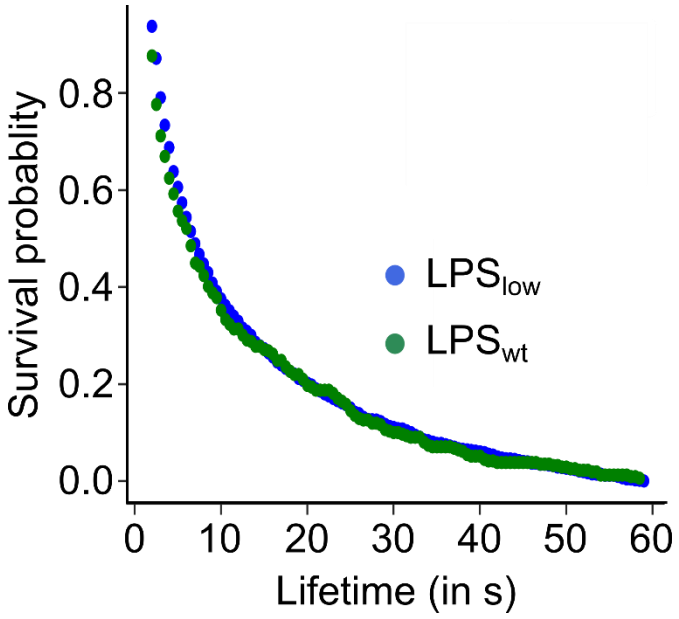

Figure 34: Bridge breakage decay kinetic are unaffected by lowered cellular LPS concentration. Lifetime distribution plots of immobile Halo-LptB tracks with (blue) and without (green) treatment of LpxC inhibitor. Results are representatives of at least two independent experiments.

4.2.2. Rate of Lpt-bridge formation is decreased when LPS synthesis is inhibited

To test if the number of bridges is affected by a decreased cellular LPS concentration we tracked the mobility of Halo-LptB in cells treated with an LpxC inhibitor. While the lifetime distribution plot was identical in the presence and absence of LpxC inhibitor, we found that the immobile fraction for Halo-LptB, which reports on the relative number of bridges, decreased substantially in the presence of the LpxC inhibitor. (Figure 35 a) Also the confinement radius

distribution was shifted to larger conferment radii, indicating more mobility, upon LpxC inhibitor treatment. (Figure 35 b)

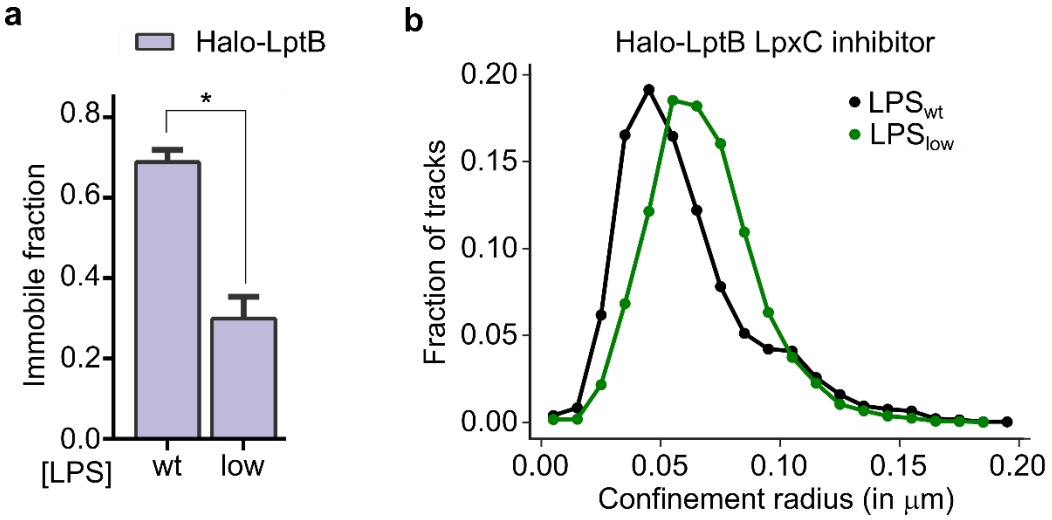

Figure 35: Bridge formation is facilitated by LPS. a, Average alpha values with standard deviations (error bars), which indicated the immobile state, gained from the CDF analysis of single-molecule Halo-LptB tracks, measured under wild type (wt) and with 0.5 MIC LpxC inhibitor treatment. *P*-value was obtained from a t-test, **P* <0.05. **b**, The corresponding confinement radius plots for the tracks are shown. Halo-LptB becomes more mobile when cells are treated with LpxC inhibitor. The number of Lpt-bridges in the cell decreases at lower cellular LPS concentration.

Since the rate of breaking bridges stayed the same, but the number of Lpt-bridges in cells is decreased, the rate of forming Lpt-bridges must be slowed down when the LPS concentration decreases. Although stable Lpt-bridges can form *in vitro* without LPS,[7] in cells, this data indicates the rate of bridge formation is promoted by LPS. Therefore, LPS is not only a substrate for bridge transport but is a structural component that facilitates the process of connecting the inner membrane and outer membrane complexes. Because we do not observe an LPS concentration

dependence on bridge decay kinetics, the rate of dissociation of the structural LPS bound to the machine must be slow relative to transport. This model suggests that LPS binding to $LptB_2FGC$ in the IM, *i.e.*, containing a preloaded structural LPS, lowers the barrier to connect to LptADE.

4.2.3. Lifetime of LptCA-fusion bridges

If a structural LPS in the inner membrane complex indeed facilitates the CA-interaction for bridge formation, we wondered if this increased stability contributes to the two observed rates for bridge breakage. Given that we observe two rates for bridge breakage, we wondered what would happen to bridge lifetimes, if we artificially stabilize the CA-interface by fusing LptC to LptA. In this artificial system the bridge is forced to break and form between the DA-interface. (Figure 36)

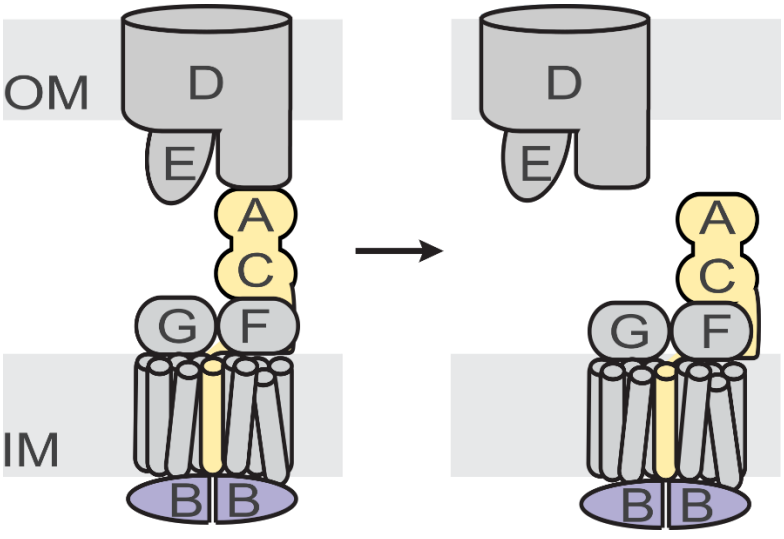

Figure 36: CA-fusion protein forces the bridge to break and form through the DA-interface. Scheme depicting the breakage of a bridge containing the CA-fusion protein. Since the CA-interface is fixed, the bridge has to break though the DA-interface.

Previous studies in the lab have shown that the CA-fusion protein supports outer membrane assembly in cells lacking both individual proteins.[176] We overexpressed the CA-fusion protein while we monitored the immobile state of LptB to obtain bridge lifetimes. Figure 37 shows the lifetime distribution for bridges containing the CA-fusion protein (blue) compared to the lifetime distribution of wild type bridges (green). The lifetime distribution for cells producing the CA-fusion protein was clearly shifted towards longer lifetimes, indicating that fusing the CA-interface stabilized the Lpt-bridge.

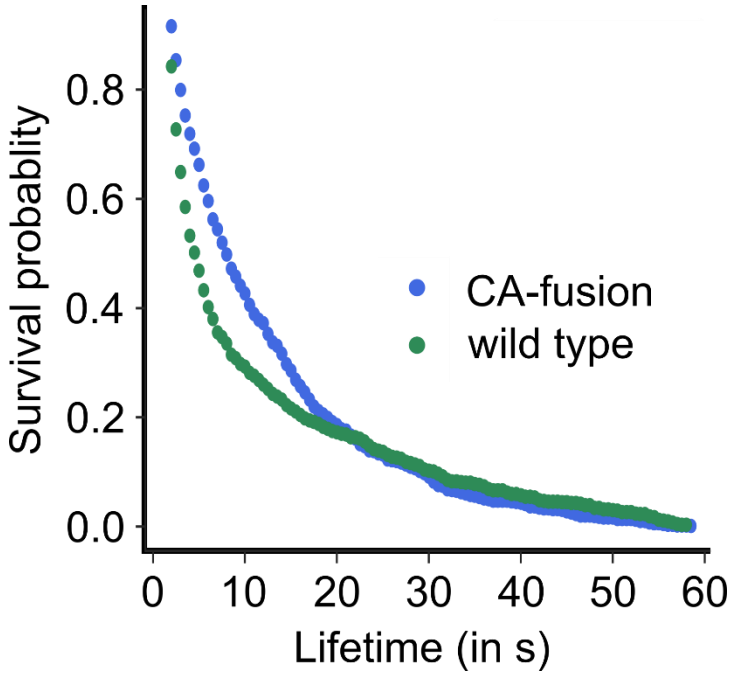

Figure 37: CA-fusion bridges showed longer lifetimes than wild type bridges. Lifetime distribution plots of immobile Halo-LptB tracks with (blue) and without (green) treatment of LpxC inhibitor. Results are representatives of at least two independent experiments.

4.2.3.1. Fitting of LptCA fusion bridge lifetimes

To get insights into the breakage mechanism of CA-fusion bridges we fitted a single exponential and a biexponential decay to the lifetime data. Interestingly, in contrast to the wild type lifetime data, the lifetimes obtained for the CA-fusion were best fit by a single exponential decay (red line). The corresponding half-life of the single exponential fit was ~8 s. (Figure 38 a, b)

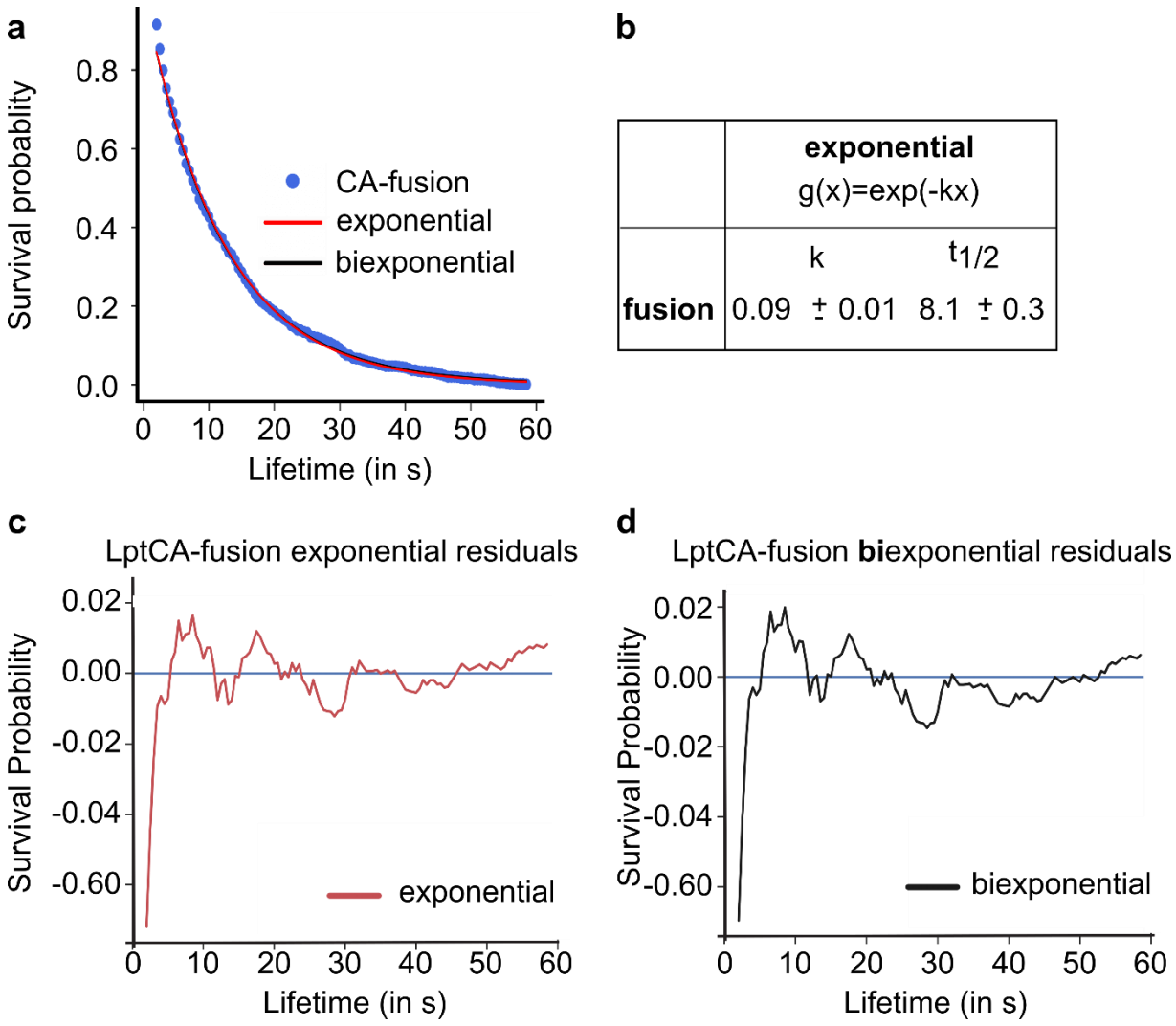

Figure 38: The lifetime distribution of CA-fusion bridges followed a single exponential decay. a, Single exponential curve (red) and biexponential curve (black) are fitted to the lifetime plot of LptB in the presence of LptC-A-fusion. (line = fit, dots = lifetime data). **b,** Fitted values of the single exponential decay

to the lifetime distribution of CA-fusion bridges. **c, d,** Residuals of the exponential (red, **c**) and biexponential (black, **d**) fit to the LptCA-fusion lifetime distribution (**a**) are shown.

Since the lifetime distribution of wild type bridges showed a biexponential behavior, the observation that the CA-fusion showed a single exponential decay implies that fragmentation at the CA-interface is one of the two bridge breakage processes observed for the wild-type bridge. Preventing breakage at this interface by fusing the CA-bond lead to a single exponential lifetime decay. Following this logic the other wild type bridge breakage process must involve fragmentation at the DA-interface. Because fixing the bond between LptC and LptA resulted in a longer bridge lifetimes (Figure 37), the faster cleavage process captured by the 4 s half-life for the wild-type bridge likely corresponds to dissociation at the CA-interface. Following the slower process captured by the 12 s half-life likely corresponds to the rupture of the DA-interface.

4.2.4. Bridges preferably form through the CA-interface

To test if fusing LptC to LptA affects the number of bridges in the cell, we monitored the change in mobility of Halo-LptB upon overproduction of the CA-fusion protein. We found that the relative number of bridges for the CA-fusion slightly decreased compared to the wild-type bridge under comparable conditions. (Figure 39) The immobile fraction of Halo-LptB determined by the CDF analysis slightly decreased and also the confinement radius distribution showed a small shift to higher mobility. If the number of CA-fusion bridges in the cell remained unchanged or slightly decreased, while the rate of breaking CA-fusion bridges was slower than for wild type

bridges, this observation implies that the rate of $LptB_2FGCA$-fusion bridge formation was slower than in the wild type case.

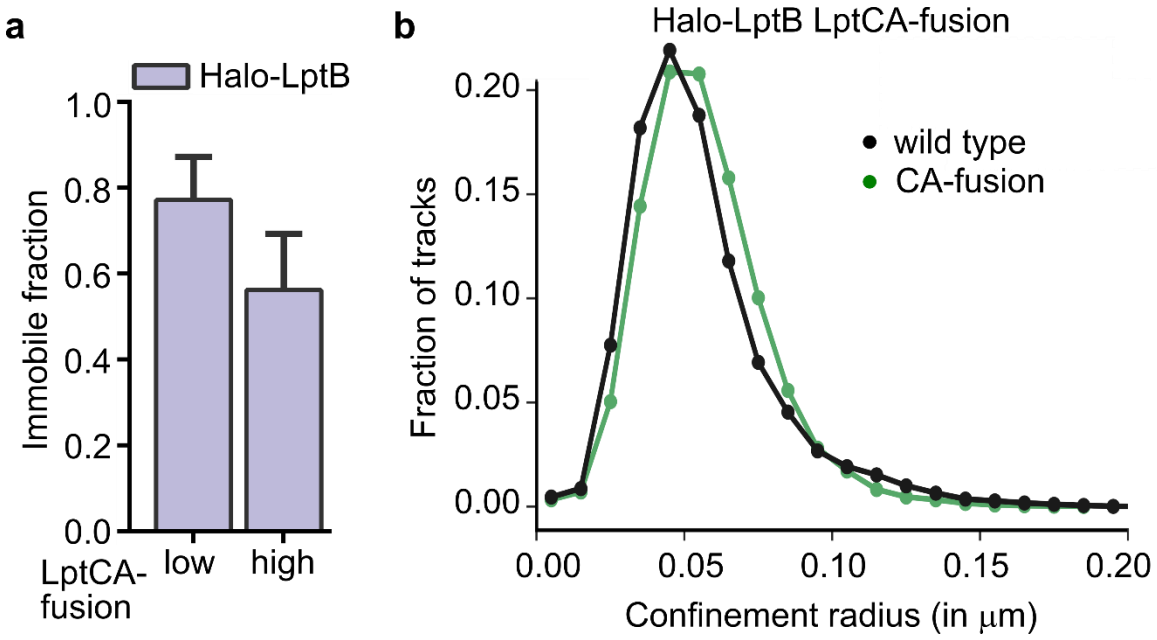

Figure 39: CA-fusion decreases the rate of formation. a, Average alpha values with standard deviations (error bars), which indicated the immobile state, gained from the CDF analysis of single-molecule LptB tracks, measured without (low) or with (high) induction of LptCA-fusion protein expression. **b,** The corresponding confinement radius plots for the Halo-LptB tracks measured with (green) and without (black) overproduction of LptCA-fusion are shown.

4.3. Discussion

In this chapter we tried to gain insights into the two remaining questions about LPS transport stated in 1.4.7.:

- What influences bridge formation and bridge breakage?
- How do bridges form and break?

We tested the effect of lowered cellular LPS concentration on bridge dynamics using an LpxC inhibitor. We found that the lifetime of bridges remained unaffected. A mechanism by which the cell measures the amount of LPS in either the outer leaflet of the inner membrane or the outer leaflet of the outer membrane could allow coordination of LPS transport with bridge lifetime. In chapter 2.3. we discussed that filling of the outer membrane by newly inserted LPS could increase the stiffness of the membrane at the site of transport and therefore lead to bridge breakage due to increased sheer forces between the two membranes. An example for how the bridge could monitor LPS levels in the inner membrane was that the bridge transports LPS until it is depleted from the inner membrane. But our data suggests this is not the case. In fact we find that lowering the concentration of LPS in the inner membrane did not affect the lifetime of the bridge.

However, while the lifetime of the bridge remained unaffected, we found that the number of bridges in the cell decreased at lower cellular LPS levels. It follows that higher LPS levels promote bridge formation and we conclude that LPS is not only a substrate of the bridge but also acts as a structural component that facilitates the interaction between the inner membrane and the outer membrane complexes. A preloaded $LptB_2FGC$ with LPS could lower the barrier to connect to LptADE. Also, Martorana *et al.* suggested recently that LPS might act as structural component of the bridge, based on the observation that components of the bridge, LptA and LptD are degraded upon treatment with an LpxC inhibitor.[177] As discussed in the introduction, the short lifetime of the bridge in cells means that LPS must be transported rapidly when the bridge is intact. Calculations show that ~70, 000 LPS molecules are transported to the outer membrane per minute.[67] If LPS transport starts before the complete bridge is assembled, it is possible for LPS to spill into the periplasm creating toxicity by activating the σ^E response. The fact that LPS is not

only a substrate of the bridge but also acts as structural component, that facilitates bridge formation, might be a way for the cell to coordinate LPS transport with bridge assembly.

Further, we showed in this chapter that fixing the interaction between LptA and LptC results in bridges with longer lifetimes, which break following a single exponential decay. Since the lifetime distribution of wild type bridges follows a biexponential decay describing two different processes we conclude that one of the two wild type bridge breaking processes is the dissociation of the CA-interaction. Because the lifetime of the bridge containing the CA-fusion protein is longer than the lifetime of wild type bridges, we concluded that the dissociation of the CA-interaction likely corresponds to the faster rate constant described by the biexponential decay, while the slower rate constant describes the rupture of the DA-interface. Based on the observation that LPS stabilized the interaction between LptC-A, we hypothesized that bridges break at the DA-interfaces when LPS is present in the bridge. In contrast, based on the fact that LptA fractionated with LptDE, we hypothesized that bridges without LPS might break at the CA-interface.

Furthermore, we were able to observe that bridges containing the CA-fusion protein form slower than wild type bridges, suggesting that fixing LptA and LptC might prevent the preferred order of bridge formation. We therefore concluded that under wild type condition LptA might first interact with the outer membrane complex LptDE and then connects to the inner membrane complex $LptB_2FGC$. This together with the observation that LptD sequesters LptA away from LptC when not in a bridge (chapter 2) may be a cellular feature designed to prevent release of LPS from the inner membrane to the periplasmic LptA when it is not connected in a bridge. In addition the levels of LptA are carefully regulated.[83, 177] Depletion of bridge components or other disruptions to the bridge cause degradation of LptA.

Taken together, our data suggest the following model for how bridges form and break in cells. (Figure 40) In the unbridged state, $LptB_2FGC$ forms at the inner membrane, and soluble LptA preferentially associates at the outer membrane to form LptADE. When cells require more outer membrane, LPS biosynthesis produces an accumulation of LPS in the inner membrane, leading to an interaction with $LptB_2FGC$ to form $LptB_2FGC$·LPS. The LPS preloaded inner membrane complex facilitates bridge formation with LptDEA. Transport occurs rapidly, locally depleting LPS from the inner membrane. There are then two different rates for the breakage of wild type bridges, which describe the breakage of two different states of the bridge in two distinct path ways. In the faster breakage process no structural LPS is bound to the bridge components anymore. In this case, rupture of the bridge occurs at the CA-interface. However, the dissociation of structural LPS from $LptB_2FGC$·LPS to the $LptB_2FGC$ complex is slow. Therefore, is also occurs that bridges break while the structural LPS is bound. We showed that the presence of LPS promotes the formation of bridges, and we have proposed that it does so by accelerating the formation of the CA-interface. Thus we hypothesize that the presence of LPS leads to the second slower bridge breakage process in which breakage occurs through rupture of the DA-interface.

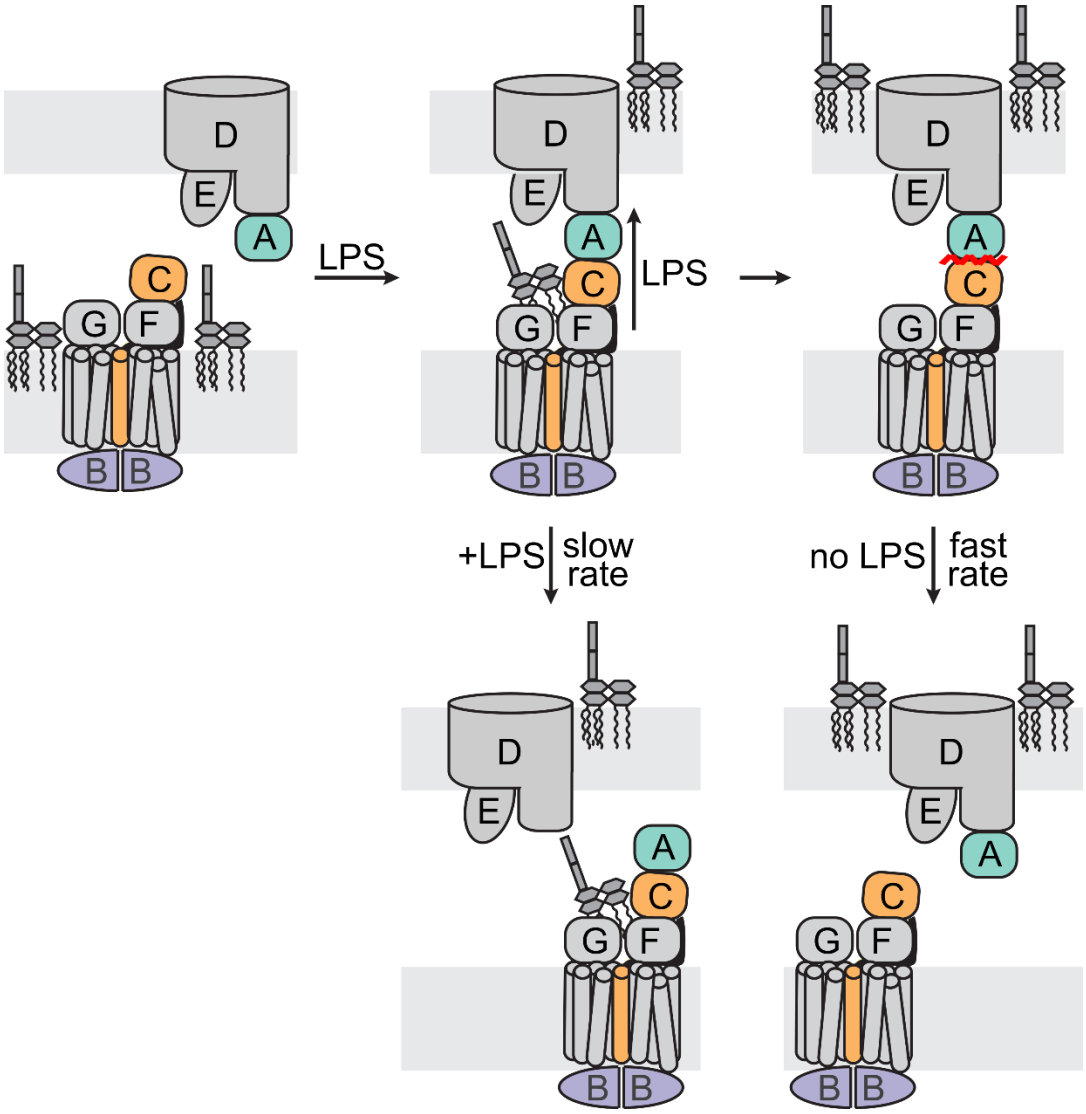

Figure 40: LPS promotes bridge formation by favoring the CA-interaction; bridges containing LPS break slower than empty bridges. Scheme depicting the hypothesized model for Lpt-bridge formation and breakage. High levels of LPS at the inner membrane interact with the inner membrane complex LptB2FGC and facilitate the interaction between LptC and LptA bound to the outer membrane complex LptDE. LPS is transported over the formed trans-envelope bridge. Bridges bound to the structural LPS are breaking slowly by dissociation of the DA-interface. Bridges without the structural LPS break quicker at the CA-interface.

In conclusion, we have provided direct evidence that Lpt-bridges exist in cells. Although sparse labeling cannot resolve the absolute number of bridges per cell, we found that at any given

time, approximately half of the Lpt membrane proteins exist in a bridge state. We have also shown that Lpt-bridges are highly dynamic and only exist for ~10 s in cells. Further, there are two types of bridges that break, likely one with and one without structural bound LPS. The lifetimes of both bridge types are very short, but the presence of LPS correlates with higher stability. Previous calculations have predicted that during cell growth ~70 000 molecules of LPS must be transported to the cell surface per minute.[67] Based on protein synthesis rates it was predicted that the copy umber of the least abundant Lpt-protein, LptC, is around 250 molecules per generation.[155] With our observation that the lifetime of the bridge is <10 s and that roughly half of the Lpt proteins exist in the bridge state, we can estimate that one Lpt-bridge transports ~10 LPS molecules per second and ~50 LPS molecules during its lifetime. This means that LPS is transported rapidly when an Lpt bridge is formed. The fact that LPS promotes bridge formation and its presence correlates with bridge stability provides a strategy to link LPS abundance to cell growth. [177]

4.4. Materials and Methods

4.4.1. Strains used in this chapter

Table 5 contains a list of the strains used in this chapter. The construction of these strains is described in chapter 2 in 2.4.1..

Table 5: List of strains for chapter 4

strain name	genotype	source
LT17	TB28 attHK022 Plac::Halo-15-aa-LptB, ΔLptB::frt	this study

4.4.2. Plasmids used in this chapter

The CA-fusion protein was amplified using primers LT247,(5‘-ATGAGTAAAGCCAGA CGTTGGGTTATCA-3’), and LT314, (5’-TTAATTACCCTTCTTCTGTGCCGG-3’), from plasmid pETCA-fusion.[176] pBAD33 was amplified using primers LT316,(5’-CCGGCACAGAAGAA GGGTAATTAATTGATTAATACCTAGGCTGCATGC-3’), and LT319,(5’-CCAACGTCTGGCTTTACTCATATGTATATCTCCTTCTTAAAGTTAAACAAA ATTATTTC-3’). The two fragments were Gibson assembled® and transformed into NovoBlue cells.

Table 6: List of plasmids for chapter 4

strain name	genotype	source
pBAD33		[21]
pETCA-fusion	Encodes LptC-LptA-fusion protein	[176]
pBAD33CA-fusion	encodes LptC-LptA-fusion protein	this study

4.4.3. Sample preparation for imaging with LpxC inhibitor

A frozen stock of LT17 was streaked out on an LB agar plate, containing 20 μM IPTG. The agar plate was incubated at 37°C overnight. The next day a single colony from the plate was incubated in M9 media, supplemented with 0.2% CAA and 0.4% Maltose as carbon source and 20 μM IPTG to induce Halo-LptB expression. The inoculated culture was serial diluted and the dilutions were grown over night at 37°C while shaking. The next day a culture at its mid exponential phase (OD600 = 0.3-0.6) was used as starter culture to produce another round of serial dilutions in the supplemented M9 media with the addition of 20 μM IPTG. 90 min before staining the cells, when the culture was around (OD600 = 0.3) cells were treated with 0.024 μM LpxC

inhibitor (PF 5081090)[49] (about 0.5 x MIC). Also, the agarose pad to fix the cells to the microscope slides was prepared with 0.024 μM LpxC inhibitor. Since the outer membrane of cells treated with LpxC inhibitor becomes leaky, the labeling dye Halo-Tag-JF549 concentration was reduced to ~12.5 pM. 1 mL of LpxC inhibitor treated culture was stained for 10-15 min. The culture was concentrated by spinning for 2 min at 8000 rpm and removing parts of the supernatant. 1 μL of the concentrated culture was pipetted onto a microscope slide. The slide was previously prepared as described in (2.4.7.). Movies for particle tracking and lifetime measurement were collected as described below. For the negative control, LT17 was imaged without the addition of an LpxC inhibitor and with the usual dye concentration of ~5 nM.

4.4.4. Sample preparation for imaging CA-fusion

pBAD33CA-fusion was transformed into LT17. A single colony of the strain containing the CA-fusion plasmids was inoculated into M9 media, supplemented with 0.2% CAA and 0.4% Maltose as carbon source, 20μM IPTG to induce Halo-LptB expression and chloramphenicol to retain the pBAD33CA-fusion plasmid. The inoculated culture was serial diluted and grown over night at 37°C while shaking. The next day a culture at mid exponential growth (OD=0.3-0.6) was used as starter culture to produce another round of serial dilutions in fresh media. 10 min before staining the cultures, when the culture is at OD600 ~0.3, 0.04 μM arabinose was added to induce the production of LptCA-fusion protein. After 10 minutes of induction the cells were stained with ~5 nM Halo-Tag-JF549 dye for 10 -15 min. The stained culture was concentrated and 1μL of the concentrated culture was pipetted onto prepared microscope slides and covered with an agar pad, prepped from the growth media with the addition of arabinose. For the negative wild-type control,

no arabinose was added to the culture or the pad. Particle tracking and lifetime measurements were conducted as described below.

4.4.5. Microscope set up for lifetime measurements

Total internal reflection fluorescence microscopy (TIRF-M) and phase-contrast microscopy was performed on a Nikon TI microscope equipped with a 100X NA 1.45 TIRF objective and an Andor Ixon EMCCD camera resulting in 160 nm pixels. With an exposure time of 500 ms, TIRF-M time-lapses were taken with streaming acquisition for 4 min at an illumination of 561 nm at a 50% laser intensity. A phase-contrast image was taken before and after the fluorescent movie was acquired to segment the outside of the cells. Movies that displayed drifts were discarded. The imaging was performed in a chamber equilibrated at 37°C.

4.4.6. Microscope set up for particle tracking

The same microscope settings as described in 4.4.5. were used with a changed exposure time and laser intensity. With an exposure time of 100 ms, TIRF-M time-lapses were taken with streaming acquisition for 400 frames min at an illumination of 561 nm at a 70% laser intensity. Again, phase-contrast images was taken before and after the fluorescent movie was acquired to segment the outside of the cells.

4.4.7. Lifetime analysis

The lifetime analysis of immobile Halo-LptB under the treatment of LpxC inhibitor and under the overproduction of LptCA-fusion protein was conducted analogous as described in 3.4.4..

Cell masks were generated from the phase contrast images using the threshold tool in Fiji.[169] The TIRF-M time-lapses were preliminary analyzed using TrackMate[170] and the data were exported to Matlab. Tracks were filtered to be inside cells using the generated cell masks, and the filtered tracks were converted into spot intensity traces. The intensity traces were filtered and fitted to a hidden Markov model using the vbFRET package to measure single molecule lifetimes.[151, 174-175] Traces that were best fitted with a two-state model were included for further analysis. Further filtering of the traces to determine the lifetime was done analogous as described in 3.4.4.. However, treatment of cells with LpxC inhibitor resulted in higher background images. Therefore, more stringent lifetime analysis parameters were used for these data and the corresponding control. Instead of a 40 counts difference between state 1 and state 2 for LpxC inhibitor data and its control a 50 count difference was set. Further only traces with 3 events were allowed instead of the 4 events. The lifetime data were exported and further analyzed with custom written python code as described in 3.4.4..

4.4.8. Single molecule tracking analysis

Tracks were constructed from the collected TIRF-M time lapses with TrackMate as described in 2.4.14.1.. Tracks were filtered to be inside cells using the phase contrast images collected before and after each TIRF-M movie as described in 2.4.14.2.1.. The confinement radius analysis and plots was conducted as described in 2.4.14.2.3.. The cumulative distribution analysis and fits was done as described in 2.4.14.2.4..

5. References

1. Kamio, Y.; Nikaido, H., Outer membrane of Salmonella typhimurium: accessibility of phospholipid head groups to phospholipase c and cyanogen bromide activated dextran in the external medium. *Biochemistry* **1976,** *15* (12), 2561-2570.

2. Osborn, M.; Gander, J.; Parisi, E.; Carson, J., Mechanism of assembly of the outer membrane of Salmonella typhimurium: isolation and characterization of cytoplasmic and outer membrane. *Journal of Biological Chemistry* **1972,** *247* (12), 3962-3972.

3. Mühlradt, P. F.; Golecki, J. R., Asymmetrical distribution and artifactual reorientation of lipopolysaccharide in the outer membrane bilayer of Salmonella typhimurium. *European journal of biochemistry* **1975,** *51* (2), 343-352.

4. Raetz, C. R.; Whitfield, C., Lipopolysaccharide endotoxins. *Annual review of biochemistry* **2002,** *71* (1), 635-700.

5. Sperandeo, P.; Lau, F. K.; Carpentieri, A.; De Castro, C.; Molinaro, A.; Deho, G.; Silhavy, T. J.; Polissi, A., Functional analysis of the protein machinery required for transport of lipopolysaccharide to the outer membrane of Escherichia coli. *Journal of bacteriology* **2008,** *190* (13), 4460-4469.

6. Chng, S.-S.; Gronenberg, L. S.; Kahne, D., Proteins required for lipopolysaccharide assembly in Escherichia coli form a transenvelope complex. *Biochemistry* **2010,** *49* (22), 4565-4567.

7. Sherman, D. J.; Xie, R.; Taylor, R. J.; George, A. H.; Okuda, S.; Foster, P. J.; Needleman, D. J.; Kahne, D., Lipopolysaccharide is transported to the cell surface by a membrane-to-membrane protein bridge. *Science* **2018,** *359* (6377), 798-801.

8. Gram, C., Ueber die isolirte Farbung der Schizomyceten in Schnitt-und Trockenpraparaten. *Fortschritte der Medicin* **1884,** *2*, 185-189.

9. Silhavy, T. J.; Kahne, D.; Walker, S., The bacterial cell envelope. *Cold Spring Harbor perspectives in biology* **2010,** *2* (5), a000414.

10. Ruiz, N.; Kahne, D.; Silhavy, T. J., Advances in understanding bacterial outer-membrane biogenesis. *Nature Reviews Microbiology* **2006,** *4* (1), 57-66.

11. Mullineaux, C. W.; Nenninger, A.; Ray, N.; Robinson, C., Diffusion of green fluorescent protein in three cell environments in Escherichia coli. *Journal of bacteriology* **2006,** *188* (10), 3442-3448.

12. Höltje, J.-V., Growth of the stress-bearing and shape-maintaining murein sacculus of Escherichia coli. *Microbiology and molecular biology reviews* **1998,** *62* (1), 181-203.

13. Sankaran, K.; Wu, H. C., Lipid modification of bacterial prolipoprotein. Transfer of diacylglyceryl moiety from phosphatidylglycerol. *Journal of Biological Chemistry* **1994,** *269* (31), 19701-19706.

14. Cowan, S.; Schirmer, T.; Rummel, G.; Steiert, M.; Ghosh, R.; Pauptit, R.; Jansonius, J.; Rosenbusch, J., Crystal structures explain functional properties of two E. coli porins. *Nature* **1992,** *358* (6389), 727-733.

15. Schirmer, T.; Keller, T. A.; Wang, Y.-F.; Rosenbusch, J. P., Structural basis for sugar translocation through maltoporin channels at 3.1 Å resolution. *Science* **1995,** *267* (5197), 512-514.

16. Nikaido, H., Molecular basis of bacterial outer membrane permeability revisited. *Microbiology and molecular biology reviews* **2003,** *67* (4), 593-656.

17. Nikaido, H.; Nakae, T., The outer membrane of Gram-negative bacteria. *Advances in microbial physiology* **1980,** *20*, 163-250.

18. Nikaido, H.; Vaara, M., Molecular basis of bacterial outer membrane permeability. *Microbiological reviews* **1985,** *49* (1), 1-32.

19. Rojas, E. R.; Billings, G.; Odermatt, P. D.; Auer, G. K.; Zhu, L.; Miguel, A.; Chang, F.; Weibel, D. B.; Theriot, J. A.; Huang, K. C., The outer membrane is an essential load-bearing element in Gram-negative bacteria. *Nature* **2018,** *559* (7715), 617-621.

20. Whitfield, C.; Trent, M. S., Biosynthesis and export of bacterial lipopolysaccharides. *Annual review of biochemistry* **2014,** *83*, 99-128.

21. Takeuchi, Y.; Nikaido, H., Persistence of segregated phospholipid domains in phospholipid-lipopolysaccharide mixed bilayers: studies with spin-labeled phospholipids. *Biochemistry* **1981,** *20* (3), 523-529.

22. Rottem, S.; Leive, L., Effect of variations in lipopolysaccharide on the fluidity of the outer membrane of Escherichia coli. *Journal of Biological Chemistry* **1977,** *252* (6), 2077-2081.

23. Herrmann, M.; Schneck, E.; Gutsmann, T.; Brandenburg, K.; Tanaka, M., Bacterial lipopolysaccharides form physically cross-linked, two-dimensional gels in the presence of divalent cations. *Soft matter* **2015,** *11* (30), 6037-6044.

24. Raetz, C. R.; Reynolds, C. M.; Trent, M. S.; Bishop, R. E., Lipid A modification systems in gram-negative bacteria. *Annu. Rev. Biochem.* **2007,** *76*, 295-329.

25. Schnaitman, C. A.; Klena, J. D., Genetics of lipopolysaccharide biosynthesis in enteric bacteria. *Microbiological reviews* **1993,** *57* (3), 655-682.

26. Rietschel, E. T.; Kirikae, T.; Schade, F. U.; Mamat, U.; Schmidt, G.; Loppnow, H.; Ulmer, A. J.; Zähringer, U.; Seydel, U.; Di Padova, F., Bacterial endotoxin: molecular relationships of structure to activity and function. *The FASEB Journal* **1994,** *8* (2), 217-225.

27. Needham, B. D.; Trent, M. S., Fortifying the barrier: the impact of lipid A remodelling on bacterial pathogenesis. *Nature Reviews Microbiology* **2013,** *11* (7), 467-481.

28. Sassi, N.; Paul, C.; Martin, A.; Bettaieb, A.; Jeannin, J.-F., Lipid A-induced responses in vivo. In *Lipid A in cancer therapy*, Springer: 2009; pp 69-80.

29. Scott, A. J.; Oyler, B. L.; Goodlett, D. R.; Ernst, R. K., Lipid A structural modifications in extreme conditions and identification of unique modifying enzymes to define the Toll-like receptor 4 structure-activity relationship. *Biochimica et Biophysica Acta (BBA)-Molecular and Cell Biology of Lipids* **2017,** *1862* (11), 1439-1450.

30. Maldonado, R. F.; Sá-Correia, I.; Valvano, M. A., Lipopolysaccharide modification in Gram-negative bacteria during chronic infection. *FEMS microbiology reviews* **2016,** *40* (4), 480-493.

31. Meneses-Echávez, J. F.; González-Jiménez, E.; Ramírez-Vélez, R., Effects of supervised multimodal exercise interventions on cancer-related fatigue: systematic review and meta-analysis of randomized controlled trials. *BioMed research international* **2015,** *2015*.

32. Simpson, B. W.; Trent, M. S., Pushing the envelope: LPS modifications and their consequences. *Nature Reviews Microbiology* **2019,** *17* (7), 403-416.

33. Amor, K.; Heinrichs, D. E.; Frirdich, E.; Ziebell, K.; Johnson, R. P.; Whitfield, C., Distribution of core oligosaccharide types in lipopolysaccharides from Escherichia coli. *Infection and immunity* **2000,** *68* (3), 1116-1124.

34. Heinrichs, D. E.; Yethon, J. A.; Whitfield, C., Molecular basis for structural diversity in the core regions of the lipopolysaccharides of Escherichia coli and Salmonella enterica. *Molecular microbiology* **1998,** *30* (2), 221-232.

35. Kalynych, S.; Morona, R.; Cygler, M., Progress in understanding the assembly process of bacterial O-antigen. *FEMS microbiology reviews* **2014,** *38* (5), 1048-1065.

36. Lerouge, I.; Vanderleyden, J., O-antigen structural variation: mechanisms and possible roles in animal/plant–microbe interactions. *FEMS microbiology reviews* **2002,** *26* (1), 17-47.

37. Wang, L.; Wang, Q.; Reeves, P. R., The variation of O antigens in gram-negative bacteria. In *Endotoxins: Structure, Function and Recognition*, Springer: 2010; pp 123-152.

38. Whitfield, C., Biosynthesis of lipopolysaccharide O antigens. *Trends in microbiology* **1995,** *3* (5), 178-185.

39. Anderson, M. S.; Raetz, C., Biosynthesis of lipid A precursors in Escherichia coli. A cytoplasmic acyltransferase that converts UDP-N-acetylglucosamine to UDP-3-O-(R-3-hydroxymyristoyl)-N-acetylglucosamine. *Journal of Biological Chemistry* **1987,** *262* (11), 5159-5169.

40. Coleman, J.; Raetz, C., First committed step of lipid A biosynthesis in Escherichia coli: sequence of the lpxA gene. *Journal of bacteriology* **1988,** *170* (3), 1268-1274.

41. Anderson, M.; Bull, H.; Galloway, S.; Kelly, T.; Mohan, S.; Radika, K.; Raetz, C., UDP-N-acetylglucosamine acyltransferase of Escherichia coli. The first step of endotoxin biosynthesis is thermodynamically unfavorable. *Journal of Biological Chemistry* **1993,** *268* (26), 19858-19865.

42. Kelly, T.; Stachula, S.; Raetz, C.; Anderson, M., The firA gene of Escherichia coli encodes UDP-3-O-(R-3-hydroxymyristoyl)-glucosamine N-acyltransferase. The third step of endotoxin biosynthesis. *Journal of Biological Chemistry* **1993,** *268* (26), 19866-19874.

43. Young, K.; Silver, L. L.; Bramhill, D.; Cameron, P.; Eveland, S. S.; Raetz, C. R.; Hyland, S. A.; Anderson, M. S., The envA Permeability/Cell Division Gene of Escherichia coli Encodes the Second Enzyme of Lipid A Biosynthesis: UDP-3-O-(R-3-HYDROXYMYRISTOYL)-N-ACETYLGLUCOSAMINE DEACETYLASE (∗). *Journal of Biological Chemistry* **1995,** *270* (51), 30384-30391.

44. Meredith, T. C.; Aggarwal, P.; Mamat, U.; Lindner, B.; Woodard, R. W., Redefining the requisite lipopolysaccharide structure in Escherichia coli. *ACS chemical biology* **2006,** *1* (1), 33-42.

45. Caughlan, R. E.; Jones, A. K.; DeLucia, A. M.; Woods, A. L.; Xie, L.; Ma, B.; Barnes, S. W.; Walker, J. R.; Sprague, E. R.; Yang, X., Mechanisms decreasing in vitro susceptibility to the LpxC inhibitor CHIR-090 in the Gram-negative pathogen Pseudomonas aeruginosa. *Antimicrobial agents and chemotherapy* **2012,** *56* (1), 17-27.

46. Barb, A. W.; Leavy, T. M.; Robins, L. I.; Guan, Z.; Six, D. A.; Zhou, P.; Bertozzi, C. R.; Raetz, C. R., Uridine-based inhibitors as new leads for antibiotics targeting Escherichia coli LpxC. *Biochemistry* **2009,** *48* (14), 3068-3077.

47. Clements, J. M.; Coignard, F.; Johnson, I.; Chandler, S.; Palan, S.; Waller, A.; Wijkmans, J.; Hunter, M. G., Antibacterial activities and characterization of novel inhibitors of LpxC. *Antimicrobial agents and chemotherapy* **2002,** *46* (6), 1793-1799.

48. Mdluli, K. E.; Witte, P. R.; Kline, T.; Barb, A. W.; Erwin, A. L.; Mansfield, B. E.; McClerren, A. L.; Pirrung, M. C.; Tumey, L. N.; Warrener, P., Molecular validation of LpxC as an antibacterial drug target in Pseudomonas aeruginosa. *Antimicrobial agents and Chemotherapy* **2006,** *50* (6), 2178-2184.

49. Montgomery, J. I.; Brown, M. F.; Reilly, U.; Price, L. M.; Abramite, J. A.; Arcari, J.; Barham, R.; Che, Y.; Chen, J. M.; Chung, S. W., Pyridone methylsulfone hydroxamate LpxC inhibitors for the treatment of serious gram-negative infections. *Journal of medicinal chemistry* **2012,** *55* (4), 1662-1670.

50. Bartling, C. M.; Raetz, C. R., Steady-state kinetics and mechanism of LpxD, the N-acyltransferase of lipid A biosynthesis. *Biochemistry* **2008,** *47* (19), 5290-5302.

51. Radika, K.; Raetz, C., Purification and properties of lipid A disaccharide synthase of Escherichia coli. *Journal of Biological Chemistry* **1988,** *263* (29), 14859-14867.

52. Crowell, D. N.; Anderson, M. S.; Raetz, C., Molecular cloning of the genes for lipid A disaccharide synthase and UDP-N-acetylglucosamine acyltransferase in Escherichia coli. *Journal of bacteriology* **1986,** *168* (1), 152-159.

53. Ray, B.; Raetz, C., The biosynthesis of gram-negative endotoxin. A novel kinase in Escherichia coli membranes that incorporates the 4'-phosphate of lipid A. *Journal of Biological Chemistry* **1987,** *262* (3), 1122-1128.

54. Garrett, T. A.; Que, N. L.; Raetz, C. R., Accumulation of a Lipid A Precursor Lacking the 4′-Phosphate following Inactivation of the Escherichia coli lpxKGene. *Journal of Biological Chemistry* **1998,** *273* (20), 12457-12465.

55. Brozek, K. A.; Raetz, C., Biosynthesis of lipid A in Escherichia coli. Acyl carrier protein-dependent incorporation of laurate and myristate. *Journal of Biological Chemistry* **1990,** *265* (26), 15410-15417.

56. Clementz, T.; Bednarski, J. J.; Raetz, C. R., Function of the htrB High Temperature Requirement Gene of Escherichia coli in the Acylation of Lipid A: HtrB CATALYZED INCORPORATION OF LAURATE (∗). *Journal of Biological Chemistry* **1996,** *271* (20), 12095-12102.

57. Clementz, T.; Zhou, Z.; Raetz, C. H., Function of the Escherichia coli msbB gene, a multicopy suppressor of htrB knockouts, in the acylation of lipid A: acylation by MsbB follows laurate incorporation by HtrB. *Journal of Biological Chemistry* **1997,** *272* (16), 10353-10360.

58. Roncero, C.; Casadaban, M. J., Genetic analysis of the genes involved in synthesis of the lipopolysaccharide core in Escherichia coli K-12: three operons in the rfa locus. *Journal of bacteriology* **1992,** *174* (10), 3250-3260.

59. McGRATH, B. C.; Osborn, M., Localization of the terminal steps of O-antigen synthesis in Salmonella typhimurium. *Journal of bacteriology* **1991,** *173* (2), 649-654.

60. Doerrler, W. T.; Gibbons, H. S.; Raetz, C. R., MsbA-dependent translocation of lipids across the inner membrane of Escherichia coli. *Journal of Biological Chemistry* **2004,** *279* (43), 45102-45109.

61. Feldman, M. F.; Marolda, C. L.; Monteiro, M. A.; Perry, M. B.; Parodi, A. J.; Valvano, M. A., The activity of a putative polyisoprenol-linked sugar translocase (Wzx) involved in Escherichia coli O antigen assembly is independent of the chemical structure of the O repeat. *Journal of Biological Chemistry* **1999,** *274* (49), 35129-35138.

62. Liu, D.; Cole, R. A.; Reeves, P. R., An O-antigen processing function for Wzx (RfbX): a promising candidate for O-unit flippase. *Journal of bacteriology* **1996,** *178* (7), 2102-2107.

63. Abeyrathne, P. D.; Daniels, C.; Poon, K. K.; Matewish, M. J.; Lam, J. S., Functional characterization of WaaL, a ligase associated with linking O-antigen polysaccharide to the core of Pseudomonas aeruginosa lipopolysaccharide. *Journal of bacteriology* **2005,** *187* (9), 3002-3012.

64. Abeyrathne, P. D.; Lam, J. S., WaaL of Pseudomonas aeruginosa utilizes ATP in in vitro ligation of O antigen onto lipid A-core. *Molecular microbiology* **2007,** *65* (5), 1345-1359.

65. Bray, D.; Robbins, P., The direction of chain growth in Salmonella anatum O-antigen biosynthesis. *Biochemical and Biophysical Research Communications* **1967,** *28* (3), 334-339.

66. Collins, L. V.; Hackett, J., Molecular cloning, characterization, and nucleotide sequence of the rfc gene, which encodes an O-antigen polymerase of Salmonella typhimurium. *Journal of bacteriology* **1991,** *173* (8), 2521-2529.

67. Lima, S.; Guo, M. S.; Chaba, R.; Gross, C. A.; Sauer, R. T., Dual molecular signals mediate the bacterial response to outer-membrane stress. *Science* **2013,** *340* (6134), 837-841.

68. Sampson, B. A.; Misra, R.; Benson, S. A., Identification and characterization of a new gene of Escherichia coli K-12 involved in outer membrane permeability. *Genetics* **1989,** *122* (3), 491-501.

69. Bos, M. P.; Robert, V.; Tommassen, J., Biogenesis of the gram-negative bacterial outer membrane. *Annu. Rev. Microbiol.* **2007,** *61*, 191-214.

70. Dartigalongue, C.; Missiakas, D.; Raina, S., Characterization of the Escherichia coliçE Regulon. *Journal of Biological Chemistry* **2001,** *276* (24), 20866-20875.

71. MacRitchie, D. M.; Buelow, D. R.; Price, N. L.; Raivio, T. L., Two-component signaling and gram negative envelope stress response systems. *Bacterial signal transduction: networks and drug targets* **2008**, 80-110.

72. Braun, M.; Silhavy, T. J., Imp/OstA is required for cell envelope biogenesis in Escherichia coli. *Molecular microbiology* **2002,** *45* (5), 1289-1302.

73. Bos, M. P.; Tefsen, B.; Geurtsen, J.; Tommassen, J., Identification of an outer membrane protein required for the transport of lipopolysaccharide to the bacterial cell surface. *Proceedings of the National Academy of Sciences of the United States of America* **2004,** *101* (25), 9417-9422.

74. Wu, T.; McCandlish, A. C.; Gronenberg, L. S.; Chng, S.-S.; Silhavy, T. J.; Kahne, D., Identification of a protein complex that assembles lipopolysaccharide in the outer membrane of Escherichia coli. *Proceedings of the National Academy of Sciences* **2006,** *103* (31), 11754-11759.

75. Serina, S.; Nozza, F.; Nicastro, G.; Faggioni, F.; Mottl, H.; Dehò, G.; Polissi, A., Scanning the Escherichia coli chromosome by random transposon mutagenesis and multiple phenotypic screening. *Research in microbiology* **2004,** *155* (8), 692-701.

76. Sperandeo, P.; Pozzi, C.; Dehò, G.; Polissi, A., Non-essential KDO biosynthesis and new essential cell envelope biogenesis genes in the Escherichia coli yrbG–yhbG locus. *Research in microbiology* **2006,** *157* (6), 547-558.

77. Sperandeo, P.; Cescutti, R.; Villa, R.; Di Benedetto, C.; Candia, D.; Deho, G.; Polissi, A., Characterization of lptA and lptB, two essential genes implicated in lipopolysaccharide transport to the outer membrane of Escherichia coli. *Journal of bacteriology* **2007,** *189* (1), 244-253.

78. Stenberg, F.; Chovanec, P.; Maslen, S. L.; Robinson, C. V.; Ilag, L. L.; von Heijne, G.; Daley, D. O., Protein complexes of the Escherichia coli cell envelope. *Journal of biological chemistry* **2005,** *280* (41), 34409-34419.

79. Linton, K. J.; Higgins, C. F., Structure and function of ABC transporters: the ATP switch provides flexible control. *Pflügers Archiv-European Journal of Physiology* **2007,** *453* (5), 555-567.

80. Ruiz, N.; Gronenberg, L. S.; Kahne, D.; Silhavy, T. J., Identification of two inner-membrane proteins required for the transport of lipopolysaccharide to the outer membrane of Escherichia coli. *Proceedings of the National Academy of Sciences* **2008,** *105* (14), 5537-5542.

81. Narita, S.-i.; Tokuda, H., Biochemical characterization of an ABC transporter LptBFGC complex required for the outer membrane sorting of lipopolysaccharides. *FEBS letters* **2009,** *583* (13), 2160-2164.

82. Benedet, M.; Falchi, F. A.; Puccio, S.; Di Benedetto, C.; Peano, C.; Polissi, A.; Deho, G., The lack of the essential LptC protein in the trans-envelope lipopolysaccharide transport machine is circumvented by suppressor mutations in LptF, an inner membrane component of the Escherichia coli transporter. *PloS one* **2016,** *11* (8).

83. Sperandeo, P.; Villa, R.; Martorana, A. M.; Šamalikova, M.; Grandori, R.; Deho, G.; Polissi, A., New insights into the Lpt machinery for lipopolysaccharide transport to the cell surface: LptA-LptC interaction and LptA stability as sensors of a properly assembled transenvelope complex. *Journal of bacteriology* **2011,** *193* (5), 1042-1053.

84. Villa, R.; Martorana, A. M.; Okuda, S.; Gourlay, L. J.; Nardini, M.; Sperandeo, P.; Dehò, G.; Bolognesi, M.; Kahne, D.; Polissi, A., The Escherichia coli Lpt transenvelope protein complex for lipopolysaccharide export is assembled via conserved structurally homologous domains. *Journal of bacteriology* **2013,** *195* (5), 1100-1108.

85. Freinkman, E.; Okuda, S.; Ruiz, N.; Kahne, D., Regulated assembly of the transenvelope protein complex required for lipopolysaccharide export. *Biochemistry* **2012,** *51* (24), 4800-4806.

86. Ruiz, N.; Kahne, D.; Silhavy, T. J., Transport of lipopolysaccharide across the cell envelope: the long road of discovery. *Nature Reviews Microbiology* **2009,** *7* (9), 677-683.

87. Okuda, S.; Sherman, D. J.; Silhavy, T. J.; Ruiz, N.; Kahne, D., Lipopolysaccharide transport and assembly at the outer membrane: the PEZ model. *Nature Reviews Microbiology* **2016**.

88. Owens, T. W.; Taylor, R. J.; Pahil, K. S.; Bertani, B. R.; Ruiz, N.; Kruse, A. C.; Kahne, D., Structural basis of unidirectional export of lipopolysaccharide to the cell surface. *Nature* **2019,** *567* (7749), 550-553.

89. Li, Y.; Orlando, B. J.; Liao, M., Structural basis of lipopolysaccharide extraction by the LptB2FGC complex. *Nature* **2019,** *567* (7749), 486-490.

90. Sherman, D. J.; Okuda, S.; Denny, W. A.; Kahne, D., Validation of inhibitors of an ABC transporter required to transport lipopolysaccharide to the cell surface in Escherichia coli. *Bioorganic & medicinal chemistry* **2013,** *21* (16), 4846-4851.

91. Galardy, R.; Craig, L.; Printz, M., Benzophenone triplet: a new photochemical probe of biological ligand-receptor interactions. *Nature New Biology* **1973,** *242* (117), 127-128.

92. Ryu, Y.; Schultz, P. G., Efficient incorporation of unnatural amino acids into proteins in Escherichia coli. *Nature methods* **2006,** *3* (4), 263-265.

93. Okuda, S.; Freinkman, E.; Kahne, D., Cytoplasmic ATP hydrolysis powers transport of lipopolysaccharide across the periplasm in E. coli. *Science* **2012,** *338* (6111), 1214-1217.

94. Kaback, H., [13] Bacterial Membranes. In *Methods in enzymology*, Elsevier: 1971; Vol. 22, pp 99-120.

95. Kaback, H.; Stadtman, E., Proline uptake by an isolated cytoplasmic membrane preparation of Escherichia coli. *Proceedings of the National Academy of Sciences of the United States of America* **1966,** *55* (4), 920.

96. Jae, K. Y.; Rajapandi, T.; Oliver, D., SecA protein is exposed to the periplasmic surface of the E. coli inner membrane in its active state. *Cell* **1994,** *78* (5), 845-853.

97. Simpson, B. W.; Owens, T. W.; Orabella, M. J.; Davis, R. M.; May, J. M.; Trauger, S. A.; Kahne, D.; Ruiz, N., Identification of residues in the lipopolysaccharide ABC transporter that coordinate ATPase activity with extractor function. *MBio* **2016,** *7* (5), e01729-16.

98. Sherman, D. J.; Lazarus, M. B.; Murphy, L.; Liu, C.; Walker, S.; Ruiz, N.; Kahne, D., Decoupling catalytic activity from biological function of the ATPase that powers lipopolysaccharide transport. *Proceedings of the National Academy of Sciences* **2014,** *111* (13), 4982-4987.

99. Wang, Z.; Xiang, Q.; Zhu, X.; Dong, H.; He, C.; Wang, H.; Zhang, Y.; Wang, W.; Dong, C., Structural and functional studies of conserved nucleotide-binding protein LptB in lipopolysaccharide transport. *Biochemical and Biophysical Research Communications* **2014,** *452* (3), 443-449.

100. Bertani, B. R.; Taylor, R. J.; Nagy, E.; Kahne, D.; Ruiz, N., A cluster of residues in the lipopolysaccharide exporter that selects substrate variants for transport to the outer membrane. *Molecular microbiology* **2018,** *109* (4), 541-554.

101. Trent, M. S.; Ribeiro, A. A.; Lin, S.; Cotter, R. J.; Raetz, C. R., An Inner Membrane Enzyme in Salmonellaand Escherichia coli That Transfers 4-Amino-4-deoxy-l-arabinose to Lipid A: INDUCTION IN POLYMYXIN-RESISTANT MUTANTS AND ROLE OF A NOVEL LIPID-LINKED DONOR* 210. *Journal of Biological Chemistry* **2001,** *276* (46), 43122-43131.

102. Chng, S.-S.; Ruiz, N.; Chimalakonda, G.; Silhavy, T. J.; Kahne, D., Characterization of the two-protein complex in Escherichia coli responsible for lipopolysaccharide assembly at the outer membrane. *Proceedings of the National Academy of Sciences* **2010,** *107* (12), 5363-5368.

103. Qiao, S.; Luo, Q.; Zhao, Y.; Zhang, X. C.; Huang, Y., Structural basis for lipopolysaccharide insertion in the bacterial outer membrane. *Nature* **2014,** *511* (7507), 108-111.

104. Dong, H.; Xiang, Q.; Gu, Y.; Wang, Z.; Paterson, N. G.; Stansfeld, P. J.; He, C.; Zhang, Y.; Wang, W.; Dong, C., Structural basis for outer membrane lipopolysaccharide insertion. *Nature* **2014,** *511* (7507), 52-56.

105. Hagan, C. L.; Silhavy, T. J.; Kahne, D., β-Barrel membrane protein assembly by the Bam complex. *Annual review of biochemistry* **2011,** *80*, 189-210.

106. Vertommen, D.; Ruiz, N.; Leverrier, P.; Silhavy, T. J.; Collet, J. F., Characterization of the role of the Escherichia coli periplasmic chaperone SurA using differential proteomics. *Proteomics* **2009,** *9* (9), 2432-2443.

107. Ruiz, N.; Chng, S.-S.; Hiniker, A.; Kahne, D.; Silhavy, T. J., Nonconsecutive disulfide bond formation in an essential integral outer membrane protein. *Proceedings of the National Academy of Sciences* **2010,** *107* (27), 12245-12250.

108. Matsuyama, S.; Tajima, T.; Tokuda, H., A novel periplasmic carrier protein involved in the sorting and transport of Escherichia coli lipoproteins destined for the outer membrane. *The EMBO journal* **1995,** *14* (14), 3365.

109. Okuda, S.; Tokuda, H., Lipoprotein sorting in bacteria. *Annual review of microbiology* **2011,** *65*, 239-259.

110. Freinkman, E.; Chng, S.-S.; Kahne, D., The complex that inserts lipopolysaccharide into the bacterial outer membrane forms a two-protein plug-and-barrel. *Proceedings of the National Academy of Sciences* **2011,** *108* (6), 2486-2491.

111. Botos, I.; Majdalani, N.; Mayclin, S. J.; McCarthy, J. G.; Lundquist, K.; Wojtowicz, D.; Barnard, T. J.; Gumbart, J. C.; Buchanan, S. K., Structural and functional characterization of the LPS transporter LptDE from Gram-negative pathogens. *Structure* **2016,** *24* (6), 965-976.

112. Li, X.; Gu, Y.; Dong, H.; Wang, W.; Dong, C., Trapped lipopolysaccharide and LptD intermediates reveal lipopolysaccharide translocation steps across the Escherichia coli outer membrane. *Scientific reports* **2015,** *5* (1), 1-8.

113. Malojčić, G.; Andres, D.; Grabowicz, M.; George, A. H.; Ruiz, N.; Silhavy, T. J.; Kahne, D., LptE binds to and alters the physical state of LPS to catalyze its assembly at the cell surface. *Proceedings of the National Academy of Sciences* **2014,** *111* (26), 9467-9472.

114. Bos, M. P.; Tommassen, J., The LptD chaperone LptE is not directly involved in lipopolysaccharide transport in Neisseria meningitidis. *Journal of Biological Chemistry* **2011,** *286* (33), 28688-28696.

115. Chimalakonda, G.; Ruiz, N.; Chng, S.-S.; Garner, R. A.; Kahne, D.; Silhavy, T. J., Lipoprotein LptE is required for the assembly of LptD by the β-barrel assembly machine in the outer membrane of Escherichia coli. *Proceedings of the National Academy of Sciences* **2011,** *108* (6), 2492-2497.

116. Chng, S.-S.; Xue, M.; Garner, R. A.; Kadokura, H.; Boyd, D.; Beckwith, J.; Kahne, D., Disulfide rearrangement triggered by translocon assembly controls lipopolysaccharide export. *Science* **2012,** *337* (6102), 1665-1668.

117. Sperandeo, P.; Dehò, G.; Polissi, A., The lipopolysaccharide transport system of Gram-negative bacteria. *Biochimica et Biophysica Acta (BBA)-Molecular and Cell Biology of Lipids* **2009,** *1791* (7), 594-602.

118. Takeda, K.; Miyatake, H.; Yokota, N.; Matsuyama, S.-i.; Tokuda, H.; Miki, K., Crystal structures of bacterial lipoprotein localization factors, LolA and LolB. *The EMBO journal* **2003,** *22* (13), 3199-3209.

119. Okuda, S.; Watanabe, S.; Tokuda, H., A short helix in the C-terminal region of LolA is important for the specific membrane localization of lipoproteins. *FEBS letters* **2008,** *582* (15), 2247-2251.

120. Tran, A. X.; Trent, M. S.; Whitfield, C., The LptA protein of Escherichia coli is a periplasmic lipid A-binding protein involved in the lipopolysaccharide export pathway. *Journal of Biological Chemistry* **2008,** *283* (29), 20342-20349.

121. Mühlradt, P. F.; Menzel, J.; Golecki, J. R.; Speth, V., Outer membrane of Salmonella: sites of export of newly synthesised lipopolysaccharide on the bacterial surface. *European journal of biochemistry* **1973,** *35* (3), 471-481.

122. Bayer, M., Areas of adhesion between wall and membrane of Escherichia coli. *Microbiology* **1968,** *53* (3), 395-404.

123. Kellenberger, E., The 'Bayer bridges' confronted with results from improved electron microscopy methods. *Molecular microbiology* **1990,** *4* (5), 697-705.

124. Bayer, M., Zones of membrane adhesion in the cryofixed envelope of Escherichia coli. *Journal of structural biology* **1991,** *107* (3), 268-280.

125. Tefsen, B.; Geurtsen, J.; Beckers, F.; Tommassen, J.; de Cock, H., Lipopolysaccharide transport to the bacterial outer membrane in spheroplasts. *Journal of Biological Chemistry* **2005,** *280* (6), 4504-4509.

126. Ishidate, K.; Creeger, E.; Zrike, J.; Deb, S.; Glauner, B.; MacAlister, T.; Rothfield, L., Isolation of differentiated membrane domains from E. coli and S. typhimurium, including a fraction containing attachment sites between the inner and outer membranes and the murein skeleton of the cell envelope. *J. Biol. Chem* **1986,** *261*, 428-443.

127. Suits, M. D.; Sperandeo, P.; Dehò, G.; Polissi, A.; Jia, Z., Novel structure of the conserved gram-negative lipopolysaccharide transport protein A and mutagenesis analysis. *Journal of molecular biology* **2008,** *380* (3), 476-488.

128. Tran, A. X.; Dong, C.; Whitfield, C., Structure and functional analysis of LptC, a conserved membrane protein involved in the lipopolysaccharide export pathway in Escherichia coli. *Journal of Biological Chemistry* **2010,** *285* (43), 33529-33539.

129. Xie, R.; Taylor, R. J.; Kahne, D., Outer membrane translocon communicates with inner membrane ATPase to stop lipopolysaccharide transport. *Journal of the American Chemical Society* **2018,** *140* (40), 12691-12694.

130. Mühlradt, P. F.; Menzel, J.; Golecki, J. R.; Speth, V., Lateral mobility and surface density of lipopolysaccharide in the outer membrane of Salmonella typhimurium. *European journal of biochemistry* **1974,** *43* (3), 533-539.

131. Rassam, P.; Copeland, N. A.; Birkholz, O.; Tóth, C.; Chavent, M.; Duncan, A. L.; Cross, S. J.; Housden, N. G.; Kaminska, R.; Seger, U., Supramolecular assemblies underpin turnover of outer membrane proteins in bacteria. *Nature* **2015,** *523* (7560), 333-336.

132. Leake, M. C.; Chandler, J. H.; Wadhams, G. H.; Bai, F.; Berry, R. M.; Armitage, J. P., Stoichiometry and turnover in single, functioning membrane protein complexes. *Nature* **2006,** *443* (7109), 355-358.

133. Oh, D.; Yu, Y.; Lee, H.; Wanner, B. L.; Ritchie, K., Dynamics of the serine chemoreceptor in the Escherichia coli inner membrane: a high-speed single-molecule tracking study. *Biophysical journal* **2014,** *106* (1), 145-153.

134. Benn, G.; Mikheyeva, I. V.; Inns, P. G.; Forster, J. C.; Ojkic, N.; Bortolini, C.; Ryadnov, M. G.; Kleanthous, C.; Silhavy, T. J.; Hoogenboom, B. W., Phase separation in the outer membrane of Escherichia coli. *Proceedings of the National Academy of Sciences* **2021,** *118* (44).

135. Smit, J.; Nikaido, H., Outer membrane of gram-negative bacteria. XVIII. Electron microscopic studies on porin insertion sites and growth of cell surface of Salmonella typhimurium. *Journal of Bacteriology* **1978,** *135* (2), 687-702.

136. Ursell, T. S.; Trepagnier, E. H.; Huang, K. C.; Theriot, J. A., Analysis of surface protein expression reveals the growth pattern of the gram-negative outer membrane. **2012**.

137. Mamou, G.; Inns, P. G.; Sun, D.; Kaminska, R.; Housden, N. G.; Cohen-Khait, R.; Miller, H.; Storek, K. M.; Rutherford, S. T.; Payandeh, J., Spatiotemporal organization of BamA governs the pattern of outer membrane protein distribution in growing Escherichia coli cells. *bioRxiv* **2021**.

138. Chavent, M.; Duncan, A. L.; Rassam, P.; Birkholz, O.; Hélie, J.; Reddy, T.; Beliaev, D.; Hambly, B.; Piehler, J.; Kleanthous, C., How nanoscale protein interactions determine the

mesoscale dynamic organisation of bacterial outer membrane proteins. *Nature communications* **2018,** *9* (1), 1-12.

139. Lill, Y.; Jordan, L. D.; Smallwood, C. R.; Newton, S. M.; Lill, M. A.; Klebba, P. E.; Ritchie, K., Confined mobility of TonB and FepA in Escherichia coli membranes. *PLoS One* **2016,** *11* (12), e0160862.

140. Bergmiller, T.; Andersson, A. M.; Tomasek, K.; Balleza, E.; Kiviet, D. J.; Hauschild, R.; Tkačik, G.; Guet, C. C., Biased partitioning of the multidrug efflux pump AcrAB-TolC underlies long-lived phenotypic heterogeneity. *Science* **2017,** *356* (6335), 311-315.

141. Egan, A. J., Bacterial outer membrane constriction. *Molecular microbiology* **2018,** *107* (6), 676-687.

142. Rassam, P.; Long, K. R.; Kaminska, R.; Williams, D. J.; Papadakos, G.; Baumann, C. G.; Kleanthous, C., Intermembrane crosstalk drives inner-membrane protein organization in Escherichia coli. *Nature communications* **2018,** *9* (1), 1-8.

143. Stout, A. L.; Axelrod, D., Evanescent field excitation of fluorescence by epi-illumination microscopy. *Applied optics* **1989,** *28* (24), 5237-5242.

144. Kawano, Y.; Abe, C.; Kaneda, T.; Aono, Y.; Abe, K.; Tamura, K.; Terakawa, S. In *High-numerical-aperture objective lenses and optical system improved objective type total internal reflection fluorescence microscopy*, Optical Devices and Diagnostics in Materials Science, SPIE: 2000; pp 142-151.

145. Axelrod, D.; Burghardt, T. P.; Thompson, N. L., Total internal reflection fluorescence. *Annual review of biophysics and bioengineering* **1984,** *13* (1), 247-268.

146. Axelrod, D., Cell-substrate contacts illuminated by total internal reflection fluorescence. *The Journal of cell biology* **1981,** *89* (1), 141-145.

147. Axelrod, D., Total internal reflection fluorescence microscopy in cell biology. *Traffic* **2001,** *2* (11), 764-774.

148. Funatsu, T.; Harada, Y.; Tokunaga, M.; Saito, K.; Yanagida, T., Imaging of single fluorescent molecules and individual ATP turnovers by single myosin molecules in aqueous solution. *Nature* **1995,** *374* (6522), 555-559.

149. Cho, H.; Wivagg, C. N.; Kapoor, M.; Barry, Z.; Rohs, P. D.; Suh, H.; Marto, J. A.; Garner, E. C.; Bernhardt, T. G., Bacterial cell wall biogenesis is mediated by SEDS and PBP polymerase families functioning semi-autonomously. *Nature microbiology* **2016,** *1* (10), 1-8.

150. Garner, E. C.; Bernard, R.; Wang, W.; Zhuang, X.; Rudner, D. Z.; Mitchison, T., Coupled, circumferential motions of the cell wall synthesis machinery and MreB filaments in B. subtilis. *Science* **2011,** *333* (6039), 222-225.

151. Squyres, G. R.; Holmes, M. J.; Barger, S. R.; Pennycook, B. R.; Ryan, J.; Yan, V. T.; Garner, E. C., Single-molecule imaging reveals that Z-ring condensation is essential for cell division in Bacillus subtilis. *Nature microbiology* **2021,** *6* (5), 553-562.

152. Bisson-Filho, A. W.; Hsu, Y.-P.; Squyres, G. R.; Kuru, E.; Wu, F.; Jukes, C.; Sun, Y.; Dekker, C.; Holden, S.; VanNieuwenhze, M. S., Treadmilling by FtsZ filaments drives peptidoglycan synthesis and bacterial cell division. *Science* **2017,** *355* (6326), 739-743.

153. Lee, T. K.; Meng, K.; Shi, H.; Huang, K. C., Single-molecule imaging reveals modulation of cell wall synthesis dynamics in live bacterial cells. *Nature communications* **2016,** *7* (1), 1-9.

154. Domínguez-Escobar, J.; Chastanet, A.; Crevenna, A. H.; Fromion, V.; Wedlich-Söldner, R.; Carballido-López, R., Processive movement of MreB-associated cell wall biosynthetic complexes in bacteria. *Science* **2011,** *333* (6039), 225-228.

155. Li, G.-W.; Burkhardt, D.; Gross, C.; Weissman, J. S., Quantifying absolute protein synthesis rates reveals principles underlying allocation of cellular resources. *Cell* **2014,** *157* (3), 624-635.

156. Ke, N.; Landgraf, D.; Paulsson, J.; Berkmen, M., Visualization of periplasmic and cytoplasmic proteins with a self-labeling protein tag. *Journal of bacteriology* **2016,** *198* (7), 1035-1043.

157. Grimm, J. B.; English, B. P.; Chen, J.; Slaughter, J. P.; Zhang, Z.; Revyakin, A.; Patel, R.; Macklin, J. J.; Normanno, D.; Singer, R. H., A general method to improve fluorophores for live-cell and single-molecule microscopy. *Nature methods* **2015,** *12* (3), 244-250.

158. Schütz, G. J.; Schindler, H.; Schmidt, T., Single-molecule microscopy on model membranes reveals anomalous diffusion. *Biophysical journal* **1997,** *73* (2), 1073-1080.

159. Bosch, P. J.; Kanger, J. S.; Subramaniam, V., Classification of dynamical diffusion states in single molecule tracking microscopy. *Biophysical journal* **2014,** *107* (3), 588-598.

160. Kumar, M.; Mommer, M. S.; Sourjik, V., Mobility of cytoplasmic, membrane, and DNA-binding proteins in Escherichia coli. *Biophysical journal* **2010,** *98* (4), 552-559.

161. Gerding, M. A.; Ogata, Y.; Pecora, N. D.; Niki, H.; De Boer, P. A., The trans-envelope Tol–Pal complex is part of the cell division machinery and required for proper outer-membrane invagination during cell constriction in E. coli. *Molecular microbiology* **2007,** *63* (4), 1008-1025.

162. Hagan, C. L.; Kim, S.; Kahne, D., Reconstitution of outer membrane protein assembly from purified components. *Science* **2010,** *328* (5980), 890-892.

163. Gibson, D. G.; Young, L.; Chuang, R.-Y.; Venter, J. C.; Hutchison, C. A.; Smith, H. O., Enzymatic assembly of DNA molecules up to several hundred kilobases. *Nature methods* **2009,** *6* (5), 343-345.

164. Bernhardt, T. G.; De Boer, P. A., Screening for synthetic lethal mutants in Escherichia coli and identification of EnvC (YibP) as a periplasmic septal ring factor with murein hydrolase activity. *Molecular microbiology* **2004,** *52* (5), 1255-1269.

165. Guzman, L.-M.; Belin, D.; Carson, M. J.; Beckwith, J., Tight regulation, modulation, and high-level expression by vectors containing the arabinose PBAD promoter. *Journal of bacteriology* **1995,** *177* (14), 4121-4130.

166. Datsenko, K. A.; Wanner, B. L., One-step inactivation of chromosomal genes in Escherichia coli K-12 using PCR products. *Proceedings of the National Academy of Sciences* **2000,** *97* (12), 6640-6645.

167. Bernhardt, T. G.; De Boer, P. A., SlmA, a nucleoid-associated, FtsZ binding protein required for blocking septal ring assembly over chromosomes in E. coli. *Molecular cell* **2005,** *18* (5), 555-564.

168. Haldimann, A.; Wanner, B. L., Conditional-replication, integration, excision, and retrieval plasmid-host systems for gene structure-function studies of bacteria. *Journal of bacteriology* **2001,** *183* (21), 6384-6393.

169. Schindelin, J.; Arganda-Carreras, I.; Frise, E.; Kaynig, V.; Longair, M.; Pietzsch, T.; Preibisch, S.; Rueden, C.; Saalfeld, S.; Schmid, B., Fiji: an open-source platform for biological-image analysis. *Nature methods* **2012,** *9* (7), 676-682.

170. Ershov, D.; Phan, M.-S.; Pylvänäinen, J. W.; Rigaud, S. U.; Le Blanc, L.; Charles-Orszag, A.; Conway, J. R.; Laine, R. F.; Roy, N. H.; Bonazzi, D., Bringing TrackMate in the era of machine-learning and deep-learning. *bioRxiv* **2021**.

171. Harris, C. R.; Millman, K. J.; Van Der Walt, S. J.; Gommers, R.; Virtanen, P.; Cournapeau, D.; Wieser, E.; Taylor, J.; Berg, S.; Smith, N. J., Array programming with NumPy. *Nature* **2020,** *585* (7825), 357-362.

172. Newville, M.; Otten, R.; Nelson, A.; Ingargiola, A.; Stensitzki, T.; Allan, D.; Fox, A.; Carter, F., Micha l. *Dima Pustakhod, lneuhaus, Sebastian Weigand, Ray Osborn, Glenn, Christoph Deil, Mark, Allan LR Hansen, Gustavo Pasquevich, Leon Foks, Nicholas Zobrist, Oliver Frost, Alexandre Beelen, Stuermer, kwertyops, Anthony Polloreno, Shane Caldwell, Anthony Almarza, Arun Persaud, Ben Gamari, and Benjamin F. Maier. lmfit/lmfit-py* **2021,** *1* (2).

173. Okuda, S.; Sherman, D. J.; Silhavy, T. J.; Ruiz, N.; Kahne, D., Lipopolysaccharide transport and assembly at the outer membrane: the PEZ model. *Nature Reviews Microbiology* **2016,** *14* (6), 337-345.

174. Lifetime Analysis. https://bitbucket.org/garnerlab/squyres-2020/src/master/Lifetime%20Analysis/. (2020).

175. Bronson, J. E.; Fei, J.; Hofman, J. M.; Gonzalez Jr, R. L.; Wiggins, C. H., Learning rates and states from biophysical time series: a Bayesian approach to model selection and single-molecule FRET data. *Biophysical journal* **2009,** *97* (12), 3196-3205.

176. In preparation, Stephen Early, Andrew Wilson, Sebastian Rowe, Rebecca Taylor, Natividad Ruiz and Daniel Kahne.

177. Martorana, A. M.; Moura, E. C.; Sperandeo, P.; Di Vincenzo, F.; Liang, X.; Toone, E.; Zhou, P.; Polissi, A., Degradation of Components of the Lpt Transenvelope Machinery Reveals

LPS-Dependent Lpt Complex Stability in Escherichia coli. *Frontiers in molecular biosciences* **2021,** *8*.